2015

EFFECT OF HEATING AND IONIZATION OF FOUR ATOMIZING GASES ON THE SPRAY CHARACTERISTICS OF A HIGH VOLUME LOW PRESSURE SPRAY ATOMIZER

Anthony V. Adornato
University of Kentucky, tony.adornato@gmail.com

STUDENT AGREEMENT:

I represent that my thesis or dissertation and abstract are my original work. Proper attribution has been given to all outside sources. I understand that I am solely responsible for obtaining any needed copyright permissions. I have obtained needed written permission statement(s) from the owner(s) of each third-party copyrighted matter to be included in my work, allowing electronic distribution (if such use is not permitted by the fair use doctrine) which will be submitted to UKnowledge as Additional File.

I hereby grant to The University of Kentucky and its agents the irrevocable, non-exclusive, and royalty-free license to archive and make accessible my work in whole or in part in all forms of media, now or hereafter known. I agree that the document mentioned above may be made available immediately for worldwide access unless an embargo applies.

I retain all other ownership rights to the copyright of my work. I also retain the right to use in future works (such as articles or books) all or part of my work. I understand that I am free to register the copyright to my work.

REVIEW, APPROVAL AND ACCEPTANCE

The document mentioned above has been reviewed and accepted by the student's advisor, on behalf of the advisory committee, and by the Director of Graduate Studies (DGS), on behalf of the program; we verify that this is the final, approved version of the student's thesis including all changes required by the advisory committee. The undersigned agree to abide by the statements above.

Anthony V. Adornato, Student

Dr. Kozo Saito, Major Professor

Dr. James McDonough, Director of Graduate Studies

EFFECT OF HEATING AND IONIZATION OF FOUR ATOMIZING GASES ON THE SPRAY CHARACTERISTICS OF A HIGH VOLUME LOW PRESSURE SPRAY ATOMIZER

THESIS

A thesis submitted in partial fulfillment of the
requirements for the degree of Master of Science in Mechanical
Engineering in the College of Engineering at the
University of Kentucky

By

Anthony Victor Adornato

Lexington, Kentucky

Director: Dr. Kozo Saito, Professor of Mechanical Engineering

Lexington, Kentucky

2015

ABSTRACT OF THESIS

EFFECT OF HEATING AND IONIZATION OF FOUR ATOMIZING GASES ON THE SPRAY CHARACTERISTICS OF A HIGH VOLUME LOW PRESSURE SPRAY ATOMIZER

The disintegration of a liquid jet emerging from a nozzle by a high speed gas stream has been under investigation of several decades. A result of the liquid jet disintegration is droplet formation. This process is referred to as atomization. Industrial applications use atomization as a method for applying coatings to substrates. It has been reported that the use of other atomizing gases instead of compressed plant air will positively affect paint droplet size distributions, spray patterns and finish qualities; furthermore, the ionization and heating of the atomizing gas was reported to positively affect finish qualities. Although ionization techniques have been studied in the past, a lack of specific information remains about how ionization actually affects droplet formation and size, and finish quality.

To determine the effect of the different atomizing gases, heating, and ionization several methods were used. The droplet size distribution of the spray was captured with the use of laser diffraction, while the large-scale characteristics of the flow were recorded with Infrared thermography. In the process, a novel method was developed for measuring the secondary droplet breakup in the spray.

KEYWORDS: Atomization, Laser Diffraction, Infrared Thermography, Heating, Ionization

Anthony Victor Adornato

April 22, 2015

EFFECT OF HEATING AND IONIZATION OF FOUR ATOMIZING GASES ON THE SPRAY CHARACTERISTICS OF A HIGH VOLUME LOW PRESSURE SPRAY ATOMIZER

By

Anthony Victor Adornato

Dr. Kozo Saito
Director of Thesis

Dr. James McDonough
Director of Graduate Studies

April 22, 2015

This thesis is dedicated to my family and my friends. You kept me sane when it all seemed like too much and encouraged me to finish when I wanted to quit. Without you, this thesis wouldn't exist.

Calvin: "I've been thinking Hobbes"
Hobbes: "On a weekend?"
Calvin: "Well it wasn't on purpose…"

-Bill Watterson

ACKNOWLEDGEMENTS

While this thesis is an individual work, it has been greatly influenced by the efforts and insights of a great number of people. Firstly, I would like to express my most sincere gratitude to Dr. Kozo Saito for his guidance and support throughout my time in graduate school. I am also greatly appreciative of the efforts of Dr. Nelson Akafuah. His advice and guidance was always thoughtful and informative. I am also very thankful to Dr. Sean Bailey who has been one of my professors for quite a few years now, and graciously agreed to serve on my thesis defense committee.

I would be remiss if I did not mention the invaluable mentorship of Dr. Ahmad Salaimeh for working with me since my first day in graduate school. He took time out of his very busy schedule to teach me how to be a good researcher. I would also like to thank my colleagues in the IR4TD group: Dr. Tianxiang Li, Dr. John Stencel, Ms. Li Yang, Ms. Brittany Adam, Mr. Jeremiah Fugate, Mr. Justin English, Mr. Sadegh Poozesh, Mr. Nikolay Gustenyov, and my high school students: Mr. Monon Rahman and Mr. Eric Lowry.

Additionally, I would like to thank the people who I worked with at CAER, specifically Dr. Mark Crocker, Dr. John Groppo, and Mr. Michael Wilson. When I walked into their offices my first day I had no idea what I was doing, their guidance molded me into a competent engineer.

Finally I need to thank my friends and family, who helped save me from my own dumb ideas on more occasions than I care to admit.

TABLE OF CONTENTS

LIST OF FIGURES

LIST OF TABLES

CHAPTER ONE

1.0 INTRODUCTION

Automotive coatings demand an exceptional level of quality to ensure that their color, gloss and texture are as excellent as possible. These traits greatly affect the perception of the quality of the overall product in the eyes of customers (Lou and Huang 2003). Furthermore, during coating processes, it is necessary that all environmental regulations are met. For these reasons, extra care is given to painting processes during automotive production. Coating composition, together with application techniques, curing and surface characteristics determine the appearance of a coating film (Braun and Fields 1994). Several different techniques for applying coatings are used, but the most common by far is spray atomization. The quality of the atomization has a strong influence on the finished quality of finished parts (McKnight 1997).

Paint sprays consist of a large number of paint droplets dispersed in a carrier gas, often air. The distribution of the liquid and gas phases in the time domain is described by the liquid volume fraction, f_v, defined as the ratio of equivalent volume of the liquid to a given volume of the gas and liquid mixture (Sirignano 1999). The droplet number density is defined as the number of liquid droplets per unit volume.

Understanding droplet atomization processes allows for increased knowledge of the physics of the droplets and the ways that this impacts the coating quality. This quality is currently based on visualization techniques used by the paint shop operators, and solutions to quality problems are usually based on experience-based knowledge. However, continuous improvements in quality and the reduction of waste require a

deeper understanding of the underlying droplet formation and painting processes (Lou and Huang 2003). This thesis seeks to address some of these issues by studying the atomization quality of an atomizer that is used in automobile painting operations and by developing a new method for determining atomization. It also examines the effectiveness of a relatively new approach to atomization which has been claimed to increase the efficiency of automobile coating processes.

1.1 RESEARCH OBJECTIVES

The main objectives of this thesis are to investigate the use of different gases, heating and ionization during paint droplet formation and to understand to what extent these changes affect the characteristics of sprays emanating from one type of atomizer. It has been reported (Eurosider 2008) that the use of nitrogen atomizing gas instead of compressed plant air will positively affect paint droplet size distributions, spray patterns and finish qualities; furthermore, the ionization of the atomizing gas was reported to positively affect finish qualities. Although ionization techniques have been studied in the past Keith-Roach 2010), a lack of specific information remains about how ionization actually affects droplet formation and size, and finish quality. Additionally, heating of the atomizing gas has been reported to positively affect droplet breakup during atomization and the ensuing spray pattern. Although the chemical and physical properties of these gases are well known, their effects on atomization are not well known.

Secondly, a novel method for judging the atomization quality of an entire spray was developed. This method employs Weber number (We) calculations; the Weber

number is non-dimensional and can be used to predict droplet breakup, but has only been studied in single-droplet systems. Actual sprays consist of a distribution of droplets of different sizes which can be in a range of atomization regimes. A method was developed for determining the relative proportions of the spray in each of these atomization regimes, as is defined in the following. It allows for an experimenter to more thoroughly understand the processes taking place in the spray.

During this study, a range of different possible nozzle geometries were available for use on a High Volume Low Pressure (HVLP) spray atomizer. The nozzles were each evaluated during preliminary research and then the most representative of the three was chosen for use in the more extensive experiments described herein.

That data in this thesis are considered to be an example of a practical characterization approach for HVLP nozzles. This characterization could be useful for industrial applications where a user may need to tailor atomizer performance for a particular application.

1.2 LITERATURE REVIEW

Liquid atomization and the characterization of sprays in conjunction with IR thermography have been studied for decades. In Section 1.2.1, published literature on spray atomization is presented, and includes the principles of airblast atomization; the Kelvin-Helmholtz instability; the Rayleigh-Taylor instability; and secondary breakup. Section 1.2.2 offers a literature review that covers spray characterization, including droplet size distributions and droplet measurement techniques. Section 1.2.3 focuses on a

literature review of the use of IR thermography for spray characterization; it includes a summarization of the scientific principles and applications for studying the fluid dynamics of sprays.

1.2.1 Spray Atomization

A spray is a system of droplets immersed in a gaseous continuous phase. Sprays are produced as a result of atomization, which is defined as the disintegration of a liquid into droplets (Lefebvre 1989, Liu 2000). Liquid atomization can be brought about by the use of aerodynamic, mechanical, ultrasonic or electrostatic forces. The breakup of a liquid into droplets can be achieved by gas impingement in what is called two-fluid atomization, by centrifugal forces in rotary atomization, by ultrasonic vibration utilizing a piezoelectric device in ultrasonic atomization, or by electrostatic/electromagnetic fields in electrostatic atomization. Atomization processes can also be classified by the type of energy imparted that produces instabilities in the liquid element. For example, pressure energy is imparted during pressure atomization, centrifugal energy during rotary atomization, gaseous/fluid energy during two fluid atomization, and vibratory energy during ultrasonic or acoustic atomization (Lefebvre 1989, Liu 2000).

When a liquid is sprayed, it forms ligaments due to the interaction of its surface tension with air resistance (Lefebvre 1989, Marmottant and Villermaux 2004). The liquid breaks into individual droplets which have a surface tension more capable of holding them together in the face of liquid instabilities. Very large droplets will split into smaller droplets if the surrounding ambient air resistance overcomes the droplet's surface tension.

In the vast majority of industrial processes, air assisted atomizers are used in which compressed air supplies the required energy for liquid atomization. Air atomizers are the focus of this study.

1.2.1.1 Air Blast Atomization

With conventional air pressure atomizers, high velocity is imparted to the liquid by spraying it under high pressure through a nozzle; another approach is to allow the liquid to be passed through the nozzle at a relatively slow speed. In either case, after the liquid exits the nozzle it is exposed to a large volume of a fast-moving airstream. This approach is referred to as "airblast" atomization (Lefebvre 1980).

Airblast atomizers require lower pressures and produce a more consistent spray than standard pressure atomizers as well as a more thorough mixture of the air and liquid (Lefebvre 1989). This difference makes airblast atomizers ideal for use in gas turbine systems, as well as applications where a particular spray path is desired. Airblast atomization allows for the tailoring of the droplet size distribution by adjusting the air and liquid flow rates, which provides for better control in coating applications (Hund 1985).

Simple designs for an airblast atomizer will use an annular air hole located around a central liquid nozzle; more advanced designs will use secondary "pattern" air jets which impinge on the main liquid stream at some distance away from the nozzle. The use of a secondary air jet enhances atomization and the trajectory paths of the droplets, allowing

an operator to adjust the spray pattern from a circular spray pattern to a flat sheet pattern. Each of these pattern configurations is useful in different painting scenarios.

The main drawback of the airblast atomizer design is that atomization performance degrades as lower gas velocities are used because the mechanism which induces liquid instabilities necessary for droplet formation is the air pressure energy. In other words, a steady supply of relatively high speed air is required for proper performance of airblast atomizers.

1.2.1.2 Kelvin-Helmholtz Instability

Kelvin-Helmholtz (KH) instabilities arise when a shear force is applied between two fluids traveling at different velocities. For low velocities the surface tension of the interface between the two fluids can stabilize the disturbances that occur. However, the surface tension will no longer be able to stabilize the interface after a certain velocity threshold has been attained. As a consequence, interface disturbances that occur will grow and destabilize fluid flow (Kelvin 1871).

Figure 1.1 graph depicts the behavior of a fluid stream under the influence of a KH instability. The shear force between the two fluids causes undulations in the liquid jet (Meiron, Baker et al. 1982) with stable acceleration as the fluid (liquid) moves toward the gas phase and unstable acceleration as the gas phase moves toward the liquid phase. These undulations will grow as long as the velocity difference between the two fluids is high enough. The presence of undulations occurs for most practical applications because

the velocity below which undulations are damped by viscosity are relatively low (Drazin 1970, Khan, Tourigny et al. 2003).

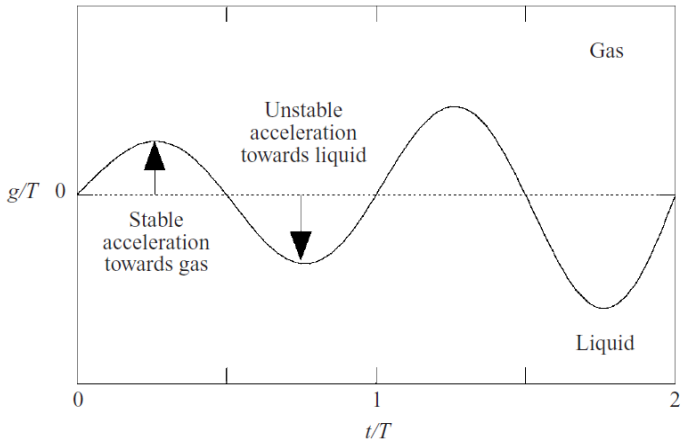

Figure 1.1: Illustration of undulations formed at a liquid-gas interface as a result of the Kelvin-Helmholtz instability (Marmottant and Villermaux 2004)

As depicted in Figure 1.1, the acceleration of the interface is oscillatory, alternatively aimed in the direction of the gas or the liquid. When acceleration is towards the more dense phase, it is unstable in the sense of Rayleigh–Taylor instabilities (Strutt 1883, Taylor 1950). Furthermore, after the fluid extends into ligaments, Kelvin-Helmholtz instability is no longer the dominant reason for droplet breakup; rather, Rayleigh-Taylor instability dominates for ligaments.

Airblast atomizers like the one in this study use a twin-fluid setup to produce a spray – liquid and gas flow outward in the same direction at the exit of the atomizer. The liquid flows at a lower velocity than the gas, with gas flow velocity about 10 times higher than the liquid flow velocity. These differences cause shear forces between the two fluids at their interface. A common setup for a plain-jet airblast atomizer is shown in Figure 1.2 (Chimonas 1986, Varga, Lasheras et al. 2003).

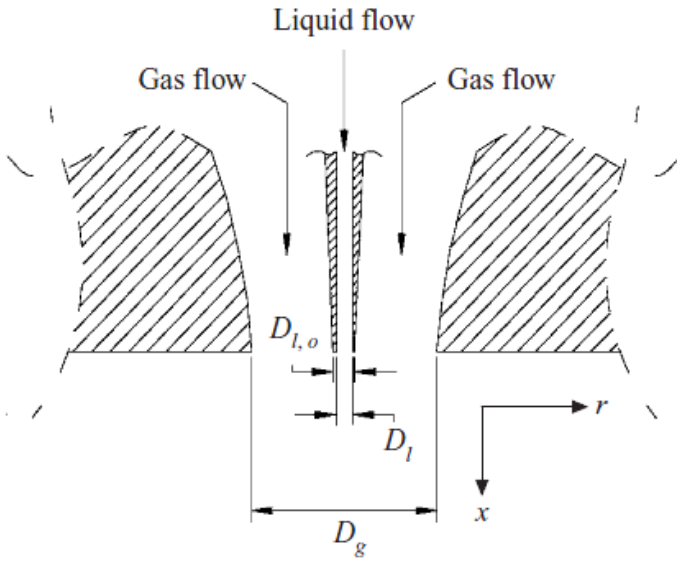

Figure 1.2: Schematic of the setup of a typical air-blast atomizer that takes advantage of Kelvin-Helmholtz instabilities to produce liquid droplets (Varga, Lasheras et al. 2003)

In Figure 1.2, the atomizer has a liquid flow nozzle and an annular air flow nozzle that completely surrounds the liquid nozzle. The fluids exit the atomizer travelling in the same direction, setting up an axi-symmetric flow. As soon as the fluids exit the nozzles they will be affected by Kelvin-Helmholtz type instability. In general, commercial air-blast atomizers are effective because this type of instability produces the liquid droplets needed for painting high-quality finishes.

1.2.1.3 Rayleigh-Taylor Instability

Rayleigh Taylor instability is a fingering-type of instability at the interface between two fluids of different densities and which occurs when the lighter fluid is

pushing a heavier fluid; “fingering” refers to the formation of distinct long, thin ligaments of the heavy fluid. These disturbances grow in size and number with time (Daly 1967).

It is instructive to visualize a Rayleigh-Taylor instability with an example presented by Sharp (Sharp 1984): Imagine the ceiling of a room plastered uniformly with water to a depth of 1 m. The layer of water will fall but it is not the lack of sufficient air pressure that enables the water to fall because atmospheric pressure is equivalent to that of a column of water 10 m thick. Rather, the air atmosphere fails as a supporting medium because it fails to constrain the air-water interface to remain flat. Independent of how carefully the water layer was prepared, small deviations from perfect planarity will be present and those portions of the fluid which lie higher than the average position will experience more pressure than is needed for their support. As a result, these portions will begin to rise, pushing aside water as they do. Simultaneously, neighboring portions of the fluid where the surface is slightly lower than average will require more than the average pressure for its support and begin to fall. In other words, air cannot supply the variations in pressure from location-to-location that is necessary to prevent interface irregularities from growing. Thereby, the initial irregularities increase in magnitude exponentially with time and the water which is moving downward concentrates in spikes with the air which is moving upward through the water consisting of round-topped columns; the water falls to the floor.

In contrast, the same layer of water lying on a denser medium would be stable because irregularities do not grow. Thus, a simple criterion can be inferred for the onset of Rayleigh-Taylor instability at the interface between two fluids of different densities: If a higher density fluid pushes a lower density fluid, the interface between the two fluids

will be stable; if a low density fluid pushes a higher density heavy fluid, the interface is unstable (Sharp 1984).

The early stages in growth of disturbances due to Rayleigh-Taylor instability can be analyzed as a linear form of the dynamic equations of the fluid. Perturbations appear on the surface of the fluid interface. The perturbations have wavelength λ and grow linearly with time (Kull 1991).

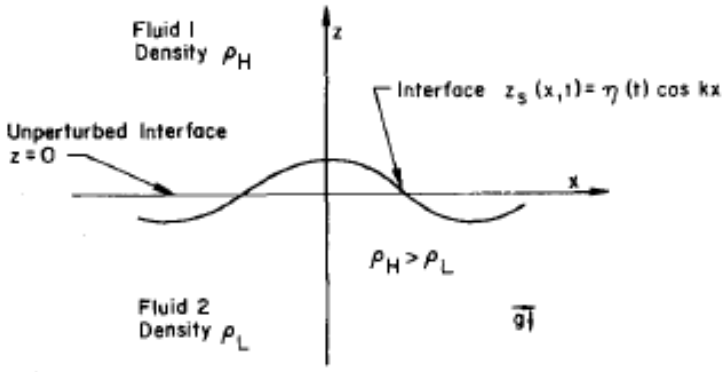

Figure 1.3: Growth of initial perturbations in a two-fluid interface as a result of Rayleigh-Taylor instability (Sharp 1984)

At the point in fluid instability depicted in Figure 1.3 the interface disturbance looks very similar to the interface that is produced at an interface by Kelvin-Helmholtz instabilities (see Figure 1.1). The less dense fluid will begin to push on the wave crest, further increasing the amplitude of the wave. After the disturbances reach a critical size of about 0.3λ, they grow nonlinearly to a size of order 2λ; their development is strongly influenced by the Atwood Number, i.e. the density ratio of the two fluids as defined in Equation 1.1. If A $\sim<$ 1, the less dense fluid moves into the more dense fluid in the form of round-topped ligaments with circular cross sections (Sharp 1984).

$$A = \frac{\left(\rho_{Heavy} - \rho_{Light}\right)}{\left(\rho_{Heavy} + \rho_{Light}\right)} \tag{1.1}$$

After crests in the higher density fluid have grown to a significant size, the fast moving air stream displaces a volume of the heavier fluid with respect to the liquid bulk. This volume is stretched into a long ligament which extends outward. The volume of the liquid ligament will remain constant, but the surface area-to-volume ratio will increase. This stretching continues until other mechanisms will break the heavier fluid into droplets (Marmottant and Villermaux 2004). The stage is characterized by the formation of liquid ligaments, the increase of the surface area-to-volume ratio of those ligaments, and the eventual breakup of the ligaments into discrete droplets which form the spray.

1.2.1.4 Secondary Droplet Breakup

Secondary atomization of droplets takes place after the bulk of the liquid has been broken into droplets because they are exposed to the turbulent flow of the atomizing gas that consists of the continuous phase of the spray. Whether the droplets are stable and will remain cohesive or are unstable and will break up is determined by the relative strength of the disruptive and cohesive forces that are acting on the droplets. The most commonly used metric to determine whether secondary droplet breakup will occur is via Weber number calculations.

The Weber number is a dimensionless physical quantity that measures the ratio of inertia forces-to surface tension (Kuneš and Kuneš 2012). The inertial force is disruptive,

while surface tension is cohesive. Droplet breakup in a two-phase flow has been very accurately predicted by using Weber number evaluations (Joseph, Belanger et al. 1999).

The Weber number is formulated by taking the ratio of the inertial force and the surface tension of the liquid droplet. The inertial force is given by:

$$F_{inertial} = \pi \rho l^3 U^2 \tag{1.2}$$

And the surface tension force is given by:

$$F_{surface\ tension} = \pi l^2 \sigma \tag{1.3}$$

A ratio of Equations 1.2-to-1.3 gives the Weber number, We:

$$We = \frac{F_{inertial}}{F_{surface\ tension}} = \frac{\pi \rho l^3 U^2}{\pi l^2 \sigma} = \frac{\rho l U^2}{\sigma} \tag{1.4}$$

where ρ is the density of the gas, l is the characteristic length of the droplet (usually its diameter), U is the relative velocity between the liquid droplet and the gas, and σ is the surface tension of the liquid droplet (Pilch and Erdman 1987).

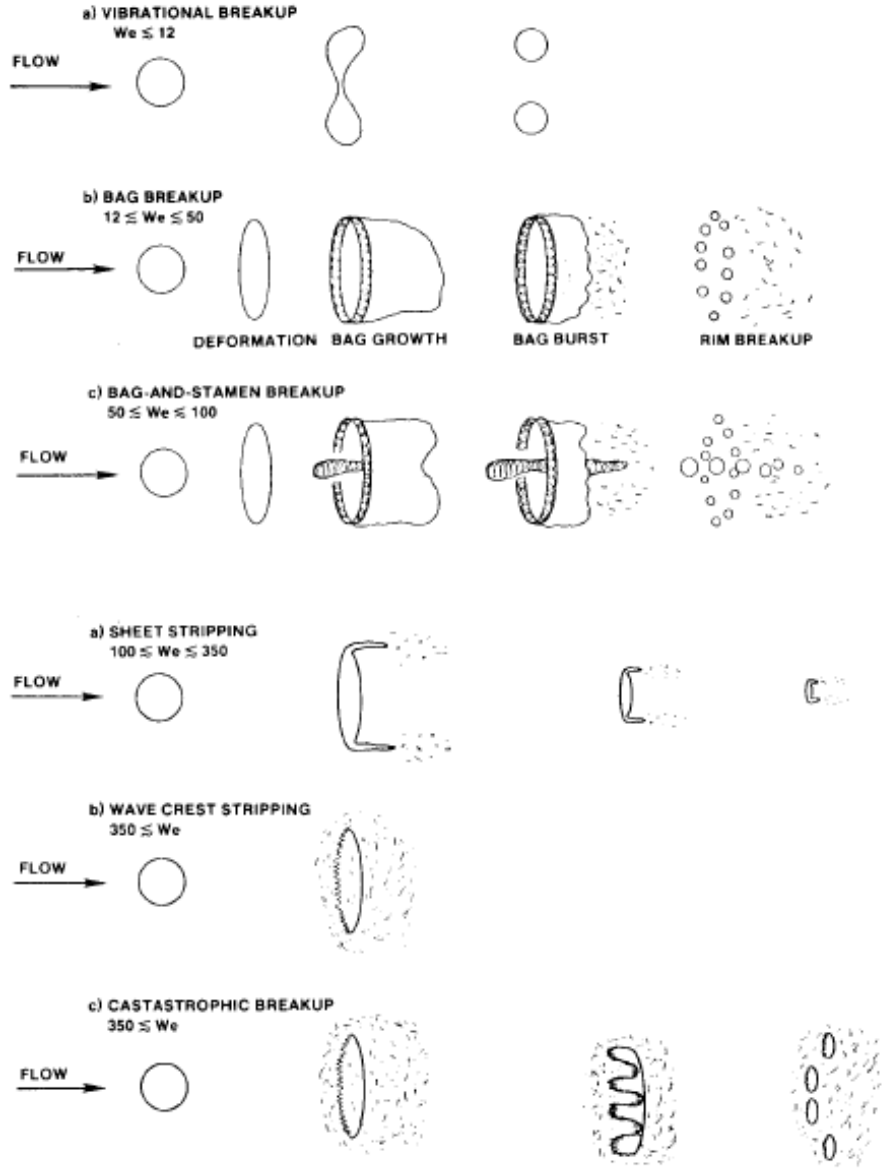

Figure 1.4 : Different secondary atomization regimes for increasing Weber numbers (Juslin, Antikainen et al. 1995)

When the Weber number is small enough (<10) the surface tension of the droplet dominates the inertial force of the gas phase; under these conditions the droplet is stable and will not break up into smaller droplets (Juslin, Antikainen et al. 1995) although vibrational breakup can occur in the same range (We < 10). During vibrational breakup,

natural frequency oscillations of the droplet can develop and, under specific conditions associated with the droplet size and gas flow, the gas phase will interact with the drop in a way that increases the amplitude of the natural oscillations which cause droplet breakup into a few large fragments. However, compared to the other droplet breakup mechanisms, vibrational breakup is very slow and is not considered overly important during liquid spraying (Sher and Sher 2011).

Figure 1.4 depicts droplet breakup during secondary atomization processes. Bag breakup is the first regime in which the inertial forces of the gas dominate surface tension forces for a Weber number range of $10 < We < 50$. The center of the droplet is extended towards the leading edge of the droplet while the more massive rim remains within the original droplet volume. The thin hollow bag breaks into a large number of small droplets, while the rim breaks into a relatively smaller number of more massive drops.

A bag-and-stamen breakup mechanism occurs at when the Weber number is between $50 < We < 100$. This regime behaves similarly to the bag regime, but with the addition of a single, long, relatively massive ligament at the middle of the drop oriented parallel to the gas flow. The thin bag again forms relatively small drops while the rim of the bag and the stamen form a few more massive drops. However, the more massive drops formed in this breakup regime are less massive than the drops in the bag regime.

The shear (also known as "sheet stripping") regime is a more energetic breakup regime than the bag-and-stamen and occurs when the Weber number is between $100 \leq We \leq 350$. The drop flattens into a disc and the edges are accelerated backwards and stripped off of the drop, forming very small satellite droplets. This is the most energetic breakup regime which occurs in the HVLP atomizers.

At extremely high Weber numbers, when We > 350, small wavelength waves form on the windward surface of the droplet. The waves are stripped off of the droplet by the gas passing over the surface of the droplet by a wave-crest stripping of droplets mechanism. Eventually large wavelength waves form on the droplets which result in the drop shattering into a number of satellite drops. This breakup happens very rapidly, with an average time to breakup being on the order of 10 μs (Lasheras, Villermaux et al. 1998, Joseph, Belanger et al. 1999).

1.2.2 Spray Characterization

It is to be realized that atomizers used in practical applications do not produce sprays of uniform droplet size. Instead, the spray is a collection of different-sized droplets. To assess and understand droplet size data in a meaningful way it is important to understand variables that may be associated with the droplet sizes, such as nozzle geometry, liquid flow rate, atomizing gas pressure and flow rate, the liquid properties and the spray angle (Lefebvre 1989). There should also be a method for describing the droplet size distribution. The measurement technique and the type of droplet distribution model size that are used have a strong effect on the results (Schick 2008).

1.2.2.1 Droplet Size Distribution

Ideally, a spray atomizer would produce droplets of exactly the same size. Unfortunately, mono-sized droplets are not produced by spray atomizers. Atomizers generate droplets with a size range covering from a few μm up to around 500 μm. Since the atomization process is not uniform, the threads and ligaments that form in liquid jets

also vary in size (Lefebvre 1989) with both the primary droplets and secondary satellite droplets having, typically, a broad size distribution. Detailed characterization of the range of droplet sizes in a spray is critical for analyzing a design of an atomizer and its operational parameters, and for validating modeling predictions. These modeling predictions will depend on spray characteristics related to droplet sizes, droplet velocities, spray patterns, spray coverage and spray angles. Also of interest are droplet break-up and coalescence. Most basically, multiphase flows are characterized by an average spray length scale, the most commonly used ones of which are D_{10} and D_{32}(Lefebvre 1989, Liu 2000).

The linear average diameter (D_{10}) is defined as the diameter of a uniform droplet set with the same number and sum of diameters as the real set, providing a simple 'average' measure with which to compare different sprays. However, most processes which utilize multiphase flows involve heat and/or mass transfer. The representative length scale used in these situations is the Sauter Mean Diameter, expressed as SMD or D_{32}, which is the diameter of a uniform droplet set with the same total volume-to-total surface area ratio as the real droplet set.

Spray characterization techniques normally record data that are in the form of number count per class size. The data are arranged into a mathematical representation referred to as a droplet size distribution and t it is most often dependent on the characterization techniques used. Some of the most common droplet size distribution functions used in industry include normal, log-normal, root normal, Nukiyama-Tanasawa, Rosin-Rammler, and upper-limit distribution function (Lefebvre 1989, Liu 2000). It should be noted that no single distribution function can characterize all

experimental measurement data of droplets sizes, and none of these functions is universally superior to any other for representing droplet size distribution (Liu 2000).

Many droplet size distributions in random droplet generation processes follow Gaussian, or a normal distribution pattern. In a normal distribution, a number distribution function, *f (D)*, may be used to determine the number of droplets of diameter *D*:

$$f(D) = \frac{dN}{dD} = \frac{1}{\sqrt{2\pi}s_n} \exp\left[-\frac{1}{2s_n^2}(D - \bar{D})^2\right] \tag{1.5}$$

where S_n is the standard deviation, and S_n^2 is the variance (Lefebvre 1989). A plot of the distribution function is the standard normal curve with the area under the standard normal curve from -∞ to +∞ equal to 1. The integral of the standard normal distribution function is the cumulative standard number distribution function *F(D)*:

$$F(D) = \frac{1}{\sqrt{2\pi}} \int_{-\infty}^{D} \exp\left[-\frac{1}{2}\left(\frac{D - D^2}{s_n}\right)^2\right] d\left(\frac{D - D^2}{s_n}\right) \tag{1.6}$$

Plotting the droplet size data on an arithmetic-probability graph will generate a straight line if the data follow normal distribution. Thus, the mean droplet diameter and standard deviation can be determined (Liu 2000).

Many droplet size distributions in natural droplet formulation and liquid metal atomization processes conform to a log-normal distribution:

$$f(D) = \frac{dN}{dD} = \frac{1}{\sqrt{2\pi}DS_g} \exp\left[-\frac{1}{2S_g^2}\left(\ln D - \ln \bar{D}_{ng}\right)^2\right] \tag{1.7}$$

where $\bar{D}_{ng}$ is the number geometric mean droplet diameter and S_g is the geometric standard deviation. Plotting droplet size data on a log-probability graph will generate a straight line if the data follow log-normal distribution (Liu 2000).

Log-normal distribution functions based on surface and volume respectively are (Liu 2000):

$$f(D^2) = \frac{dN}{dD} = \frac{1}{\sqrt{2\pi}DS_g}\exp\left[-\frac{1}{2S_g^2}\left(\ln D - \ln\overline{D}_{sg}\right)^2\right] \quad (1.8)$$

And

$$f(D^3) = \frac{dN}{dD} = \frac{1}{\sqrt{2\pi}DS_g}\exp\left[-\frac{1}{2S_g^2}\left(\ln D - \ln\overline{D}_{vg}\right)^2\right] \quad (1.9)$$

where $\overline{D}_{sg}$and $\overline{D}_{vg}$ are the geometric surface and volume means droplet diameters, respectively. These diameters can be determined once the number of the geometric mean droplets' diameters and the geometric standard deviation are known:

$$\ln\overline{D}_{sg} = \ln\overline{D}_{ng} + 2S_g^2 \quad (1.10)$$

$$\ln\overline{D}_{vg} = \ln\overline{D}_{ng} + 3S_g^2 \quad (1.11)$$

$$\ln \mathrm{SMD} = \ln\overline{D}_{ng} + 2.5S_g^2 \quad (1.12)$$

In other atomization processes, the droplet size distribution follows a root-normal distribution pattern (Liu 2000):

$$f(D) = \frac{dN}{dD} = \frac{1}{\sqrt{2\pi}DS_s}\exp\left[-\frac{1}{2S_s^2}\left((D/MMD)^{1/2} - 1\right)^2\right] \quad (1.13)$$

Where S_s is the standard deviation and MMD is the mass mean diameter.

Perhaps the most widely-used distribution function is now that of Rosin-Rammler, given by the following relation:

$$Q = 1 - exp\left[-\frac{D}{X}\right]^q \quad (1.14)$$

where Q is the fraction of total volume of droplets smaller than D, and X and q are constants. The exponent q is a measure of the spread of droplet sizes; a larger value of q corresponds to a more uniform droplet size.

In many applications, mean droplet size is the most important factor because it can be interpreted as a measure of atomization quality. It is also convenient to use only mean droplet size in calculations involving discrete droplets, such as for multiphase flow and mass transfer processes (Lefebvre 1989). Various definitions of mean droplet size have been employed in different applications, as summarized in Table 1.1 and adopted from (Liu 2000).

Table 1.1: Mean Droplet Diameters and their applications (Liu 2000)

Symbol	Common Name	a	b	Definition	Application
D_{10}	Arithmetic Mean (Length)	1	0	$\frac{\sum N_i D_i}{\sum N_i}$	Comparison
D_{20}	Surface Mean (Surface Area)	2	0	$\left[\frac{\sum N_i D_i^2}{\sum N_i}\right]^{1/2}$	Surface Area Controlling
D_{30}	Volume Mean (Volume)	3	0	$\left[\frac{\sum N_i D_i^3}{\sum N_i}\right]^{1/3}$	Volume Controlling (Hydrology)
D_{21}	Length Mean (Surface Area- Length)	2	1	$\frac{\sum N_i D_i^3}{\sum N_i D_i}$	Absorption
D_{31}	Length Mean (Volume-Length)	3	1	$\left[\frac{\sum N_i D_i^3}{\sum N_i}\right]^{1/2}$	Evaporation, Molecular Diffusion
D_{32}	Sauter Mean (SMD) (Volume-Surface)	3	2	$\frac{\sum N_i D_i^3}{\sum N_i D_i^2}$	Mass Transfer Reaction
D_{43}	Herdan Mean (De Brouckere or Herdan) (Weight)	4	3	$\frac{\sum N_i D_i^4}{\sum N_i D_i^3}$	Combustion, Equilibrium

The expressions for the mean droplet diameters as shown in Table 1.1 takes the form of a generalized equation as follows:

$$D_{ab} = \left[\frac{\int_{D_{min}}^{D_{max}} D^a \left(dN/dD\right) dD}{\int_{D_{min}}^{D_{max}} D^b \left(dN/dD\right) dD}\right]^{1/(a-b)} \quad (1.15)$$

Or

$$D_{ab} = \left[\frac{\sum N_i D_i^a}{\sum N_i D_i^b}\right]^{1/(a-b)} \quad (1.16)$$

where D_{min} and D_{max} are the minimum and maximum droplet diameters respectively, and a and b have any value according to the effects considered in Table 1.1. SMD is perhaps the most widely used; it is the diameter whose ratio of volume-to-surface area is the same as that of the entire droplet sample.

In characterizing the droplet size distributions, at least two parameters are typically necessary: a representative droplet diameter, (e.g. mean droplet size) and a measure of droplet size range (e.g. standard deviation or q). Many representative droplet diameters have been used in specifying distribution functions, definitions for which and the relevant relationships are summarized in Table 1.2. The relationships are derived on the basis of the Rosin-Rammler distribution function in Equation (1.14).

Many authors (Li and Tankin 1987, Semiao, Andrade et al. 1996, Dumouchel and Boyaval 1999, Ayres, Caldas et al. 2001, Cao 2002) have used maximum entropy formalism to derive a probability density function for predicting droplet size distributions. Liu (Liu 2000) provided a detailed summary of empirical and analytical correlations for droplet size distribution, see Table 1.2.

Table 1.2: Definition of Representative Droplet Diameters (Liu 2000)

Symbol	Definition	Position in Q-D Plot	Relationship
$D_{0.1}$	10% of total volume of droplets are of smaller diameter than this value	Q = 10%	$\frac{D_{0.1}}{X} = (0.1051)^{1/q}$ $\frac{D_{0.1}}{MMD} = (0.152)^{1/q}$
$D_{0.5}$	Mass Mean Diameter (MMD) 50% of total volume of droplets are of smaller diameter than this value	Q = 50% Left hand or right hand side of Dpeak for q > or < 3.2585	$\frac{MMD}{X} = (0.693)^{1/q}$ $\frac{MMD}{SMD} = (0.963)^{1/q}\Gamma\left(1 - \frac{1}{q}\right)$
$D_{0.632}$	Characteristic diameter 63.2% of total volume droplets are of smaller diameter than this value	Q = 63.2%	X (X in the Rosin-Rammler Distribution Function)
$D_{0.9}$	90% of total volume of droplets are of smaller diameter than this value	Q = 90%	$\frac{D_{0.9}}{X} = (2.3025)^{1/q}$ $\frac{D_{0.9}}{MMD} = (3.32)^{1/q}$
$D_{0.999}$	Maximum Diameter 99.9% of total volume of droplets are of smaller diameter than this value	Q = 99.9%	$\frac{D_{0.999}}{MMD} = (9.968)^{1/q}$
D_{peak}	Peak diameter value of D corresponding to peak of droplet size frequency distribution curve.	Peak point corresponding to $d^2Q/dD^2 = 0$	$\frac{D_{peak}}{X} = \left(1 - \frac{1}{q}\right)^{1/q}$ $\frac{D_{peak}}{MMD} = \left(1.428 - \frac{1.4428}{q}\right)^{1/q}$ $\frac{D_{peak}}{SMD} = \left(1 - \frac{1}{q}\right)^{1/q}\Gamma\left(1 - \frac{1}{q}\right)$

1.2.2.2 Droplet Measurement Techniques

A wide range of techniques are used for measuring droplet sizes of sprays. In general, although they were developed at different times and for different applications,

the goal within each techniques is to determine the droplet size in a spray without altering its properties (Liu 2000). Ideally the use of a technique will not disturb the motion of the spray. Additionally, the measurement technique should have an ability to measure a large range of different particle sizes and physical properties. Many of the techniques that have been developed for solid particle measurement are very effective, but often require physical collection of the spray. This is not ideal for liquid droplets, since they do not retain their size and shape like solid particles. Different industries have developed their own measurement equipment, but almost all of it falls into one of the following five categories (Allen 1990):

1. Inertial techniques, impingement, impaction and sedimentation
2. Filtration
3. Electrostatic precipitation
4. Thermal precipitation
5. Optical measurement

For solid particles at high concentrations, it is sufficient to use simple inertial classification techniques which operate on the principle that particles with a high inertia will move more rapidly across flow streams than will particles with low inertia. This differentiation allows for the classification of particles by aerodynamic size, and usually provides for the physical collection of the particles. The differences in various inertial techniques are usually related to providing high inertial conditions for the particles and conditioning the direction of flow in relation to the collection surface.

The simplest technique is horizontal sedimentation in which the flow passes horizontally over or at the top of a collection surface with the force of gravity causing

particles to settle into the collection chamber. Larger particles will settle closer to the inlet and smaller particles will settle further away.

Another technique is the cascade impactor in which a series of jets, with each operated at higher-and-higher speeds, are used to impinge droplets onto collection plates. The larger particles are removed from the flow at speeds lower than are the smaller particles. Aerosol centrifuges, vertical elutriators, cyclones and sedimentation chambers are also employed; each of these techniques has advantages and limitations (Gieseke 1980).

Filtration uses a porous medium to capture the droplets in a flow. It uses many of the collection mechanisms on which other techniques are based, including diffusion, interception, charge and sedimentation. For example, large droplets will follow a path deviating from streamlines as they approach a fiber and then impinge onto the fiber surface. In general, droplets only need to touch the fiber to be captured in the filter.

The advantage of filters (especially fiber filters) is their ability to allow for large volumes of gas to pass through the filter while maintaining a relatively low operational pressure loss. This capacity makes them ideal for use in industrial settings where flow rates can be extremely high. Filters are very useful for solid particles and liquid droplets for the purpose of separation from the gas stream. The disadvantage of filters is that liquid droplets will agglomerate in the filter and cannot be used for measurements (Hickey 2004).

Electrostatic precipitation techniques are used to collect solid particles for subsequent examination via microscopy. The method precipitates particles out of an aerosol according to the charge that they carry when they are passed between two plates or

surfaces across which a large potential difference is established. Deposition is related to the ratio of particle charge-to-its inertia with particles having the highest charge-to-inertia ratio depositing before particles having lower ratios(Parker 1997).

Electrostatic precipitators (ESP's) are extremely useful for even very small particle diameters because their charge-to-inertia ratio is also high. Because they can also be scaled very effectively, ESP's are widely used in power generation settings where ultra-small fly ash particulate has to be removed from stack gases even when a coal boiler combusts upwards of 2000 tons of coal per day. This attribute makes it not only an efficient measurement technique, but also a cleaning technique as well (Lowe 1953). The disadvantage of this method is when the particles in question do not have a high charge-to-inertia ratio, in which case the particles will pass through the ESP collector (Hickey 2004).

Thermal precipitation sampling is another technique for measuring droplet sizes. It depends on the observed phenomenon that aerosol particles, placed within a thermal gradient as established between two surfaces at different temperatures, tend to move in the direction of the lower temperature. The force producing this motion originates from the physical interaction of the molecules of the suspending gas with the particles (Allen 1990). Because fluids tend to reach thermal equilibrium, the gas molecules will tend to move away from the heated surface and have a greater component of velocity in the direction of the temperature increase. The result is that there will be a net force on the particle toward the colder direction. This force is generated by the impingement of the non-isothermal gas particles on the solid particles. In other words, the hot particles traveling toward the cold region will tend to push the particle in that direction And the

force developed is effective even if the particle itself has a constant temperature throughout (Keng and Orr 1966).

Hence, thermal precipitation is useful because it is operational independent of whether or not the particles undergo heating and independent of the thermal conductivity of the particles. However, the thermal force works well only for very small particles, such as microorganisms, and is not useful for particles larger than 5μm in diameter. Because of this limitation, it is mostly used in the biotechnology field (Orr, Gordon et al. 1956).

The previously discussed techniques effectively separate solid particles from an aerosol flow but are generally unable to handle the separation and measurement of liquid droplets. In contrast to solid particulate, the best way to measure the droplets in an aerosol spray is with optical methods, the most accurate of which is Phase Doppler Anemometry (PDA) (Durst 1975). PDA is a laser-Doppler velocimeter method for non-intrusive measurements of droplet diameters and velocities of spherical particles. Its measurement relies on a time delay that occurs when light scattered by intersecting lasers arrives at two separate photo detectors. It is very sensitive and is able to detect droplets even in the micrometer range.

However, the accuracy of the PDA measurements depends on the crossing angle of the laser beams, the direction of observation of the probe volume, the refractive indices of the media, and the droplet size. It also requires a skilled operator to ensure that the apparatus is providing the proper results. PDA is not capable of providing highly accurate results for non-spherical droplets/particles (Durst 1975, Qiu and Sommerfeld 1992, Sommerfeld and Qiu 1995). Because paint droplets are highly non-spherical near

to a nozzle of a paint sprayer, the application of PDA methods in this region would not be useful. However, paint droplets are highly spherical after secondary breakup, and PDA becomes useful.

The Malvern Particle Analyzer used during this research is a widely used particle analyzer based on Fraunhofer diffraction effects. In it, the diffraction pattern is formed by interaction between a parallel beam of monochromatic light and moving droplets (Malvern Instruments). For a mono-disperse sprays, the diffraction pattern comprises a series of alternate light and dark concentric rings whose spacing is related to the droplet size. For a poly-disperse sprays, the diffraction pattern comprises a number of patterns with series of overlapping diffraction rings, each of which is produced by a different group of droplets sizes (Hirleman 1988, Weber and Hirleman 1988, Muhlenweg and Hirleman 1998). A receiver lens focuses the diffraction patterns onto a photodetector that measures light energy distributions, with the detector consisting of 31 photosensitive rings surrounding a central circle; each ring is most sensitive to a particular small range of droplet sizes. The measured light energy distribution is then converted to a droplet size distribution with the measured data analyzed in terms of a histogram with 15 size classes or presented in a format of normal, log-normal, or Rosin-Rammler modes. Modern particle sizers have the ability to detect particles down to 0.1μm and are useful over a wide range of particle size between 0.1 to 2000μm (Malvern Instruments , Hirleman 1988).

1.2.3 Infrared Thermography

We know that any object that is above absolute 0 K (-273.16 °C) will emit radiation in in the Infrared (IR) band of the electromagnetic spectrum. For IR detectors, the IR spectral band is further subdivided into four smaller bands, including: the near IR (0.75-3 μm); the middle IR(3-6 μm); the far IRIR (6-15 μm); and the extreme IR (15-1000 μm). At the short-wavelength end the IR spectrum is the boundary between IR and deep-red visible light. At the long-wavelength end, IR wavelengths merge with microwave radio waves in the millimeter range. Figure 1.5**: Electromagnetic Spectrum** illustrates the different spectral bands of electromagnetic radiation.

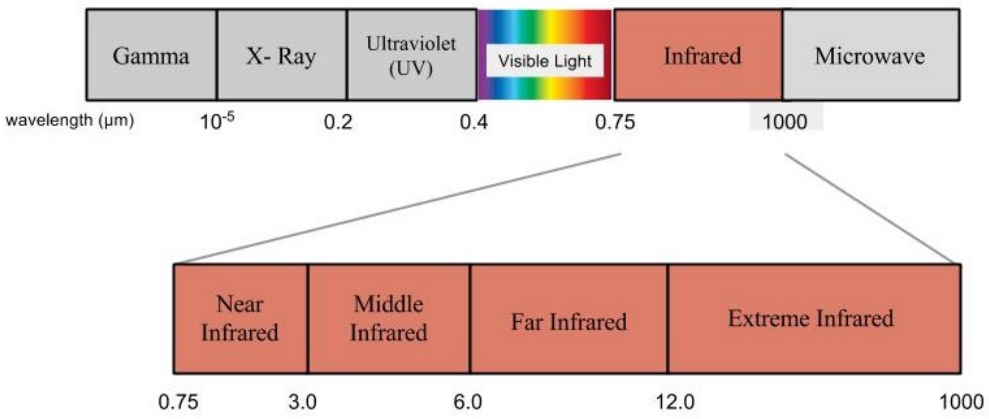

Figure 1.5: Electromagnetic Spectrum

IR thermography is a non-contact, non-intrusive technique, and allows for the visualization of thermal energy emitted by a body as a consequence its non-zero Kelvin

surface temperature. IR thermography should be considered a two-dimensional technique of temperature measurement.

1.2.3.1 Principles of Infrared Thermography

IR thermography data acquisition depends on the use of special camera optics and a IR detector which absorbs the IR radiation emitted by a body and converts it into an electrical signal. Max Planck (Planck 1901) showed that for a blackbody the spectral distributions of hemispherical emissive power and radiant intensity are expressed as a function of the wavelength and the absolute blackbody temperature. The equation is given as:

$$E_{\lambda b} = \frac{C_1}{\lambda^5 (e^{C_2/\lambda T} - 1)} \tag{1.17}$$

In the above equation, $E_{\lambda b}$ is the blackbody monochromatic radiation intensity; C_1 and C_2 are the first and second radiation constants respectively; λ is the wavelength of the radiation being considered, and T is the absolute temperature of the blackbody. By differentiating Planck's Law with respect to λ and taking the maximum radiation intensity, Wien's Displacement Law is obtained:

$$\lambda_{max} = \frac{2898}{T} \tag{1.18}$$

This mathematically expression shows that depicted colors will vary from red-to-orange-to–yellow-to-green-to-blue as the temperature (in Kelvin) of a thermal radiator increases. By integrating Planck's Law over the entire spectrum, the total hemispherical radiation is found:

$$E_b = \sigma T^4 \tag{1.19}$$

where σ is the Stefan-Boltzman constant.

Equation (1.19) describes the maximum radiation emitted from a blackbody at a given temperature. Although most items we want to measure are not perfect blackbodies, they closely approximate a black body within certain spectral intervals. The energy emitted by a real object, E_λ, generally represents only a portion of the radiation emitted by a blackbody. By introducing the quantity,

$$\varepsilon_\lambda = \frac{E_\lambda}{E_{\lambda b}} \tag{1.20}$$

which is called the spectral emissivity coefficient, Equation (1.19) can be rewritten for real objects by multiplying it by ε_λ.

IR measurements are generally performed using two different spectral windows: short wave (SW) - between 3-6 μm - and long wave (LW) - between 8-12 μm.

The performance of an IR system is evaluated in terms of thermal sensitivity, scan speed, image resolution, and intensity resolution. The sensitivity is generally expressed as the Noise-Equivalent Temperature Difference (NETD), which represents the difference in temperature at two points in the image which corresponds to a signal that is equal to the background noise of the camera (Aydin, Mantiuk et al. 2008). Some new systems are able to detect temperature differences of 20 mK at ambient temperature. The scan speed is the rate at which an entire image is updated; for older systems the scan speed is expressed as scan rate per line or scan rate per field. Newer systems are characterized by acquisition speeds higher than 1600 Hz.

The image resolution is defined as the Instantaneous Field of View (IFOV) of the detector (Poropat 1993). Modern systems are able to produce images composed of tens of thousands of pixels, which are smaller than the resolution elements of the detectors. The intensity resolution (dynamic range) is the number of grey shades which compose the thermal image. The most recent generation of cameras provides 14-bit recording and allows for very small temperature variations to be measured in a hot ambient environment (FLIR Systems 2015).

1.2.3.2 Applications of Infrared Thermography to Thermal Fluid Dynamics

IR thermography has found uses in many industries, including medicine, agriculture, manufacturing, environmental technology, non-destructive testing, turbomachinery and building inspection (Schulz 2000, Clark, McCann et al. 2003, Avdelidis and Moropoulou 2004, Meola, Carlomagno et al. 2004, Lahiri, Bagavathiappan et al. 2012). New technology is able to create thermal images with high thermal and spatial resolutions and allows for the use of IR thermography for applications that require a high degree of sensitivity, such as in a spray with numerous, distinct, and fast-moving droplets. The goal in this situation is not to acquire the absolute temperature of the spray, but rather to obtain a relative temporal and spatial distribution of the thermal radiation intensity. Originally, IR thermography was used in space missions to examine the integrity of space vehicles. In the past few decades IR thermography has become one of the most versatile, non-intrusive measurement techniques used in research and industrial applications.

A look at the literature shows great potential for using IR thermography to visualize thermo-fluids. Gartenberg (Gartenberg, Rodriguez et al. 1989) was able to measure the temperature difference between flows before and after the transition to turbulence, and to define heat transfer coefficients along an airfoil. IR thermography has been used to map the film cooling holes on a gas turbine engine using the same techniques (Schulz 2000). Jet impingement cooling was also studied (Meola, Carlomagno et al. 2004) and both the wall adiabatic temperature as well as the wall temperature were measured successfully using IR thermography. Later, the technique was used to measure the transient free convection from a vertical surface with mounted obstacles; it was observed that the thermal plumes observed with the IR camera matched with the flow wakes of the obstacles (Polidori 2003). In another study, the heat transfer from a rotating disk with a small impinging jet was measured (Astarita and Cardone 2008) using IR visualization techniques.

The use of IR thermography for visualizing two-phase flow was first developed by Akafuah and Salazar (Akafuah, Salazar et al. 2009, Akafuah, Salazar et al. 2010). In it, IR thermography was used to examine the density of a paint spray when contrasted against a blackbody background and was successful in determining the density of the spray at a given point in the flow and in describing the macro-scale characteristics of the spray. This technique has also been verified as useful with rotary atomizer sprays. In this thesis, this technique will be utilized for characterizing sprays from a twin-fluid airblast atomizer which, although produces droplets in a different way than does a rotary atomizer, but establishes droplets having a spray pattern that is similar enough to a rotary

atomizer that the technique can be used for the current study without major modifications.

CHAPTER TWO

2.0 EXPERIMENTAL APPARATUS

A discussion of the experimental apparatus is presented in four sections. In Section 2.1, the apparatus for the IR visualization and characterization used in this thesis are presented; Section 2.2 presents the apparatus for the visual imaging; Section 2.3 presents the apparatus for droplet size analysis; and, lastly, Section 2.4 describes the apparatus for the atomizer setup that was used in all of the experiments.

2.1 APPARATUS FOR IR VISUALIZATION AND CHARACTERIZATION

The basic experimental apparatus for the IR visualization and characterization comprised of an IR camera, a background radiation source, and a high-speed data recorder. Brief descriptions of each of these are provided below.

2.1.1 Infrared Camera

The imaging device used to capture the spray envelope was an IR camera, FLIR ThermoVision^{TM} SC4000. The SC4000 uses an Indium Antimonide (InSb) type detector, has a 3-5 μm spectral range and a 320 x 256 pixel deterctor. The SC4000 Focal Plane Array (FPA) system uses a Complementary-Metal-Oxide-Semiconductor (CMOS) readout integrated circuit (ROIC). FPA systems include a matrix of detectors to resolve the field of view (FOV). These detectors require cooling well below the ambient

temperature of the laboratory to allow for high sensitivity and low noise. The cooling is performed by an integrated Sterling closed cycle cooler which is capable of cooling the detectors to 70 K (FLIR Systems 2015).

The SC4000 has a 14-bit dynamic range, defined as the ratio between the largest and smallest possible values of a changeable quantity (in this case, IR radiation intensity). The Camera has a noise equivalent temperature difference (NETD) or noise equivalent irradiance of 18 mK (Myszkowsi 2008).

Figure 2.1: FLIR ThermoVision^{TM} SC4000 (FLIR Systems 2015)

NETD is usually used to characterize the sensitivity of FPAs. NETD is the temperature change of a scene required to produce a signal equal to the root mean square (rms) noise. It is a system level parameter that depends on parameters such as the f number of the optics used. For low background applications, noise equivalent power (NEP), or noise equivalent irradiance (NEI) is usually used as a figure of merit. It is the radiant flux power necessary to produce a signal equal to the rms noise (Tidrow 2000).

2.1.2 Background Radiation Source

The IR camera works by mapping surface temperatures. Since the liquid in a spray is at or close to the ambient temperature of the laboratory, it is necessary to provide a temperature contrast imaging with the IR camera. To achieve this, a uniformly heated background was placed behind the spray that provided the needed temperature contrast for visualizing the spray field. In addition, the uniform set temperature of this background also provides a reference point for the temperature of the spray field.

The background radiation source used was an IR-160/301 Blackbody System from IR Systems Development. The IR-160/301 Blackbody System is an extended area type flat plate emitter with special high emissivity coating having 0.96 (±0.02) average emissivity. Its surface dimensions were 304 mm by 304 mm. The system has a temperature controller accurate to within 0.1°C, a temperature range from ambient to 350°C, and a wavelength range between 1 to 99 μm. Temperature sensing was also accomplished by means a Pt Resistance Temperature Detector (RTD) and a Type T thermocouple (Infrared Systems 2014).

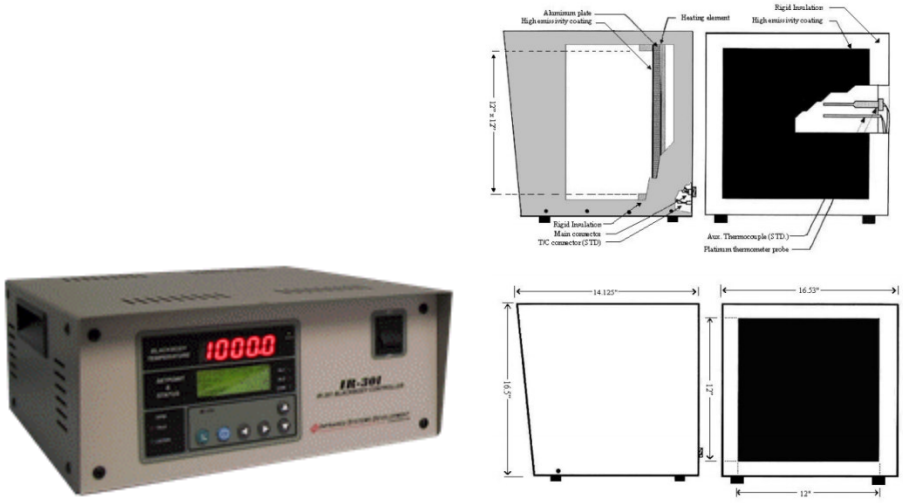

Figure 2.2: IR-160/301 Blackbody System (Infrared Systems)

2.1.3 High Speed Data Recorder

The higher frame rate settings for the IR camera generate large amounts of data and prevented use of a standard data transfer cable for the IR camera because the captured images could not be exported in real time. Hence, a DVR Express Core Camera Link Base, high-speed data recorder (HSDR) from IO Industries was used during the filming at the highest frame rates without dropping any of the recorded frames. Dropped frames are typical when too high of a data rate is used, which causes the computer controlling the IR camera to accept but not to export all frames, thereby effectively lowering the frame rate. The HSDR allows a maximum input clock frequency of 85 MHz and supports both 16bit as well as RGB inputs. The images and video were stored on the HSDR until they could be exported and analyzed at a later time (Ion Industries 1991).

Figure 2.3: DVR Express Core Camera Link Base (Ion Industries 1991)

2.2 APPARATUS FOR VISUAL IMAGING

The basic experimental apparatus for the visual imaging comprised of a visual camera, a camera lens, and work lights. Brief descriptions of each of these are provided below.

2.2.1 Visual Camera

The imaging device used to capture the spray envelope in the visual spectrum was a digital camera, Canon EOS 5D mark iii. The 5D mark iii has a 21.1 megapixel full-frame complementary metal-oxide semiconductor (CMOS) sensor, with a 3:2 aspect ratio (width: height). This configuration is equivalent to full frame 35 mm film. The ISO ranged from 100-64,000 and could be changed either manually or automatically. The shutter is a vertical mechanical shutter and its speed can be adjusted from 1/8,000 to 30 seconds either automatically or manually. The camera was able to take up to 3.9 frames

per second, and could record images in both RAW and jpeg formats for later processing (Canon USA 2015).

Figure 2.4: Canon EOS 5D mark iii (Canon USA 2015)

2.2.2 Camera Lens

The lens used on the 5D mark iii camera was a Canon EF 28-135 mm; it is based on the EF lens mount that is compatible with all models of Canon single lens reflex (SLR) cameras. The lens array was made of 16 different elements, arranged into 12 groups; the lens body had integrated image stabilization and a ring-type ultrasonic motor (USM) to allow for automatic focusing of the image; the lens had a focal length range of 28 to 135 mm, and an aperture range of 1:3.5-5.6; and, the minimum focus distance for the lens was 50 cm (Canon USA 2015).

Figure 2.5: Canon EF 28-135 mm lens (Canon USA 2015)

2.2.3 Work Lights

The liquid droplets in the spray were not strong emitters of IR radiation, and were difficult to image with the camera alone. To help illuminate the spray, six Utilitech work lights were used. Each of the lights had a RX7 type Halogen bulb rated at 500 Watts; hence, each of these lights emitted 8000 lumens. The lights were integrated onto an adjustable stand that was be positioned as needed (Lowes 2015).

Figure 2.6: Utilitech work light (Lowes 2015)

2.3 APPARATUS FOR DROPLET SIZE ANALYSIS

The experimental apparatus for droplet size analysis was a laser diffraction droplet size analyzer. A brief description it is provided below.

2.3.1 Laser Diffraction Droplet Analyzer

To analyze and model the behavior of the spray, the droplet size distribution needed to be measured. A Malvern Spraytec particle size analyzer was used.

The Malvern Spraytec has a 4 mW Helium-Neon (He-Ne) laser that emits light at a wavelength of 632.8 nm. Light is emitted from the emitter tower and was scattered as it passed through the spray, the measurement zone which was 9mm. The receiver module has a 300 mm lens that focuses the light onto a series of detectors and allowed for a droplet size detection range between 0.1 to 900 μm. The control and analysis software

then uses the full Mie Theory to completely solve the equations for the interactions between the light and droplets. Operation of the system required the user to input the refractive index of the spray material. Although the refractive index of water is well known, the refractive index of water-borne metallic base coat and solvent-borne clear coat could only be estimated (Malvern Instruments).

Figure 2.7: Malvern Spraytec particle size analyzer (Malvern Instruments)

2.4 APPARATUS FOR THE ATOMIZER

The atomizer and the equipment that supplied air and liquid were kept constant during all of the experiments. The basic experimental apparatus for the atomizer comprised of an atomizer gun, a material feed container, an ionizer, a gas pressure vessel, a spray booth, and air filters. Brief descriptions of each of these are provided below.

2.4.1 Atomizer Gun

The spray gun used to atomize different liquids during the study was a Krautzberger HS25 HV3 spray gun, which is shown in Figure 2.8. It is a twin fluid atomizer which uses the kinetic energy of a fast flowing air stream to break the liquid stream into droplets. The liquid opening is located at the center of a nozzle, and an annular air hole is located concentrically around it. The liquid and the atomizing gas were dispensed separately and then mixed in the spray of the gun. The liquid material can be supplied at pressures up to 0.4 MPa and temperatures up 50°C. The atomizing gas used to break the liquid into droplets could also be supplied at pressures up to 0.4 MPa.

The spray gun also incorporated pattern air holes, which are used to shape the spray for better application to a substrate. The amount of air passing through the pattern air holes was controlled by an adjustable knob on the back of the gun, and enabled the shape of the spray to be tailored to better suit the part that was being coated. The parts of the spray gun that come into contact with the liquid coating materials were made of aluminum (housing), stainless steel (material needle and nozzle) and brass and plastic (gaskets) (Krautzberger GmbH 2013).

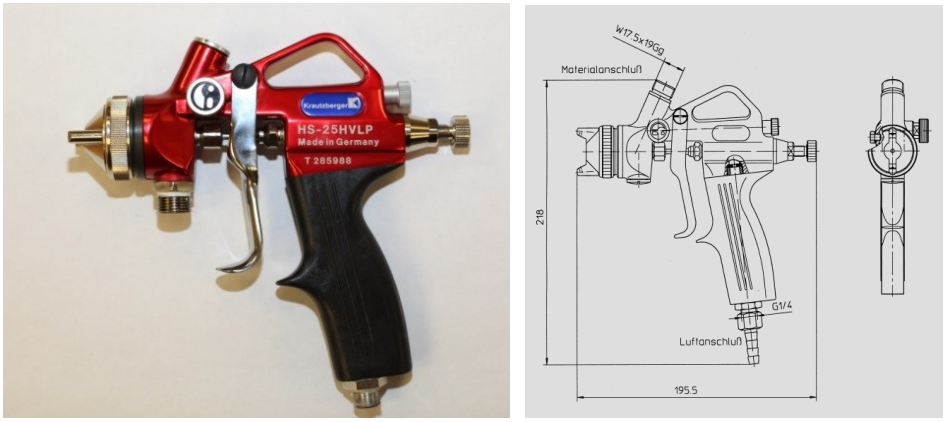

Figure 2.8: Krautzberger HS25 HV3 spray gun (Krautzberger GmbH 2013)

2.4.2 Sprayer Nozzles

There are several different nozzles that can be used on the atomizer gun. Each of the different nozzles provides a different spray pattern as well as different droplet sizes. Krautzberger manufactures spray nozzles for a wide variety of purposes.

Figure 2.9 shows the four different nozzles that were used for the experiments in this thesis. The nozzles are named HV3, E, F2 and F4. All of the nozzles have the same liquid opening of 1.2 mm, as well as pattern air holes which shape the spray from an axi-symmetric pattern to a flat fan shape. For all of the experiments, measurements were taken across the narrow dimension of the fan.

The main differences between the nozzles are in the shape, size, and orientation of the air openings. The HV3 nozzle has the largest total area for air openings, giving it the lowest relative atomizing gas velocity as well as the highest droplet size. The F2 nozzle has the smallest total area for atomizing gas to exit the nozzle. This gives it a higher gas velocity and a smaller droplet size. The F4 nozzle is identical to the F2 nozzle except that some of the air openings around the center are angled into the center of the flow instead of pointing directly outward. The E nozzle has a larger area for the air to exit than the F2 and F4 nozzles, but a smaller area than the HV3 nozzle. Each of these nozzles can be used for different situations when a specific droplet size and spray pattern is desired.

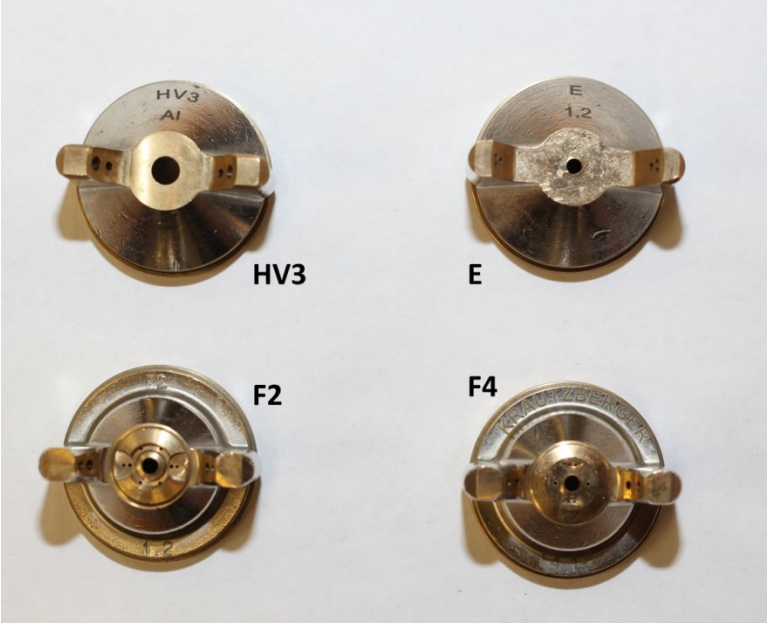

Figure 2.9: Four different nozzles for the atomizer gun which were used in the experiments (Krautzberger GmbH 2013)

2.4.2 Material Feed Container

To provide liquid to the gun, a Krautzberger pressure-operated material feed container was used. The container, which is shown in Figure 2.10, had a capacity of 2 liters and was constructed of stainless steel. After liquid was placed inside, adjustment of a pressure control valve enabled pressure variations inside the container that gave desired flow rates of liquid from the container to the atomizer gun. The pressure in the container forced the liquid out of the material feed exit and into the atomizer gun (Krautzberger GmbH 2014).

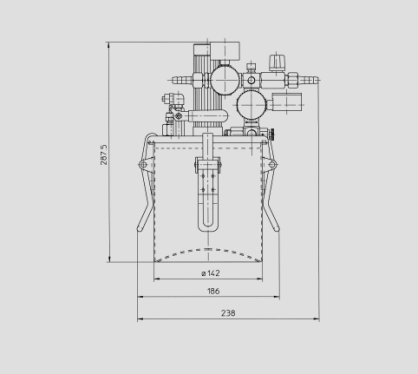

Figure 2.10: Krautzberger pressure-operated material feed container (Krautzberger GmbH 2014)

2.4.3 Ionizer

To ionize the atomizing gas, an Ion Systems Air Ionizing Cartridge W/Air Flow Sensor Model 92-6110 was used. The device is shown in Figure 2.11. The ionizer had a 120 Volt AC power supply and transformation of it into a steady-state DC ion emission. The ionizer was installed in-line with the atomizing gas flow, and provided a charge to the gas through two tungsten emitters that were placed in the middle of the flow. The ionizer provided a 25 Volt charge 15 cm away from the nozzle of the spray gun. The ionizer also contained a sensor that would automatically produce charged ions when desired. When ionization was not required, the sensor was deactivated and the device did not affect the flow (Simco-Ion 2012).

Figure 2.11: Air Ionizing Cartridge W/Air Flow Sensor Model 92-6110 (Simco-Ion 2012)

2.4.4 Compressed Gas Cylinder

The atomizing gases used during the experiments were laboratory-grade. A Taylor-Wharton model XL50-HP compressed gas cylinder was used to store the compressed gas; it had a volume of 176 liters and could be pressurized up to 2.4 MPa. The device is shown in Figure 2.12. A pressure regulator on the exit of the pressure vessel allowed for the correct gas feed to be provided to the rest of the system. An additional pressure regulator with a blow-off valve was included on the vessel to prevent the possibility that thermal expansion of the gas within the cylinder would creating unwanted pressure build up in the vessel (Taylor Wharton 2014). Each of the different gas cylinders was held in the laboratory unopened until its specific contents were to be used during the experiments.

Figure 2.12: Taylor-Wharton model XL50-HP compressed gas cylinder (Taylor Wharton 2014)

2.4.5 Spray Booth

A Paasche FABSF horizontal draft spray booth was used to provide adequate airflow to keep VOC concentration in the spray area to a minimum and to remove liquid droplets from the measurement zone. The device is shown in Figure 2.13. The booth used an 18 inch diameter, ¼ horsepower aluminum fan to draw air out of the laboratory and through the exhaust. The fan had a rated capacity of 1960 CFM. The booth held six (6) single-use filters to capture the liquid droplets flowing in the gas flow (Paasche Airbrush 2012).

Figure 2.13: Paasche FABSF horizontal draft spray booth (Paasche Airbrush 2012)

2.4.6 Air Filters

The filtration of the droplets in the paint booth was achieved using CHEMCO FMP-18 fiberglass paint arrestors, shown in Figure 2.14. These filters measured 50.8 x 50.8 cm and were made of a fiberglass microfiber with an efficiency rating of 99.23%. These filters were single-use items and needed to be replaced often to ensure that the efficiency of droplet collection remained high (Chemco Manufacturing 2000).

Figure 2.14: CHEMCO FMP-18 fiberglass paint arrestors (Chemco Manufacturing 2000)

CHAPTER THREE

3.0 EXPERIMENTAL APPARATUS

The experimental setups are presented in the following four sections. In Section 3.1, the setup for the atomizer used in all of the experiments for this thesis is presented; Section 3.2 presents the apparatus for the laser diffraction measurements; Section 3.3 presents the setup for the visual imaging; and, lastly, Section 3.4 discusses the setup for the IR thermal imaging measurements.

3.1 ATOMIZER SETUP

The configuration for the paint atomizer was kept constant for all of the experiments that were performed. It included the compressed gas cylinder, a pressure vessel, material feed container, a pressure control valve, and the water supply.

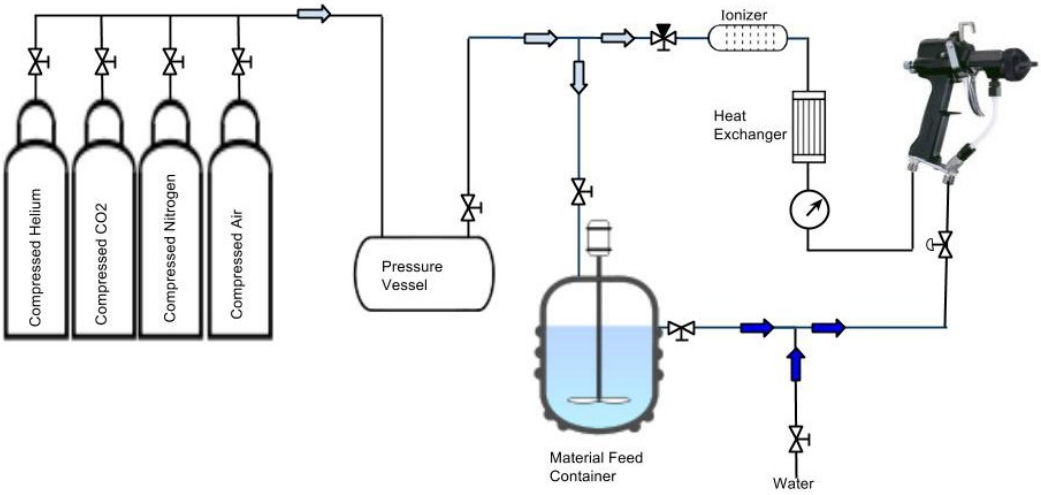

Figure 3.1: Setup for the atomizer gun used in all of the experiments

The process for using the appropriate gas was as follows. Depending on the gas to be used, a gas cylinder was opened to the piping system; although all of the gases were attached to the setup, only the valve corresponding to the gas being used was opened. Between usages of different gases, the lines were purged to eliminate any contamination between a currently-used gas and the previous one. From the compressed gas cylinder, the gas line fed into the pressure vessel installed to ensure that the compressed gas was warmed to the ambient temperature in the laboratory. This process was necessary, particularly for the nitrogen, because its cylinder contained liquid nitrogen.

The atomizing gas was then supplied to the gun through a pressure control valve which regulated its pressure within the atomizing spray gun. The pressure gauge for the gun was located at its inlet, a position which enabled the most accurate metering of the pressure within the spray gun.

Besides water, both water-based metallic paint and solvent-base clear coat were also assessed. The water was from the tap with no treatment other than to control its temperature. When either water-based metallic paint or solvent-based clear coats were sprayed, they were first contained in the material feed container, the container was then pressurized with the correct atomizing gas, and an integrated pressure regulator was adjusted to set flow rates of the paint. A pair of valves allowed the setup to be switch between these two supply options as needed.

3.2 LASER DIFFRACTION SETUP

Droplet size distributions were determined for the sprays using laser diffraction. Its setup included the atomizer gun, droplet size analyzer and the paint booth, shown in Figure 3.2. The analyzer was placed on a stable mounting platform in front of the paint booth at a fixed location ensuring that the paint droplets would be removed from the measurement zone by the paint booth equipment after the droplets passed through the laser illumination position only once and ensure proper positioning for acquiring laser diffraction data. Typically, this location and associated distances were measured from the front of the laser to the tip of the nozzle of the atomizer gun.

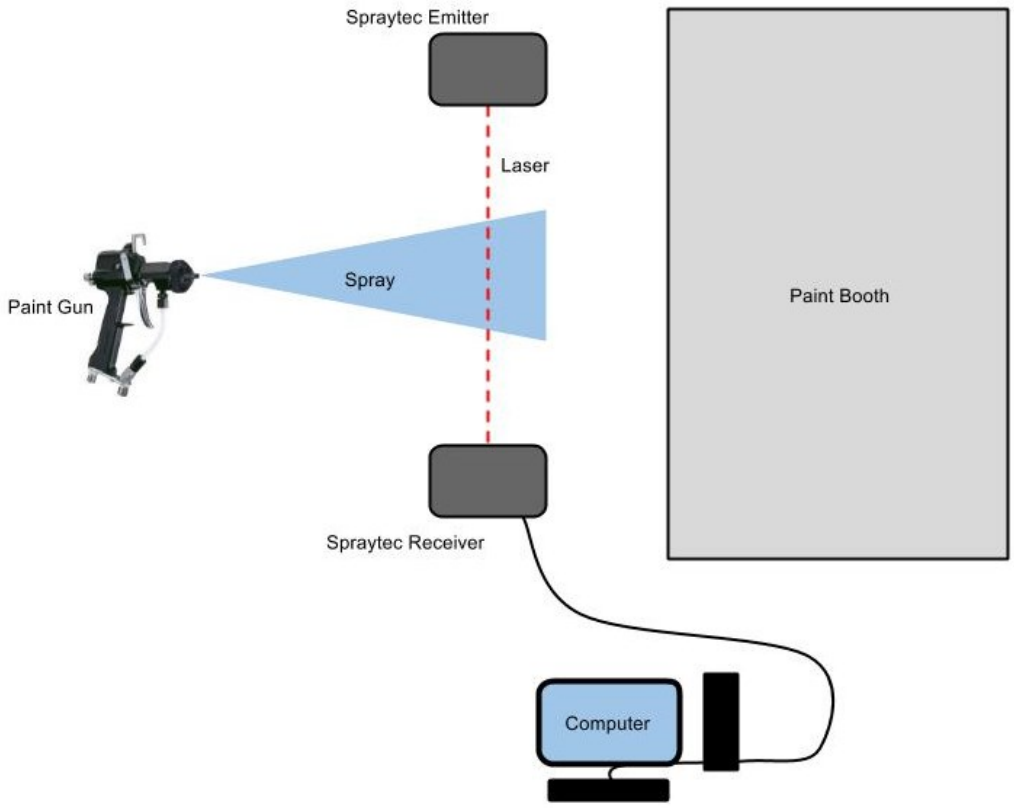

Figure 3.2: Experimental setup for the laser diffraction measurements

The Emitter tower produced laser light and the Receiver tower detected the laser beam and measure the angle of diffraction caused by the spray. The readings from the detector were acquired by a computer which also ran the Spraytec operating and analysis software. This software relied on the readings from the device and physical parameters of the fluid as input by the user to calculate the size of the droplets in the spray.

The spray was removed from the measurement zone and the room, in general, by the paint booth. It was located behind the Spraytec system, and provided a horizontal draft that ensured that spray particles only pass through the laser measurement region one time before they are removed.

The droplet size distribution measurement process involved the following steps:

1. The laser diffraction device was activated and the physical properties of the liquid used in the spray were input into the control software. The device automatically calibrated itself using these input parameters before every measurement.
2. The atomizer settings for the experiment were selected and the spray booth was activated and given time to come to steady state operation.
3. The atomizer gun is triggered and the spray is passed through the measurement zone. Once the atomizer reached steady state the measurement was started and recorded for 10 seconds.
4. The raw light diffraction data is sent to the computer with the control and analysis software. The software uses the information supplied by the user to generate a droplet size distribution for the spray. The droplet size distribution data was exported and then analyzed in Microsoft Excel.

3.3 THERMAL IMAGING SETUP

The setup for the thermal imaging (shown in Figure 3.3) includes the IR camera, the background radiation source, the atomizer gun, the high speed data recorder and the paint booth. The IR energy is emitted from the background radiation source and the spray attenuates the radiation. The camera detects the amount of radiation that reaches the camera and constructs an image. The camera was set in a position focusing on the middle of the spray field, and the background radiation source was placed behind the spray at the same height. The high speed data recorder was attached to the IR camera, and the control computer was attached to the camera as well. The paint booth ensured that the spray droplets only pass through the image once and are then removed.

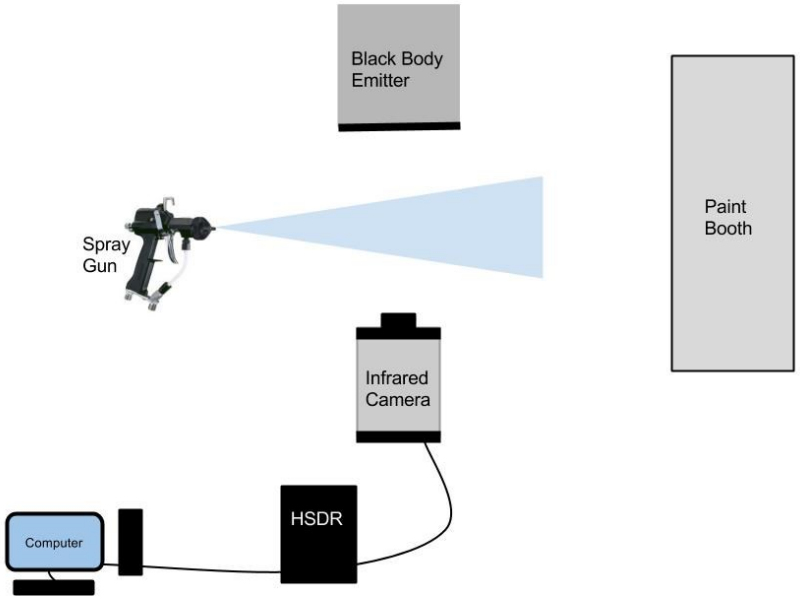

Figure 3.3: Experimental setup for the IR imaging measurements

The IR camera detects the difference in radiation that reaches the camera. To ensure that there is a temperature difference the background was set to 40°C. The temperature setting allows for a contrast from the spray, which is at the ambient temperature of the lab, measured at an average of 22°C. The background temperature was allowed to reach within 0.1°C of the selected temperature before the experiments began. Once the temperature stabilized, the desired experimental level was set for the atomizer.

The thermal imaging process involves the following steps:

1. The atomizer settings for the experiment are selected and the spray booth is activated and given time to come to steady state operation. The background radiation source is set to 40°C and allowed to reach within 0.1°C of the set point.
2. The thermal camera is activated and a frame rate of 400 fps with an integration time of 2 ms is selected. The camera core is allowed to come to its steady state operating temperature.
3. The measurement is started before the spray gun is activated so that a reference frame of the background is recorded. The atomizer is triggered shortly after the recording is started. The atomizer is run for 8 seconds and then stopped. The IR video is stopped shortly after the spray has left the imaging zone.
4. The videos are exported from the HSDR into MATLAB for post-processing and analysis.

3.4 VELOCITY MEASUREMENT SETUP

For some of the experiments that were conducted it was important to know the velocity of the atomizing gas. The setup for the velocity measurement includes the hotwire anemometer and the spray gun. The atomizing gas is emitted from the spray gun without the liquid flow. The hotwire anemometer is placed in the middle of the flow at a predetermined distance from the nozzle and the velocity of the gas is recorded. The setup for the velocity measurement is shown in Figure 3.4.

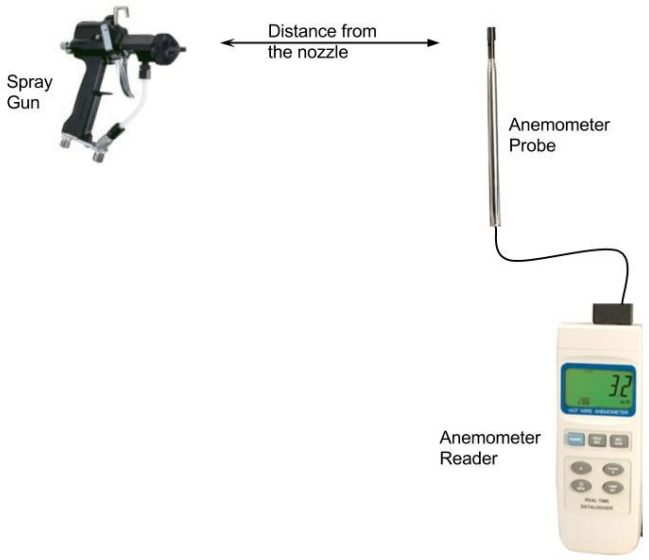

Figure 3.4: Experimental setup for the measurement of the atomizing gas velocity

3.5 TEST CONDITIONS

There are a number of factors which can be varied, including the atomizing gas pressure, the atomizing gas type, the liquid flow rate, the liquid composition, the nozzle, the distance from the nozzle, the heating, and the ionization. Several different tests will be conducted which will illuminate the effect of these different factors on the spray.

The first set of experiments will examine how the different nozzles will affect the spray envelope and the droplet size. The four nozzles will be tested while also varying the atomizing gas pressure, the liquid flow rate, and the distance from the nozzle. The atomizing gas, liquid composition, heating and ionization will be kept constant. At the end of the experiments a representative nozzle will be chose and will be kept constant for the rest of the experiments.

The next set of experiments will gather additional data and formulate a method for visualizing the breakup of droplets within the spray. This will require the use of the droplet size data from the previous experiments as well as measurements of the atomizing gas velocity, the liquid surface tension, and the atomizing gas density.

Once the method for visualizing the weber number has been developed, an immediately apparent result is the ideal distance between the sprayer nozzle and the target. The knowledge of the distance where the secondary droplet breakup is completed can be combined with the droplet diameter data to make an estimate of the ideal distance.

The next set of experiments investigates the effect of changing the gas composition and the liquid type. The variables which will be held constant are the atomizing gas pressure, the liquid flow rate, the nozzle type, the heating, the ionization,

and the distance from the nozzle. This will serve to determine if the composition of the atomizing gas will have an effect on the droplet diameter and the spray angle.

The last set of experiments will investigate the effect of ionizing and heating the ionizing gas. The variables which will be held constant are the atomizing gas pressure, the liquid flow rate, the nozzle type, the heating, the ionization, and the distance from the nozzle. These experiments will determine whether the heater and the ionizer have an effect that is significant enough to be included in a standard atomizer setup.

CHAPTER FOUR

4.0 RESULTS AND DISCUSSION

A comparison of the differences in atomization caused by the nozzle geometry is presented in Section 4.1; Section 4.2 presents a method for evaluating the atomization behavior using the Weber number; Section 4.3 presents the results of the experiments for selecting the location in the spray where the secondary atomization is no longer present. Section 4.4 presents the effects of different atomizing gases on the atomization behavior of several liquids; and, finally, Section 4.5 presents the effect of heating and ionizing the atomizing gas on the atomization of the spray.

4.1 EFFECT OF NOZZLE GEOMETRY ON ATOMIZATION PERFORMANCE

Section 4.1 presents the results for the comparison of nozzles at low liquid flow rates and over the range of pressures. Section 4.1.1 presents the results and discussion for the droplet size distribution at the low flow rate. Section 4.1.2 presents the visual imaging results for the same experimental levels. Next, Section 4.1.3 presents the experimental results of the different nozzles at the high liquid flow rate. Section 4.1.4 presents and discusses the results for the IR imaging at the high liquid flow rate. Finally, Section 4.1.5 discusses the findings of these experiments and presents the ideal nozzle to be used for the other experiments.

4.1.1 Droplet Size Distribution at low liquid flow rate

The results for the droplet size distribution in Figure 4.1. The droplet size *D43* vs. the distance from the nozzle for four different nozzles with a liquid flow rate of 200 cc/min, and an atomizing gas pressure of 0.1 MPa shows the D_{43} of the four different nozzles tested at the beginning of the research project and the evolution of droplet sizes as the spray increased in distance from the nozzle. The nozzles tested are labeled as HV3, E, F2 and F4.

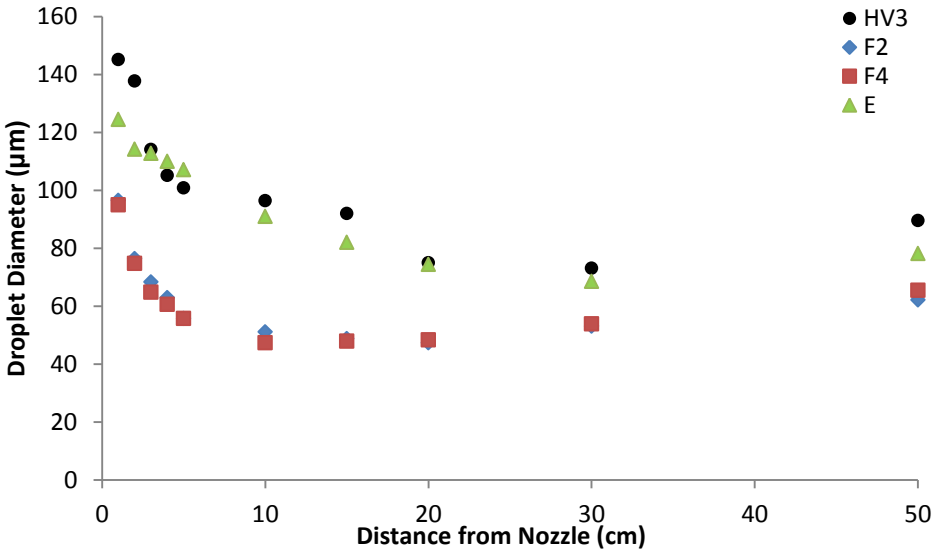

Figure 4.1. The droplet size D_{43} vs. the distance from the nozzle for four different nozzles with a liquid flow rate of 200 cc/min, and an atomizing gas pressure of 0.1 MPa

Figure 4.1 shows that the F2 and F4 nozzles produced sprays that behaved similarly; for the 10 measurements that were taken for each nozzle, the value of the average droplet diameter differed by a maximum value of 3.75 µm at 10cm from the nozzle. The droplet diameters from the F2 and F4 nozzles decreased quickly between 0-10 cm from the nozzle, and attained minimum diameters 10 cm from the nozzle. The

sprays from HV3 and E nozzles behaved similarly to each other but differently from the F2 and F4 nozzles. Both HV3 and E nozzles atomized the liquid with droplet diameters decreasing in value over the first 30 cm of travel before reaching minimum droplet sizes.

It is notable that the droplets begin to increase in size far away from the nozzle after they reach their minimum droplet size. This is due to the coalescence of the droplets due to the droplets colliding and recombining (Elshanawany and Lefebvre 1980).

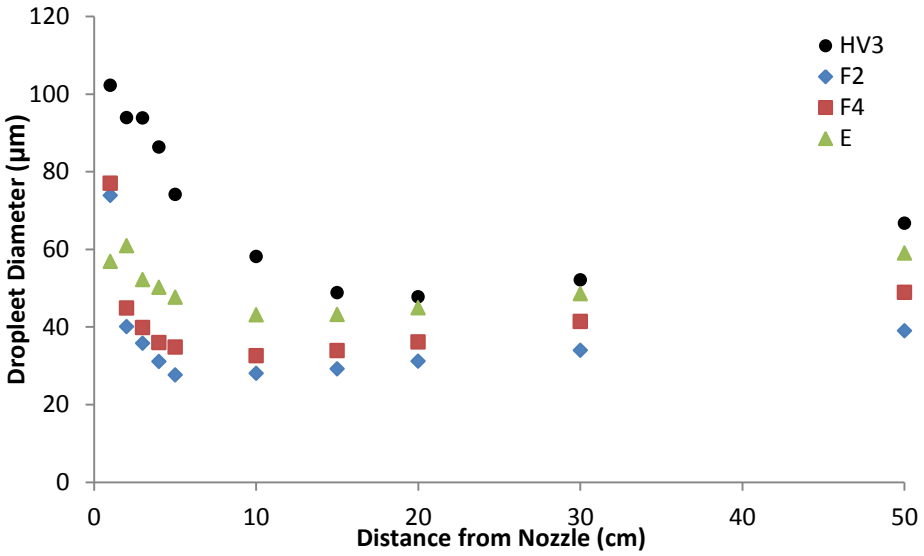

Figure 4.2. The droplet size D_{43} vs. the distance from the nozzle for four different nozzles with a liquid flow rate of 200 cc/min, and an atomizing gas pressure of 0.15 MPa

Figure 4.2 shows that at a higher atomizing gas pressure the atomization behavior of the different nozzles began to separate. All of the sprays had smaller droplet sizes at the higher atomizing gas pressure, which is expected for constant liquid flow rates and increasing atomizing gas pressure. The F2 and F4 nozzles still behaved similarly, but the F2 nozzle produced a smaller average droplet size over the entire length of the spray (50

cm). The HV3 nozzle produced the highest droplet size as it did at a lower gas pressure, and the E nozzle began to behave more similarly to the F2 and F4 nozzles than to HV3.

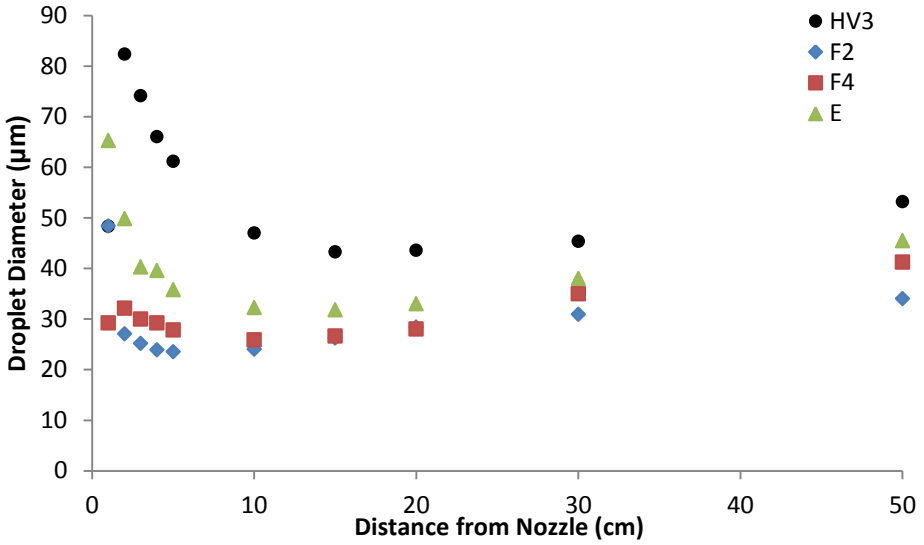

Figure 4.3. The droplet size D_{43} vs. the distance from the nozzle for four different nozzles with a liquid flow rate of 200 cc/min, and an atomizing gas pressure of 0.2 MPa

At even higher air pressure of 0.2 MPa, as depicted in Figure 4.3, the atomization behavior of the different nozzles was even more distinguishable. All of the sprays had smaller droplet sizes than at the two lower atomizing gas pressures, which is consistent with the data in Figure 4.2 in comparison to Figure 4.1. The E nozzle for the liquid flow rate of 200 cc/min and 0.2 MPa showed an atomization behavior similar to that of F2 and F4 nozzles although the droplet diameters from the E nozzle were larger. The HV3 nozzle shows a large spike in droplet size between the 1 cm and 2 cm measurements (the HV3 measurement at 1cm is hidden behind the F2 measurement at the same point). This increase in droplet size was not observed for any of the other nozzles under the same flow rate conditions and is believed to be a consequence of the differences in air pattern holes

within the face of the nozzle which forced the initial droplets from HV3 to coalesce, as is discussed in the following, thereby increasing the droplet sizes.

Figure 4.4. A picture of the HV3 nozzle type

The primary function of the air pattern holes shown in **Figure 4.4** is to influence the shape of the spray and change it from axi-symmetric into a flat fan pattern. Without these air holes, the spray from the nozzle would expand outward in a circular pattern. Instead, for HV3, the pattern air impinges on the spray and forces its shape into a flat fan.

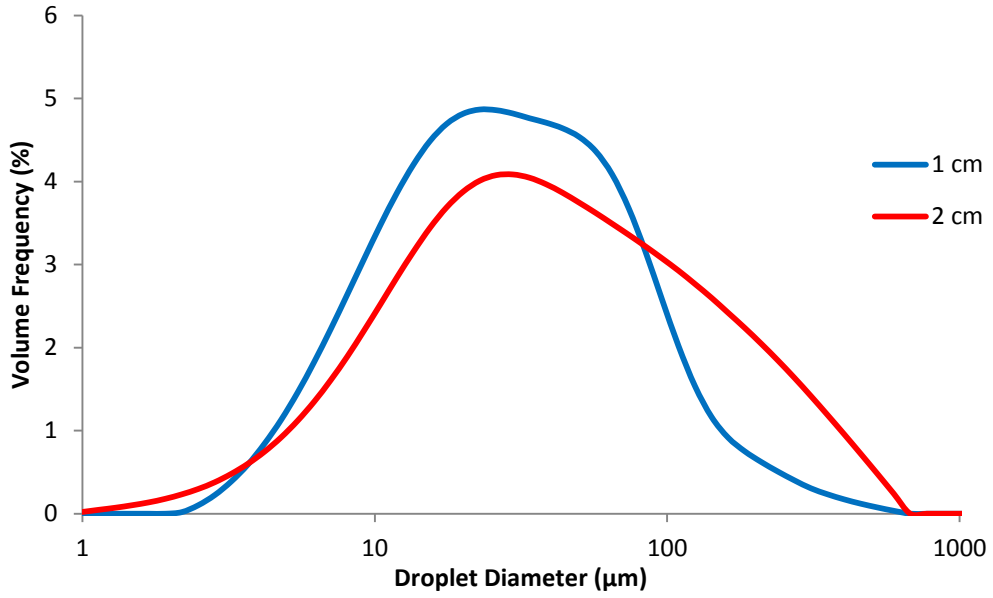

Figure 4.5. The volume frequency vs. the droplet diameter, for the HV3 nozzle with a liquid flow rate of 200 cc/min and an atomizing gas pressure of 0.2 MPa

Figure 4.5 shows that the droplet size distribution for the E nozzle was clearly not normal at 1 cm from the nozzle, but this is to be expected since primary atomization occurs in the area immediately before this measurement zone where a range of droplet sizes are produced, which are not normally distributed. In other words, secondary atomization has not yet forced the droplets into a more regular distribution. At 2 cm from the nozzle the pattern air converges onto the spray, the influx of which forces the droplets back into each other and recombination. This behavior can be seen in the droplet size distribution for 2 cm in Figure 4.5.

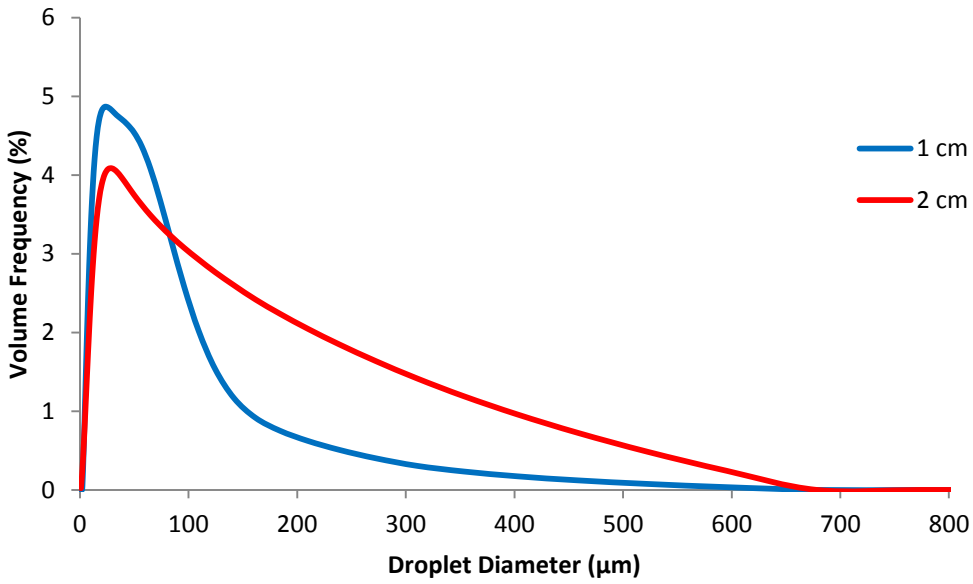

Figure 4.6. The volume frequency vs. the droplet diameter, for the HV3 nozzle with a liquid flow rate of 200 cc/min and an atomizing gas pressure of 0.2 MPa

Figure 4.6 also shows droplet size information-versus-distance from the nozzle but the droplet size is plotted linearly instead of on a log-scale. In this view it is evident that there are more small droplets at the 1 cm measurement location with the 2 cm position containing a much higher percentage of droplets at larger sizes.

From Figure 4.1- 4.5, it is evident that the design of the nozzle that is used greatly affects the behavior of the spray, even when using the same operating conditions. Upon more closely examining the geometry of the air holes in the nozzles it was determined that the number and arrangement of the air holes greatly affected atomization behavior. The HV3 nozzle produced the largest droplets of all the nozzles, and at high gas pressures created a spike in the droplet size. The F2 and F4 nozzles provided atomization behavior that was consistent across all operating conditions. The E nozzle produced atomization

that was similar to the F2 and F4 nozzles at high pressure, but was more similar to the HV3 nozzle at lower pressures.

4.1.2 Infrared Imaging Results at Low liquid Flow Rate

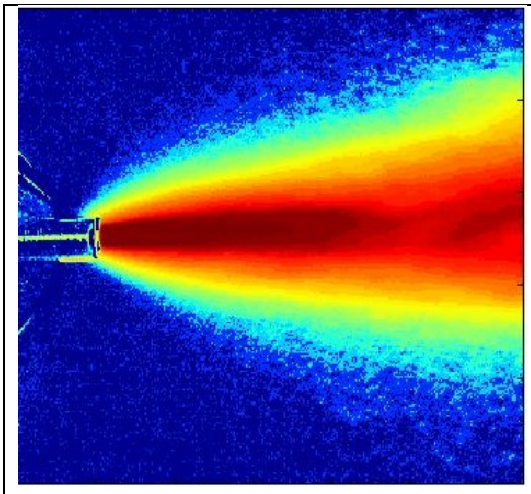

E

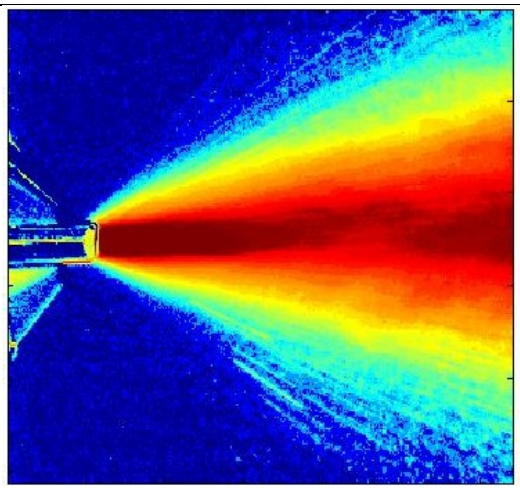

HV3

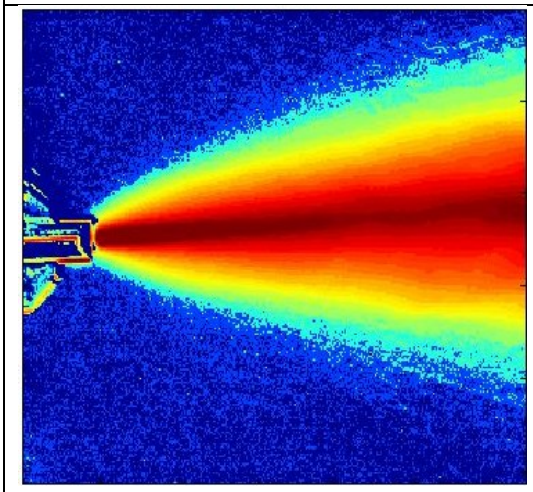

F2

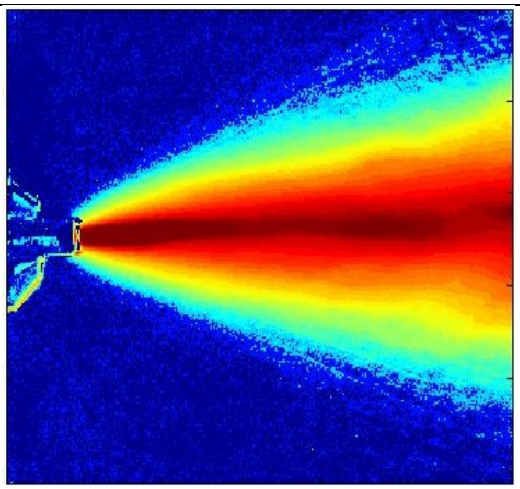

F4

200 cc/min @ 0.1 MPa

Figure 4.7. IR imaging histogram of the spray for several nozzles with a liquid flow rate of 200 cc/min and an atomizing gas pressure of 0.1 MPa

Figure 4.7 shows IR images of sprays from the four nozzles spraying water at a liquid flow rate of 200 cc/min and air at an atomizing gas pressure of 0.1 MPa. Although F2 and the F4 nozzles were very similar in design and produced almost identical droplet size distributions, their spray patterns differed noticeably. For example, the F2 nozzle had more area in red which indicates that its spray toward the middle of the pattern was denser than that from the F4 nozzle. The F4 nozzle had a more narrow spray pattern than did F2, and at the middle of the spray was more concentrated but with entire spray area not as evenly distributed as for F2. The HV3 nozzle showed the widest spray pattern of all of the nozzles and had a large area of blue, which indicates that there was a relatively large amount of the spray at the edge of the pattern in comparison to the other nozzles.

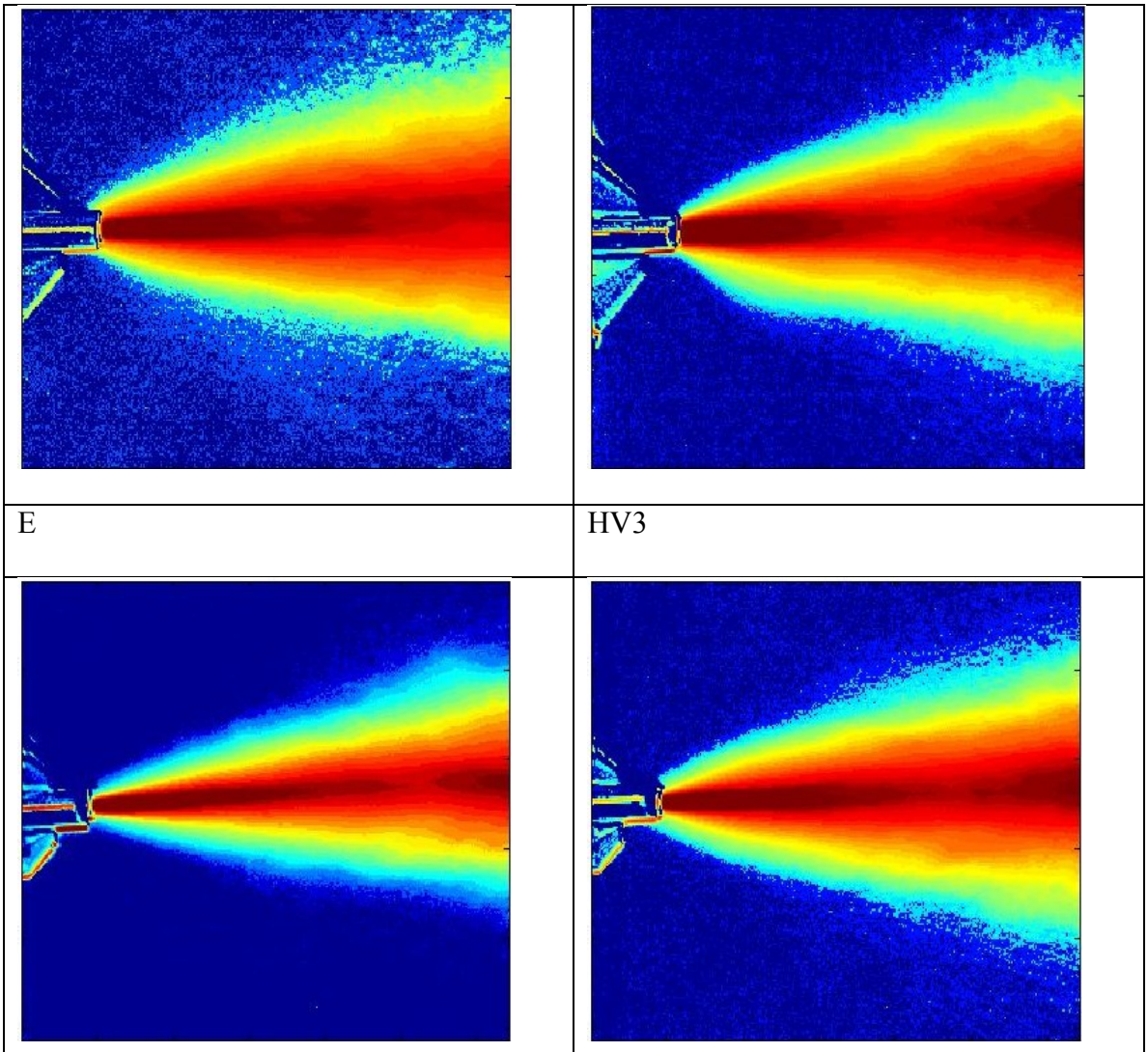

Figure 4.8. IR imaging histogram of the spray for several nozzles with a liquid flow rate of 200 cc/min and an atomizing gas pressure of 0.15 MPa

Figure 4.8 shows that at 200 cc/min and 0.15 MPa the E nozzle now has the widest spray pattern with a large yellow area in the spray. This indicates that the spray is not concentrated towards the middle as much as the other nozzles, but is more evenly spread out. The F4 nozzle shows that the edge of the spray is not as smooth as the F2

nozzle, which does not show as many stray droplets (droplets that are outside the bulk of the spray) around the edges. It is desirable to minimize the number of stray droplets in order to produce a more consistent coating on the substrate.

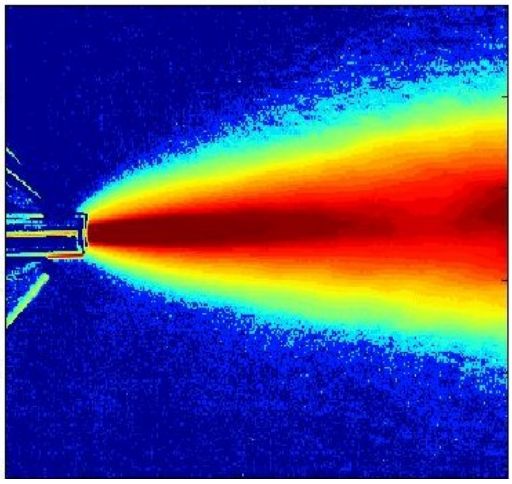

E

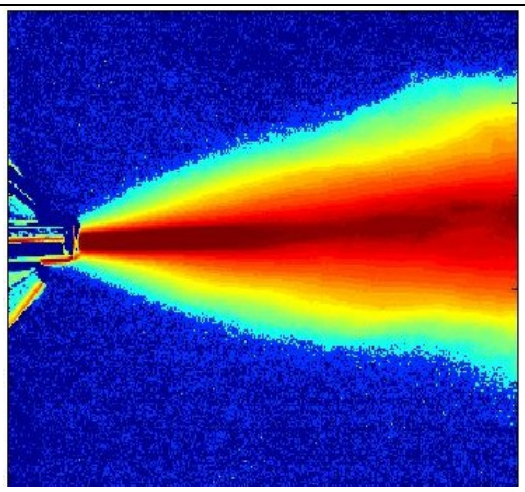

HV3

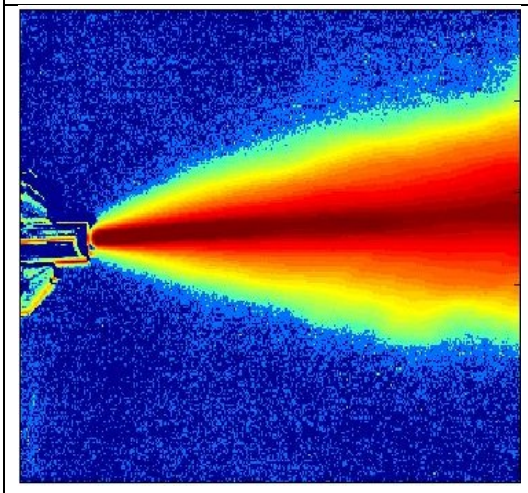

F2

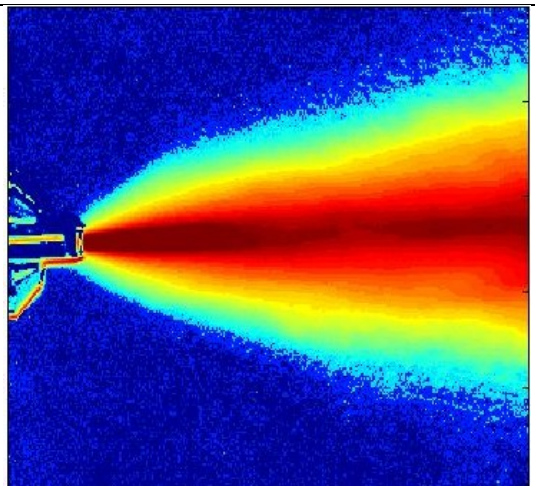

F4

200 cc/min @ 0.2 MPa

Figure 4.9. IR imaging histogram of the spray for several nozzles with a liquid flow rate of 200 cc/min and an atomizing gas pressure of 0.2 MPa

Figure 4.9 shows that the HV3 nozzle has the narrowest spray pattern of the 200 cc/min and 0.2 MPa experimental condition. The F2, F4 and E nozzles all show droplet size distributions that are roughly the same across the length of the spray. This is consistent with these imaging results which show only minor differences in the spray pattern. This is the liquid flow rate and atomizing gas pressure that produces the smallest droplet sizes, and the droplet sizes for the nozzles are all relatively similar. It can be seen that as the atomizing gas pressure increases the differences between the nozzles decrease and the flows become more similar.

4.1.3 Droplet Size Distribution at High Liquid Flow Rate

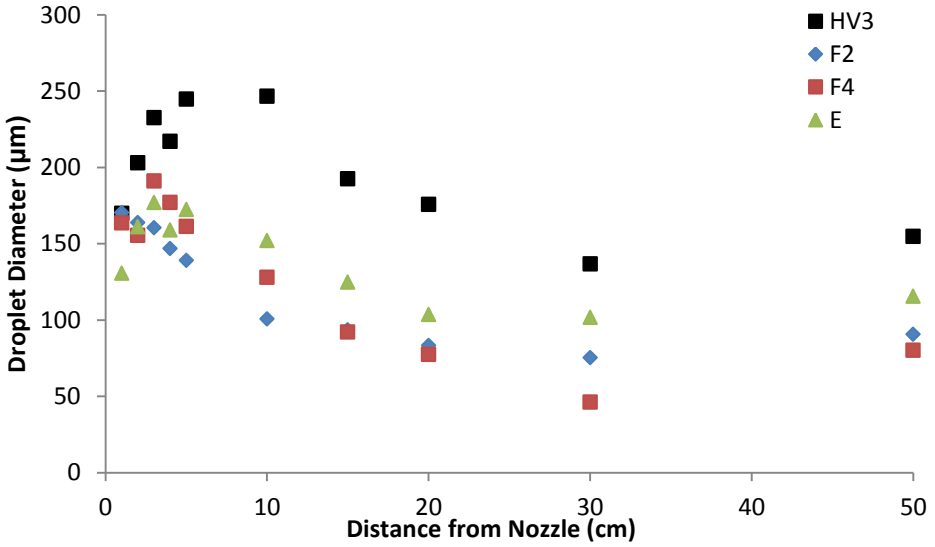

Figure 4.10. The droplet size D_{43} vs. the distance from the nozzle for four different nozzles with a liquid flow rate of 400 cc/min, and an atomizing gas pressure of 0.1 MPa

Figure 4.10 presents droplet diameter-versus-distance from the spray nozzles at a liquid flow rate of 400 cc/min. All nozzles produced initial droplet sizes near 150 µm, which then increased in value over the first few cm from the nozzles before secondary atomization decreased the size of the droplets. The droplets for F2 and the F4 nozzles reached their minimum size at 30 cm from the nozzles, while the E nozzle reached its minimum droplet size at 20 cm from the nozzle. The HV3 nozzle behaves differently than the other three nozzles a droplet size that continued to increase until at 10 cm from the nozzle. In general, the droplets sizes in Figure 4.10 are much larger than at the same atomizing gas pressure but a lower liquid flow rate. Although the inertial force of the atomizing gas remained constant, it was spread over a larger volume of liquid which resulted in inferior atomization in comparison to when the liquid flow rate was 200 cc/min.

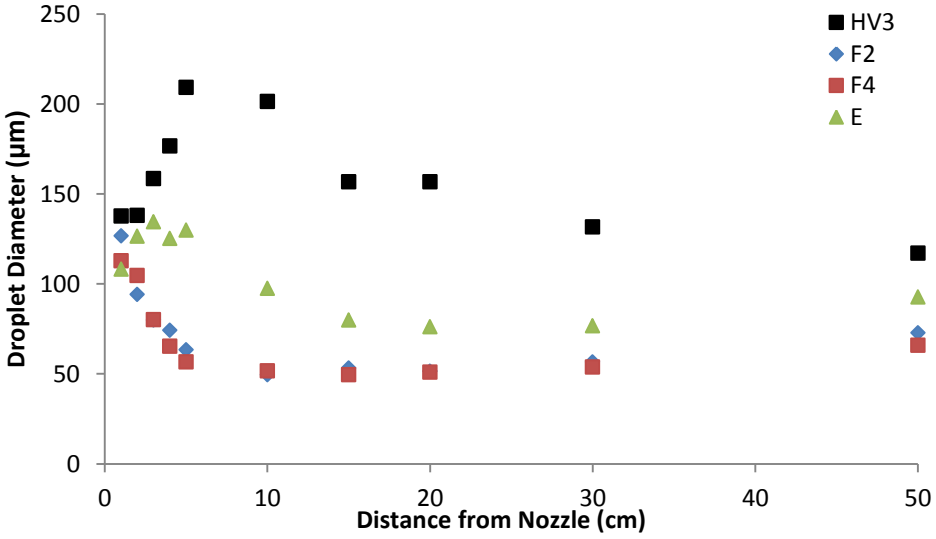

Figure 4.11. The droplet size D_{43} vs. the distance from the nozzle for four different nozzles with a liquid flow rate of 400 cc/min, and an atomizing gas pressure of 0.15 MPa

The behavior of the HV3 nozzle at a liquid flow rate of 400 cc/min and 0.15 MPa gas pressure, shown in Figure 4.11, follows a trend seen in Figure 4.10 although use of a higher atomizing gas pressure produced greater atomization of the liquid into smaller droplets. The E nozzle behavior in Figure 4.11 was similar to that in Figure 4.10, with droplet sizes increasing slightly between 1 cm to 5 cm from the nozzle, and then decrease to a minimum droplet size at 20 cm from the nozzle. The F2 and F4 nozzles both follow a different trend than before with both producing similar droplet sizes as the other nozzles close to the nozzle but then had significantly decreased sizes up to near 10 cm from the nozzle. This difference implies that secondary atomization within F2 and F4 was a much stronger influence than in HV3 and E nozzles.

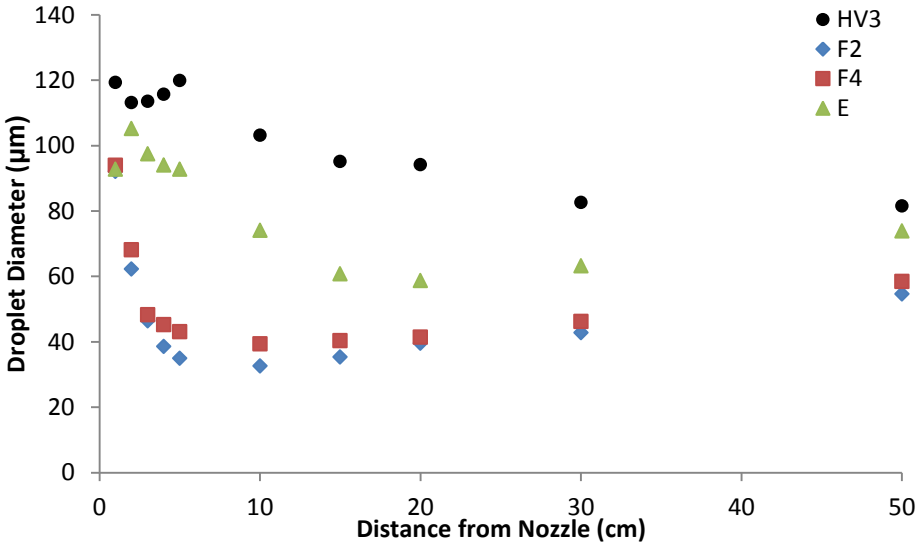

Figure 4.12. The droplet size D_{43} vs. the distance from the nozzle for four different nozzles with a liquid flow rate of 400 cc/min, and an atomizing gas pressure of 0.2 MPa

When the liquid flow rate was 400 cc/min and the gas pressure was increased to 0.2 MPa, the data in Figure 4.12 shows that changes in the droplet diameters as a function

of distance from the nozzle were minimized in comparison to the other atomizing gas pressures used with this flow rate. The droplet size still increased until 5 cm from the nozzle, but the effect was not nearly as significant as for the other operating conditions. In contrast, the F2 and F4 nozzles produced a pattern of decreasing droplet sizes from 1 cm until 10 cm from the nozzle, whereas the E nozzle exhibited a blend of behaviors observed under other flow conditions with droplet sizes increasing briefly and then decreasing to a minimum at the 20 cm mark.

The results Figure 4.10, 4.11 and 4.12 display several interesting trends. All droplets for all of the nozzles had roughly equivalent sizes at 1 cm from the nozzle; this observation suggests that very close to the nozzle the geometry of the atomizer is less important than the liquid flow rate and the atomizing gas pressure with the relationship between those two variables representing the main factor controlling primary atomization.

Furthermore, the geometry/configuration of the atomizer nozzles was observed to be an important factor that drives secondary atomization behavior, as represented by the number of air holes and their location. The F2 and F4 nozzles had very similar designs and, consequently, their atomization profiles were very similar. The HV3 and the E nozzles both had different designs, and their atomization behaviors differed from each other as well as from F2 and F4 nozzles. Hence, under similar conditions of liquid flow and gas pressure, the geometry of the nozzle is a main factor causing differences in atomization behavior, although the exact features of each nozzle which could cause different behaviors were not studied during this research.

4.1.4 Infrared Imaging Results at High Liquid Flow Rate

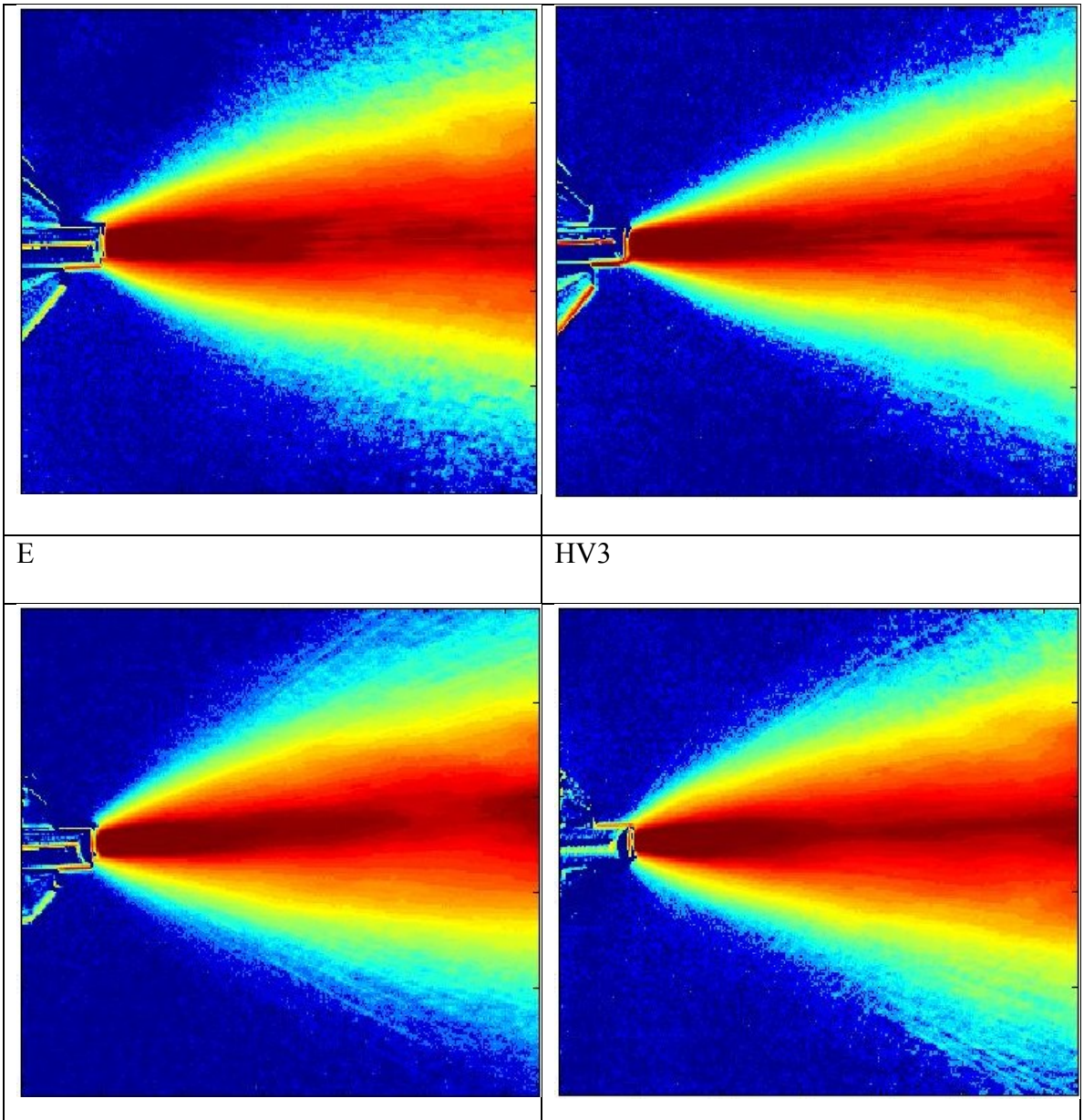

Figure 4.13. IR imaging histogram of the spray for several nozzles with a liquid flow rate of 400 cc/min and an atomizing gas pressure of 0.1 MPa

As presented in Figure 4.13, at the higher liquid flow rate the most obvious characteristic that was observed was an increased width in the spray patterns. As discussed previously, such widening is expected because of a decrease in the effect of the inertial force of the atomizing gas when higher liquid volume flow rates were used.

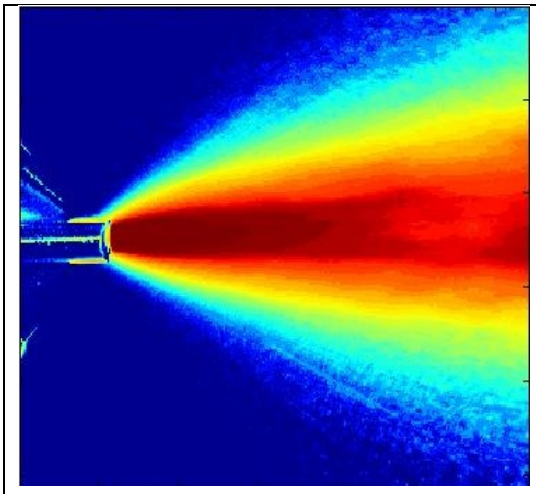	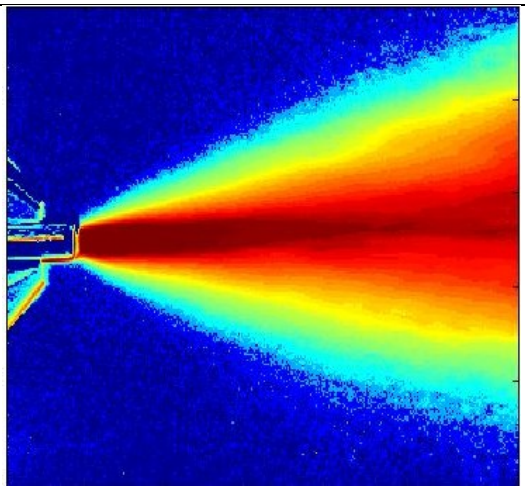
E	HV3
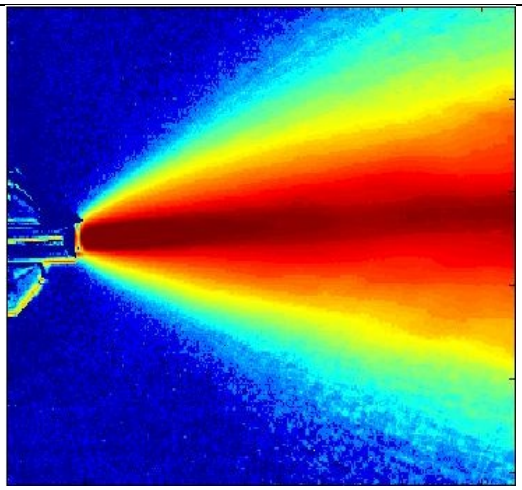	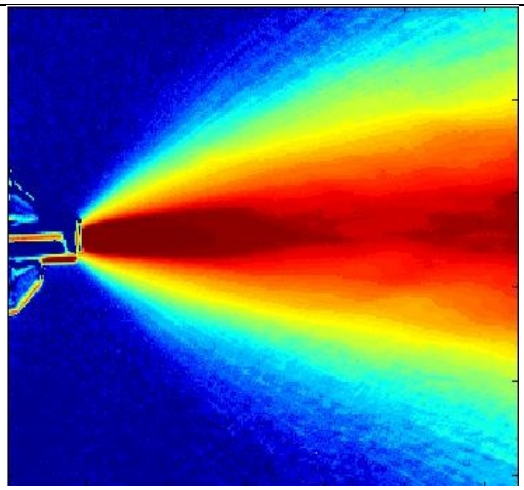
F2	F4
400 cc/min @ 0.15 MPa	

Figure 4.14. IR imaging histogram of the spray for several nozzles with a liquid flow rate of 400 cc/min and an atomizing gas pressure of 0.15 MPa

At the same 400 cc/min liquid flow rate and with gas pressure increased to 0.15 MPa, Figure 4.14 shows that the spray patterns remained very wide, with the HV3 nozzle showing a smaller spread pattern than the other nozzles. The HV3 nozzle also had reduced amounts of stray droplets around the edge of the spray pattern. In contrast, the F4 nozzle produced a high number of large droplets at the edge of the spray. This behavior suggests that the pattern air in the nozzle was not sufficient to form the liquid droplets into a consistent, well-defined spray envelope.

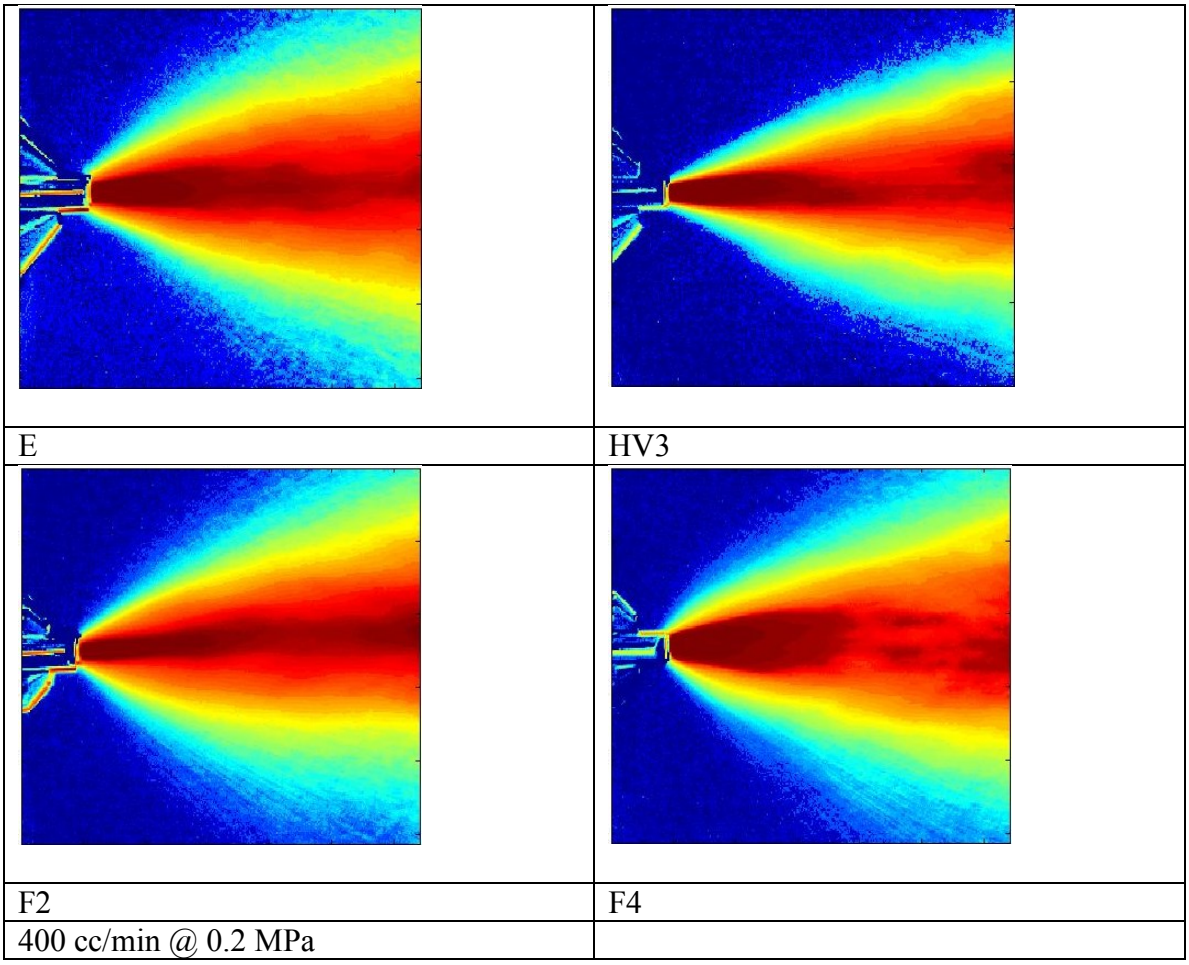

Figure 4.15. IR imaging histogram of the spray for several nozzles with a liquid flow rate of 400 cc/min and an atomizing gas pressure of 0.2 MPa

At a liquid flow rate of 400 cc/min and atomizing gas pressure of 0.2 MPa, the HV3 nozzle produced the narrowest spray envelope whereas the E, F2 and F4 nozzles all behaved similarly with wider envelopes and large numbers of large droplets at the edges of the sprays. Away from the nozzle at the right edge of the images (12 cm), the F4 nozzle had the most consistent density of spray of the four nozzles as evidenced by a more even red/orange coloration in the IR images than the other nozzles. However, areas still existed within the spray that had very high IR attenuation in the middle as evidenced by the presence of dark red coloration.

Hence, the behavior of the spray envelope changed with the atomizing gas pressure, nozzle design and the liquid flow rate. Of the three factors, the most important was the liquid flow rate with a 200 cc/min flow characterized by the relatively narrow spray envelopes with a small number of large, stray droplets at the edge of the main envelope. When the liquid flow rate was 400 cc/min, the spray envelopes were wider regardless of the nozzle or the atomizing gas pressure. The highest liquid flow rate also produced more droplets that were detected outside of the main spray envelope.

The nozzle geometry was not a main factor influencing spray patterns but it had an effect on the behavior of the spray. At the low 200 cc/min liquid flow rate, the F2 and F4 nozzles had the smallest spray envelopes whereas the HV3 and the E nozzles produced sprays that spread over a wider area. At the high, 400 cc/min liquid flow rate, the E nozzle behaved similarly to the F2 and F4 nozzles, especially as higher atomizing gas pressures were used; however, at the 400 cc/min liquid flow rate the nozzle geometry was relatively less important than it was at lower liquid flow rates.

4.1.5 Discussion of Results

The different nozzles were tested for the purpose of providing different atomization behaviors as operating conditions were varied over values typically of use in the nozzles. When the smallest possible droplet size would be required, the data points to F2 or F4 nozzle as the best. However, this thesis research did not seek to establish which nozzle was the "best" of the four because that superlative is highly dependent on the application at hand. Rather, the purpose of selecting one nozzle on which to focus during the majority of research for this thesis was to identify which exhibited a consistent behavior over the range of operational variables studied that was representative of a general spray application.

Sections 4.1.2 Infrared Imaging Results at Low liquid Flow Rate and 4.1.4 Infrared Imaging Results at High Liquid Flow Rate presented the results from IR imaging of the sprays for the four nozzles under the different atomizing gas pressures and liquid flow rates. Although the four nozzles showed some differences, it was concluded that nozzle geometry was not the main factor that influenced the spray envelope. Rather, the main factor affecting the results was the liquid flow rate; when the liquid flow rates were low, the spray envelopes were narrower than when the liquid flow rates were high. At the high liquid flow rate only minor differences existed in the IR images for the different nozzles.

Sections 4.1.1 Droplet Size Distribution at low liquid flow rate and 4.1.3 Droplet Size Distribution at High Liquid Flow Rate presented and discussed the droplet sizes from the four nozzles over a range of atomizing gas pressures and liquid flow rates. The nozzles exhibit some common results like: the HV3 nozzle

consistently produced the largest droplet sizes; the F2 and F4 nozzles consistently had very similar behavior to each other and produced the smallest droplet sizes; and the E nozzle consistently produced droplets that were of intermediate size, falling in value between the large droplets of the HV3 nozzle and the very small droplets of the F2 and F4 nozzles. These results mean that the E nozzle incorporated aspects of both the high (HV3) and low (F2 and F4) droplet size generation capacities, and was a good choice for a "representative" nozzle that was used during the remainder of thesis research.

4.2 WEBER NUMBER FORMULATION

This section presents the formulation of a method to measure the volume frequency of different Weber number-controlled breakup regimes in a spray. Section 4.2.1 presents the surface tension measurements; Section 4.2.2 discusses the method for determining gas densities; Section 4.2.3 presents the method for estimating liquid velocities; Section 4.2.4 describes measurements of the gas densities; Section 4.2.5 presents the droplet size distribution data; Section 4.2.6 discusses the regime cut-offs; and, finally, Section 4.2.7 gives an explanation spray visualization.

4.2.1 Surface Tension

Surface tension is the tendency of a fluid to minimize the surface area of the interface between two materials which are interacting (Daly 1969). The cohesion of the fluid will result in a greater force towards the fluid itself than to the other material. The exact force of this attraction is dependent on the different materials that are at the

interface. For water, the surface tension when interacting with different gases is small enough that it can be ignored. In fact, the difference between the surface tension for different gases is less than the variation of the values for different models of the surface tension. Figure 4.16 shows different models for the surface tension of water when interacting with the different gases (Gittens 1969, Cini, Ficalbi et al. 1971, Cini, Loglio et al. 1972, Kayser 1976). Each model is labeled by the gas with which the liquid water is interacting.

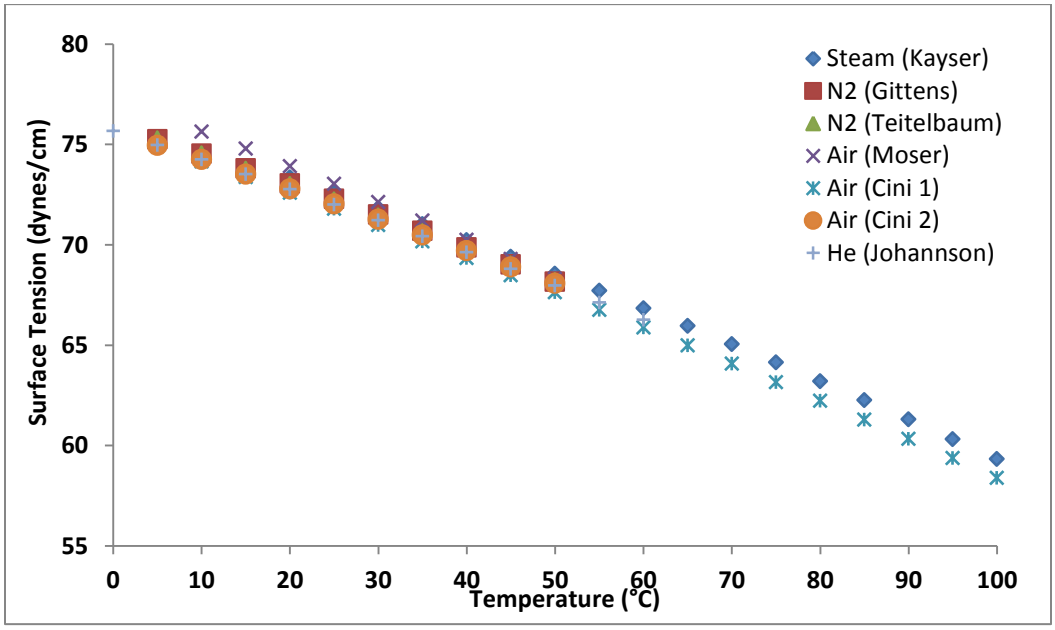

Figure 4.16. Surface Tension of Water vs. Temperature for several different models of water and gas interaction

Table 4.1: Table of temperature changes in the value of the surface tension for several different models of the water-gas interface

T (°C)	Steam (Kayser)	N2 (Gittens)	N2 (Teitelbaum)	Air (Moser)	Air (Cini 1)	Air (Cini 2)	He (Johansson)
0							75.67
5		75.25	75.31		74.91	74.95	74.96
10		74.54	74.55	75.64	74.15	74.24	74.25
15		73.81	73.79	74.79	73.38	73.52	73.51

20	73.36	73.06	73.03	73.92	72.59	72.78	72.76
25	72.60	72.29	72.25	73.03	71.79	72.03	72.00
30	71.82	71.50	71.46	72.13	70.99	71.27	71.22
35	71.03	70.69	70.67	71.20	70.16	70.49	70.43
40	70.22	69.87	69.87	70.25	69.33	69.70	69.62

The results of these models show that the surface tension behavior is expected to be almost identical regardless of the gas. In general, the surface tension is higher at temperatures near freezing and then decreases to ¾ of this cold value for temperatures near the boiling point of water. However, at normal experimental temperatures used during this research (20-25^{o} C), the value of the surface tension will not vary by more than 2 dynes/cm regardless of the type of atomizing gas that is used. This small change is regarded generally as not large enough for surface tension to significantly affect outcomes of the model (Gittens 1969, Cini, Ficalbi et al. 1971, Cini, Loglio et al. 1972, Johansso.K and Eriksson 1972, Kayser 1976, Vargaftik, Volkov et al. 1983).

4.2.2 Gas Density

The gas density used in the calculation of Weber numbers is also a function of the gas temperature. To determine this temperature, a K-type thermocouple was placed at different distances from the nozzle and the temperature of the atomizing gas (without liquid flow) was measured. This procedure was repeated for 30 points in the flow; it was found, as displayed in Figure 4.17, which the temperature dropped as the gas left the nozzle, then quickly returned to the ambient temperature of the room. This behavior is

consistent with that predicted by the ideal gas law (Kautz, Heron et al. 2005, Kautz, Heron et al. 2005).

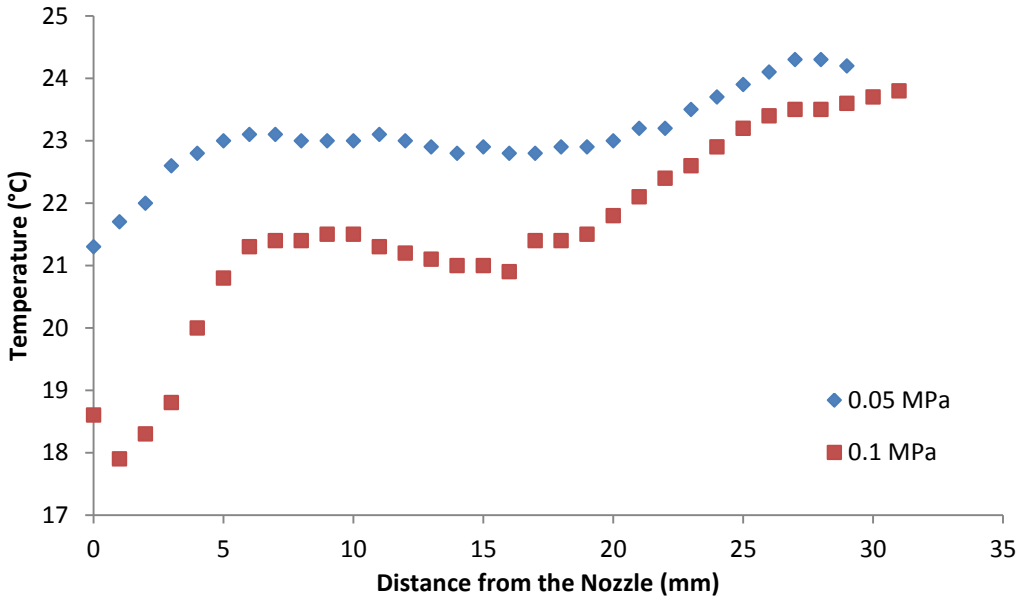

Figure 4.17. Temperature vs. distance from the nozzle for air with an atomizing gas pressure of 0.05 and 0.1 MPa at an ambient temperature of 24°C

Figure 4.17 shows the extent to which the atomizing gas temperature varied at various distances from the nozzle when the ambient laboratory temperature was 24°C. Within approximately 25 mm from the nozzle, the atomizing gas temperature equilibrated to the ambient temperature. The temperature decrease was greater at higher atomizing gas pressure; for example, the 0.1 MPa results were 2.7°C lower at the nozzle than were the 0.05 MPa results although this initial temperature difference was overcome at the same distance from the nozzle for both pressure levels. Depending on the gas that was used to atomize the droplets, the temperature of the gas can affect the density enough to change Weber Numbers in a noticeable way.

4.2.3 *Liquid Velocity*

The liquid velocity was calculated by measuring both the volumetric flow rate of the liquid and the nozzle diameter of the spray gun. The measurement of liquid velocity followed from the Bernoulli equation, as well as the conservation of mass (Çengel and Boles 2011). The liquid velocity at the exit was calculated with

$$P_1 + \frac{1}{2}\rho_1 v_1^2 + \rho_1 g z_1 = P_2 + \frac{1}{2}\rho_2 v_2^2 + \rho_2 g z_2$$

$$A_1 v_1 = A_2 v_2 \,.$$

Here P is the pressure, ρ is the density, g is the acceleration due to gravity, v_1 is the velocity of the gas in the gun, v_2 is the exit velocity at the nozzle, A is the cross-sectional area, and z is the height above or below the nozzle. These equations can be rearranged to solve for the exit velocity (v_2) of the liquid at the nozzle exit, with the result

$$v_2 = \sqrt{\frac{2P_1}{\rho\left(1 - \left(\frac{A_2}{A_1}\right)^2\right)}}\,.$$

For simplicity, the liquid velocity was assumed to be constant over the entire length of the spray. This approximation is appropriate at distances close to the nozzle, but becomes less accurate as the distance from the nozzle increases. To impart more accurate droplet velocity data would require PIV measurements of the droplets at various distances from the nozzle.

4.2.4 *Gas Velocity*

The gas velocities were measured with a hot-wire anemometer (1, 2, 3, 4, 5, 10, 15, 20, 30 and 50 cm from the nozzle). To ensure precise measurements, the liquid flow

was set to 0 cc/min, each point in the flow and each atomizing gas pressure were measured three times and then the results of each setting averaged together. Generally the measurements varied by less than 0.2 m/s, as can be visualized in Figure 4.18.

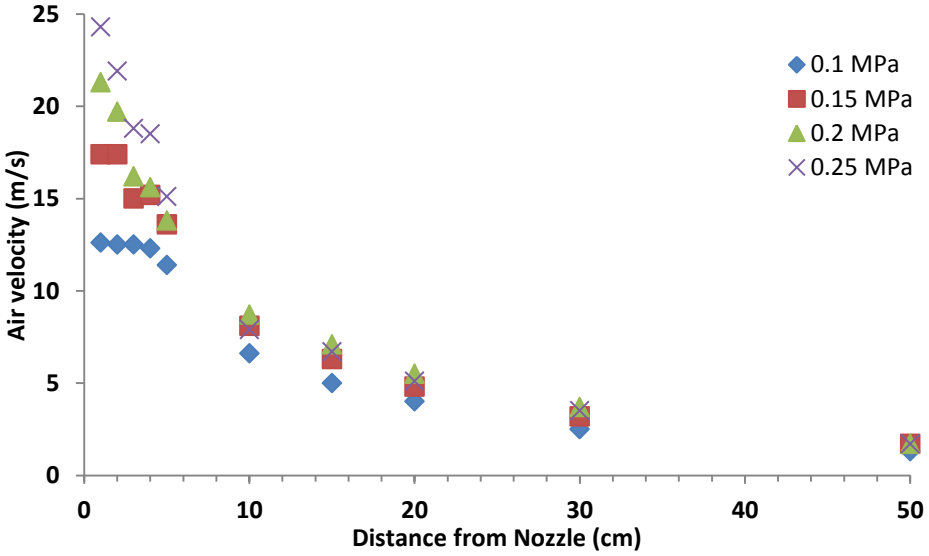

Figure 4.18. Air velocity vs. distance from the nozzle for air at a range of atomizing gas pressures

If the gas exiting the nozzle was expanding freely, it would be expected to have a velocity profile that decreased with $1/x^2$, where x is the distance from the nozzle tip. However, the actual drop in gas velocity was closer to $1/x$, which is a consequence of the geometry of the nozzle which forces the spray into a flat fan shape that expanded primarily in the vertical direction with little expansion in the horizontal direction.

As the pressure of the atomizing gas was increased, the initial spray velocity also increased as well. For the low pressure (0.1 MPa) tests the velocity of the gas remained constant over the first five centimeters of flow before decreasing. This result is due to the geometry of the gun and spray as well as the lower amount of drag that the relatively

slow moving gas experiences. At 0.15 MPa gas pressure, a similar behavior was noted but the velocity was constant for only the first two cm after exiting the nozzle. At 0.2 MPa, the velocity dropped quickly as soon as the gas exited the nozzle. Due to the nature of the flow, spray velocities at all liquid pressures will begin to converge as the distance from the nozzle is increased; in fact, spray velocities were all within 1.1 m/s of each other at 10 cm from the nozzle and within 0.5 m/s of each other at 50 cm.

4.2.5 Droplet Diameter

Liquid droplet sizes were measured using the Spraytec laser diffraction system; it provides an entire droplet size distribution within the flow and enables the development of information that fully describes the spray. Instead of choosing only representative droplet sizes, like in D_{32} or D_{v50} data, the entire droplet size distribution, as displayed in Figure 4.19, can be used to illustrate the dynamic and heterogeneous behavior of the flow.

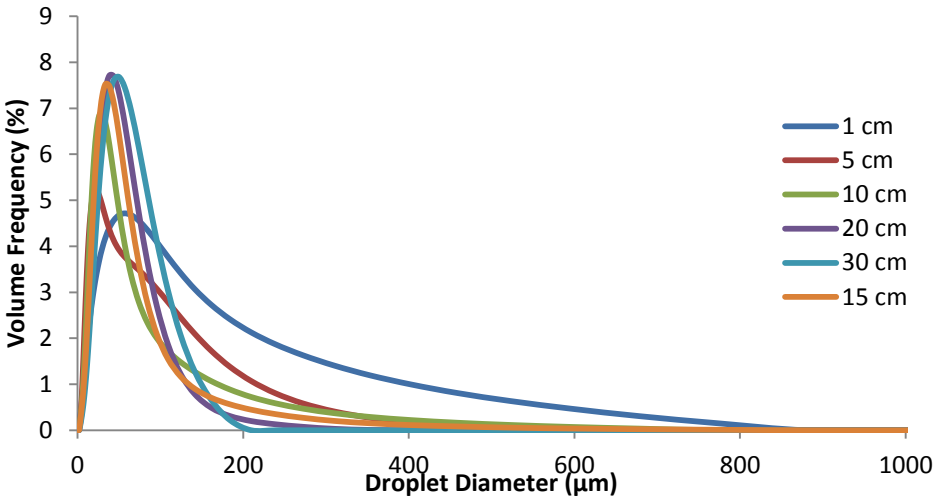

Figure 4.19. Volume frequency vs. droplet diameter for the E nozzle with a liquid flow rate of 200 cc/min and an atomizing gas pressure of 0.1 MPa at several different measurement distances

Figure 4.19 displays droplet size distribution by a percentage of the total volume within the spray. In general, most of the spray volume was contained in droplets that were smaller than 200 µm. Although a small amount of the total volume was contained in large (> 200 µm) droplets and would seem to be an insignificant portion of the spray, they are actually a source of many of the problems that are encountered during spray coating processes and should be minimized whenever possible.

Another way to visualize the droplet size distributions is to plot the droplet diameter on a log scale; this type of display demonstrates that the spray was distributed in a log-normal manner, with the bulk of the spray droplets sizes in the 10-100 µm range. This type of plot makes it easier to examine spreads in the distributions and to compare spray quality from one operating condition to another.

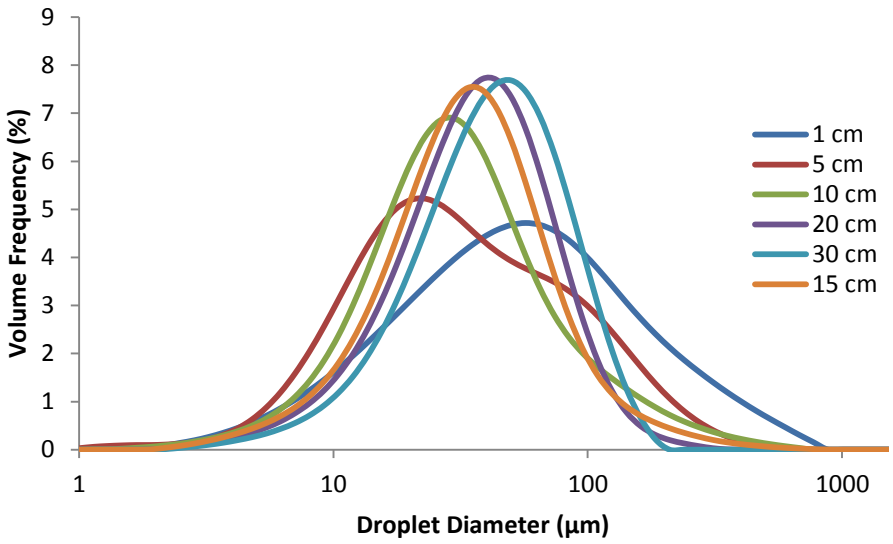

Figure 4.20. Volume frequency vs. droplet diameter for the E nozzle with a liquid flow rate of 200 cc/min and an atomizing gas pressure of 0.1 MPa at several different measurement distances

4.2.6 Regime Cut-Offs

Since the Spraytec provides the entire distribution for a spray, it was possible to calculate fractions of the spray that was within each of the atomization breakup regimes discussed previously. To accomplish this, the Weber number equation was rearranged to solve for the droplet size following

$$We = \frac{F_{inertial}}{F_{surface\ tension}} = \frac{\pi\rho l^3 U^2}{\pi l^2 \sigma} = \frac{\rho l U^2}{\sigma} \tag{4.1}$$

$$D_l = We\frac{\sigma}{\rho\left(U_l - U_g\right)^2} \tag{4.2}$$

where U_l is the liquid velocity, U_g is the atomizing gas velocity, ρ is the atomizing gas density, σ is the liquid surface tension, and l is the length scale, which will be represented by the droplet diameter.

The values of the Weber number for each of the breakup regimes are known (Pilch and Erdman 1987). When this preceding equation is combined with gas density, the surface tension, and the liquid and gas velocities, the droplet sizes corresponding to pertinent ranges of the Weber number can be calculated. After the droplet sizes were known within upper and lower limits of each breakup regime, the droplet distribution was used to compute the total area under the curve for each of the regimes. An illustration of this calculation and approach is shown in Figure 4.21.

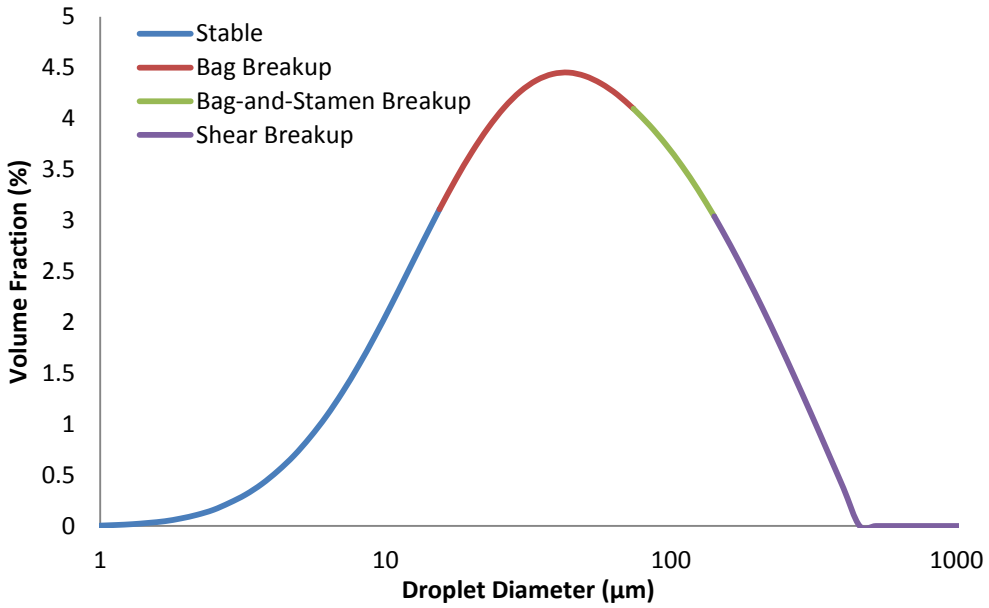

Figure 4.21. Visualization of the droplet diameters which are in different atomization regimes imposed onto the droplet size distribution for the E nozzle with a liquid flow rate of 200 cc/min, atomizing gas pressure of 0.1 MPa, at 3 cm from the nozzle.

In general, a fraction of the total volume of the spray was represented in each of the breakup regimes at a given distance from the nozzle. Changing the location of this distance changed the volume fractions within each regime. Hence, by plotting the area

under each curve for each of the regimes at each distance from the nozzle enabled a comprehensive picture of spray evolution.

4.2.7 Visualization of the Spray

For each spray, 10 measurements were taken for each of the experimental variables of gas and liquid flow rates, but instead of visualizing the distribution at each distance point, it was advantageous to calculate the percentage of the spray volume contained within each breakup regime for each point. From this approach, a visualization of spray evolution was accomplished for the entire spray which provided an understanding of the dynamic behavior of the spray.

For example, Figure 4.22 illustrates a typical behavior of the spray. The first model result was that the spray contained about 30% of the volume of the flow in the bag regime, 25% in the bag-and-stamen regime, 40% in the shear regime, and only about 5% stable droplets. As the distance from the nozzle increased, the percentage of the flow in the stable regime increased steadily until it a distance of 10 cm was attained, at which point a slower increase was observed to 100% of the flow volume was contained in stable droplets, i.e. stable with respect to Weber number breakup.

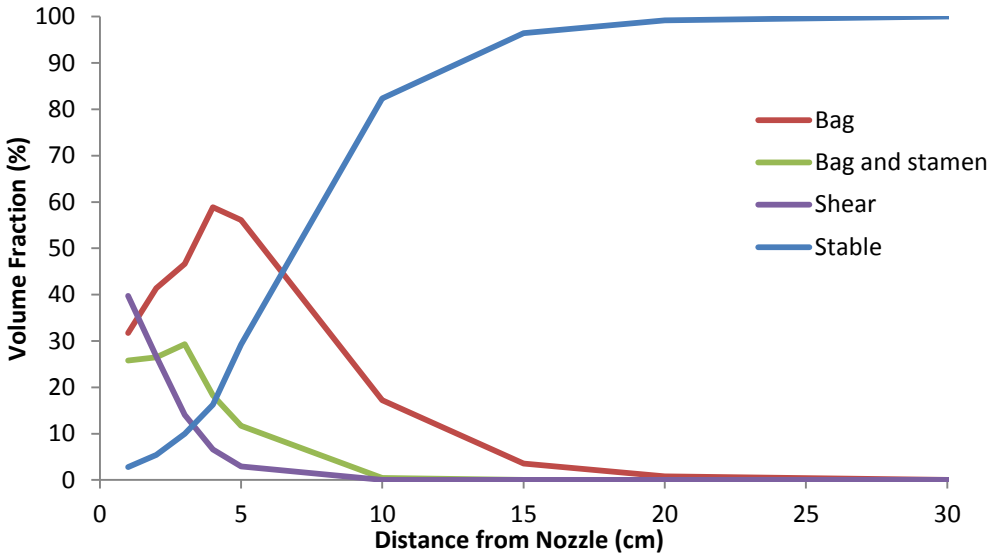

Figure 4.22. Volume fraction of the breakup regimes vs. Distance from the nozzle for the HV3 nozzle at a liquid flow rate of 200 cc/min and an atomizing gas pressure of 0.1 MPa

In general, the shear regime decreased very quickly at increasing distances from the nozzle; this decrease is a result of an atomization regime in which the inertial force most strongly dominates surface tension forces. The bag-and-stamen regime also decreased, but not at the rapid rate observed for the shear regime. For the bag-and-stamen regime, the slight increase observed in volume fraction at ~3 cm from the nozzle could be due to having unstable droplets in the shear regime that had been decreased in size to a point where they were also unstable in the bag-and-stamen regime.

The behavior of the bag regime was distinct from the other regimes in which a very obvious maximum was determined at 5 cm from the nozzle. This behavior may be due to many of the droplets which were unstable in the shear and bag-and-stamen regimes began breaking into smaller satellite droplets which were also unstable in the bag regime; if so, they would undergo additional atomization before finally becoming small

enough to be stable. This regime is the lowest energy of all the breakup regimes, and also occurs during longer time scales. As a result, the bag regime persisted until the spray was 20 cm away from the nozzle.

4.3 SELECTION OF IDEAL DISTANCE FROM NOZZLE

This section uses the method presented in Section 4.2 Weber Number Formulation and combines it with the results in Section 4.1 effect of nozzle geometry on atomization performance to determine positions in the flow which are most representative of the atomization behavior of the spray. In particular, the Weber number method for evaluating sprays has an advantage of providing a more detailed analysis of the flow, including an estimation of an ideal distance from a substrate at which the spray gun should be positioned. This ideal distance is one at which the droplet size distribution is the smallest and has the narrowest distribution. Additionally, the ideal distance would also be one at which atomization has been completed and the atomizing gas velocity is relatively low. Each of these factors will be considered in the selection of an ideal distance for placing a substrate from the nozzle.

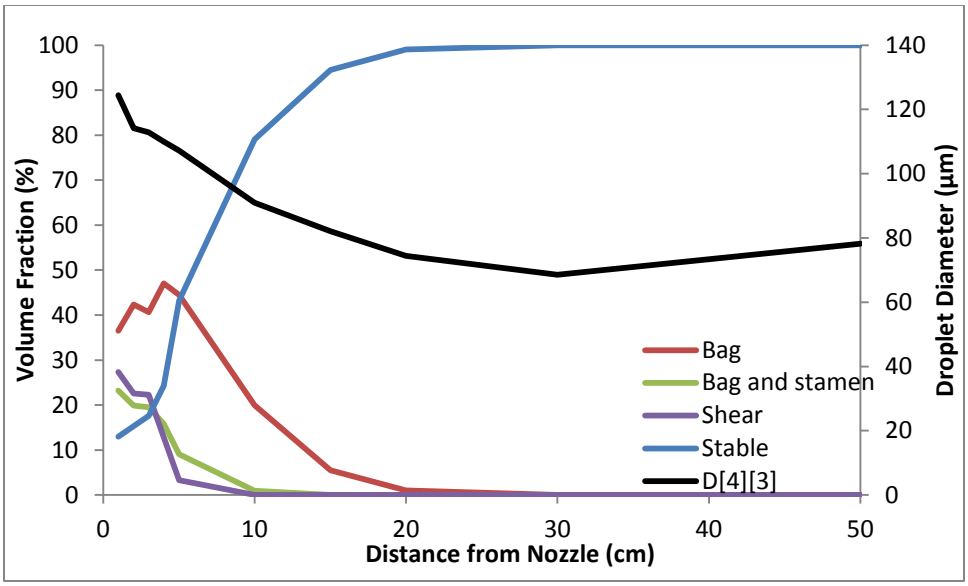

Figure 4.23. Volume fraction of Weber number regimes vs. distance from the nozzle for the E nozzle with a liquid flow rate of 200 cc/min and an atomizing gas pressure of 0.1 MPa

A minimum droplet size occurred at 30 cm from the nozzle and the breakup regime was before 20 cm from the nozzle. At 20 cm from the spray nozzle atomization is nearly complete but a small amount remains in the bag regime as evidenced by a 6 µm decrease in the droplet size. This small amount of continued breakup of the droplets is insufficient to rule out 20 cm as an acceptable distance but suggested that the ideal distance from the nozzle was in the range of 20-30 cm from the nozzle.

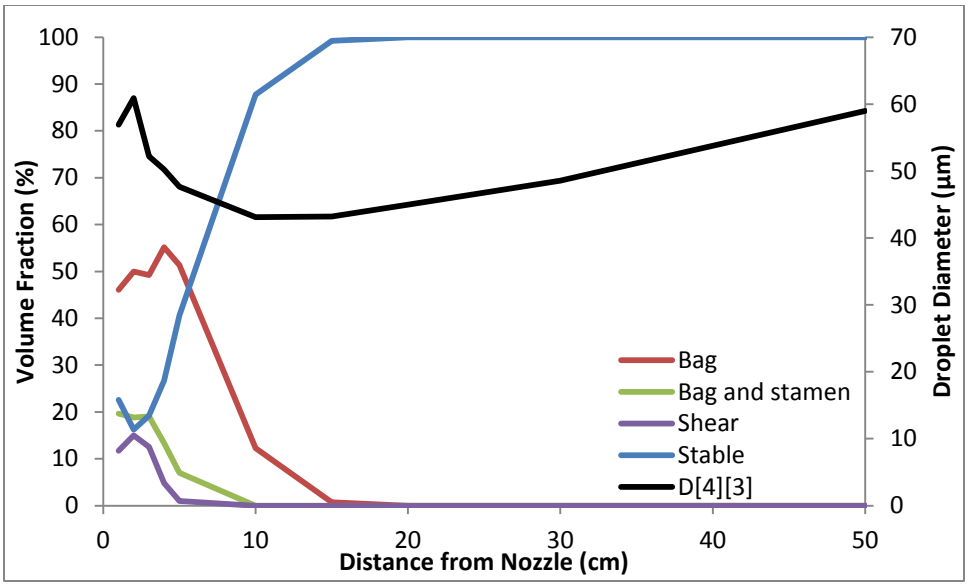

Figure 4.24. Volume fraction of Weber number regimes vs. distance from the nozzle for the E nozzle with a liquid flow rate of 200 cc/min and an atomizing gas pressure of 0.15 MPa

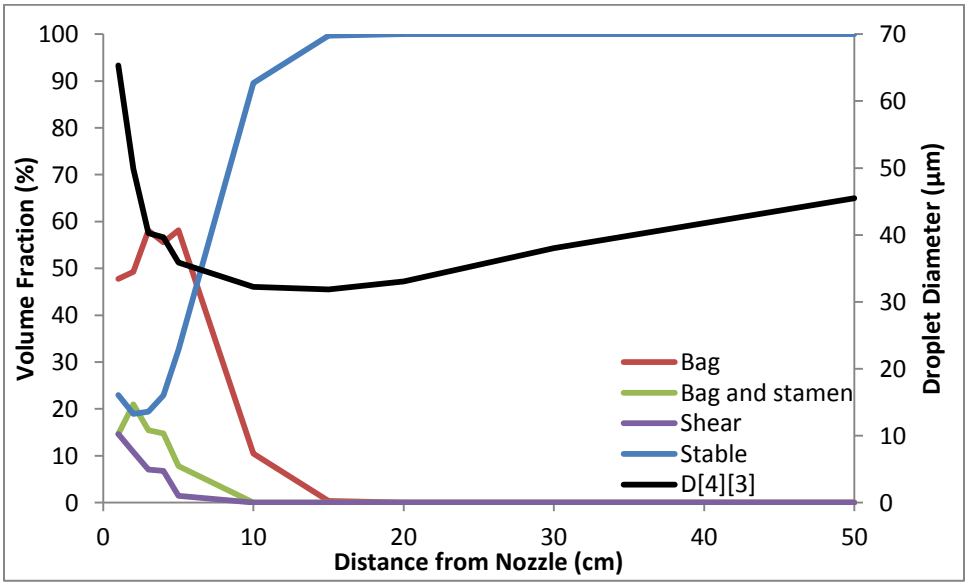

Figure 4.25. Volume fraction of Weber number regimes vs. distance from the nozzle for the E nozzle with a liquid flow rate of 200 cc/min and an atomizing gas pressure of 0.2 MPa

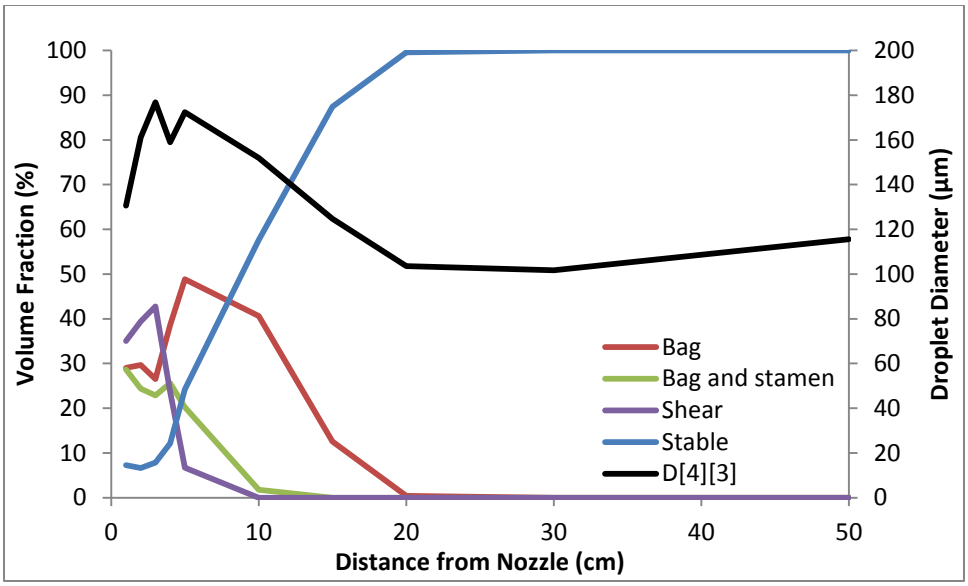

Figure 4.26. Volume fraction of Weber number regimes vs. distance from the nozzle for the E nozzle with a liquid flow rate of 400 cc/min and an atomizing gas pressure of 0.1 MPa

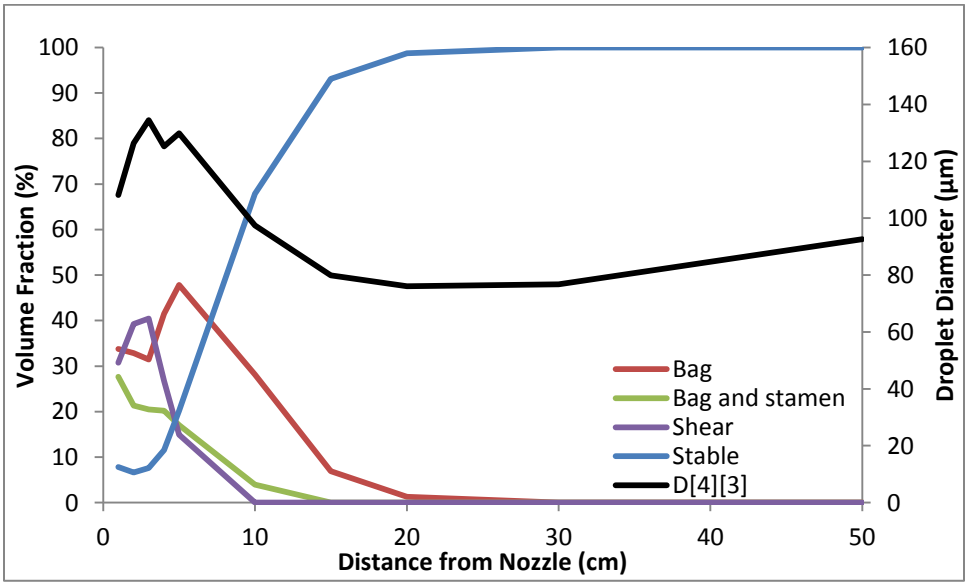

Figure 4.27. Volume fraction of Weber number regimes vs. distance from the nozzle for the E nozzle with a liquid flow rate of 400 cc/min and an atomizing gas pressure of 0.15 MPa

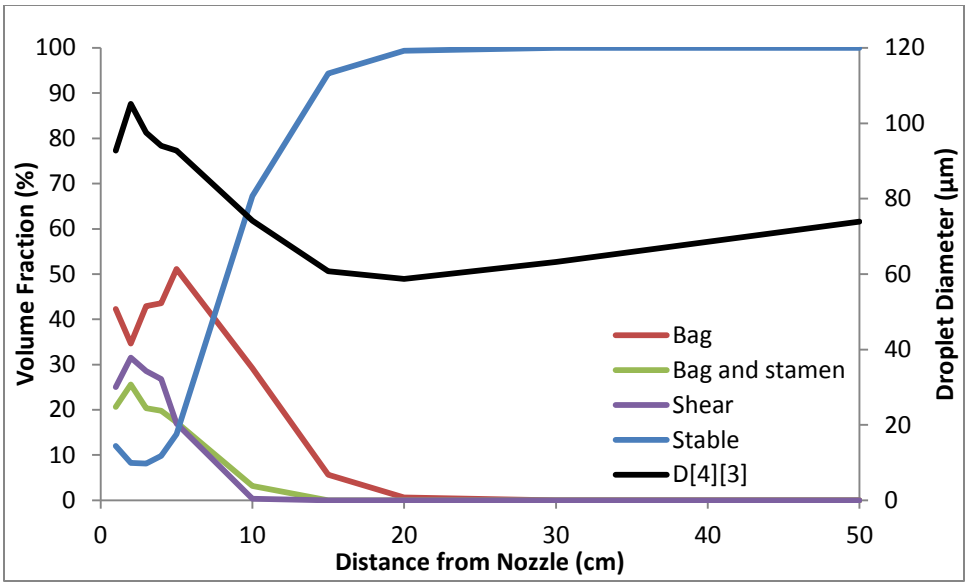

Figure 4.28. Volume fraction of Weber number regimes vs. distance from the nozzle for the E nozzle with a liquid flow rate of 400 cc/min and an atomizing gas pressure of 0.2 MPa

However, at a 200 cc/min liquid flow rate and atomizing gas pressures of 0.15 MPa and 0.2 MPa the minimum droplet sizes occurred at 10 cm from the nozzle and complete atomization finished at 15 cm from the nozzle. These caveats imply different phenomena occur during spraying that are not revealed simply by droplet size analyses. Of course, the first phenomenon to consider is secondary atomization which still occurred at 15 cm from the nozzle. A second phenomenon to also be considered is the recombination of the droplets which causes an increase in the average droplet sizes. The dynamics of these two phenomena are expected to be operational under all spraying conditions but more evident under specific conditions like those displayed in Figure 4.26 and Figure 4.27. An overall result is that there minimal change in droplet size could be measured, and either 20 cm or 30 cm from the nozzle would give similar results.

When the liquid flow rate is 400 cc/min the minimum droplet size consistently occurred at 20 cm, and the Weber number data showed that the higher-energy shear and bag-and-stamen regimes decreased to 0% of the volume by a distance of 10 cm from the nozzle. The bag regime for all atomizing gas pressures decreased to less than 1% of the volume by 20 cm and always was 0% by 30 cm. The droplet sizes at 30 cm was less than 2 μm smaller than at 20 cm, see Figure 4.26 and Figure 4.27, whereas droplet sizes differed by 5 μm in Figure 4.28.

Hence, a representative or ideal point of atomization performance is the location where atomization no longer is a major factor influencing droplet sizes. This representation also considers minimizing the effects of droplet recombination on droplet sizes. Therefore, the data in the figures within this section demonstrate that changes of the breakup regimes occurred at several different distances from the nozzle, depending on the operational conditions.

However, by examining all of the data it was concluded that the most representative or ideal location for measuring atomization performance was 20 cm from the nozzle. This location was consistently where atomization had been completed and minimum droplet sizes detected. If minimum droplet sizes were measured at another location, the differences between droplet sizes at 20 cm and the other distance were less than 5 μm.

4.4 EFFECT OF GAS COMPOSITION ON ATOMIZATION OF SEVERAL LIQUIDS

Previously the ideal settings and distance from the nozzle were found for the spray. This section discusses and then uses ideal operational settings and distance from the nozzle to investigate effects of using different atomizing gases on the spray droplet size distributions. Air, Nitrogen, CO_2 and Helium were tested with solvent-based clear coat, water-borne metallic base coat, and tap water (with a 40 µm filter to remove impurities). This portion of the thesis investigation focused on the results of the spray 20 cm from the nozzle.

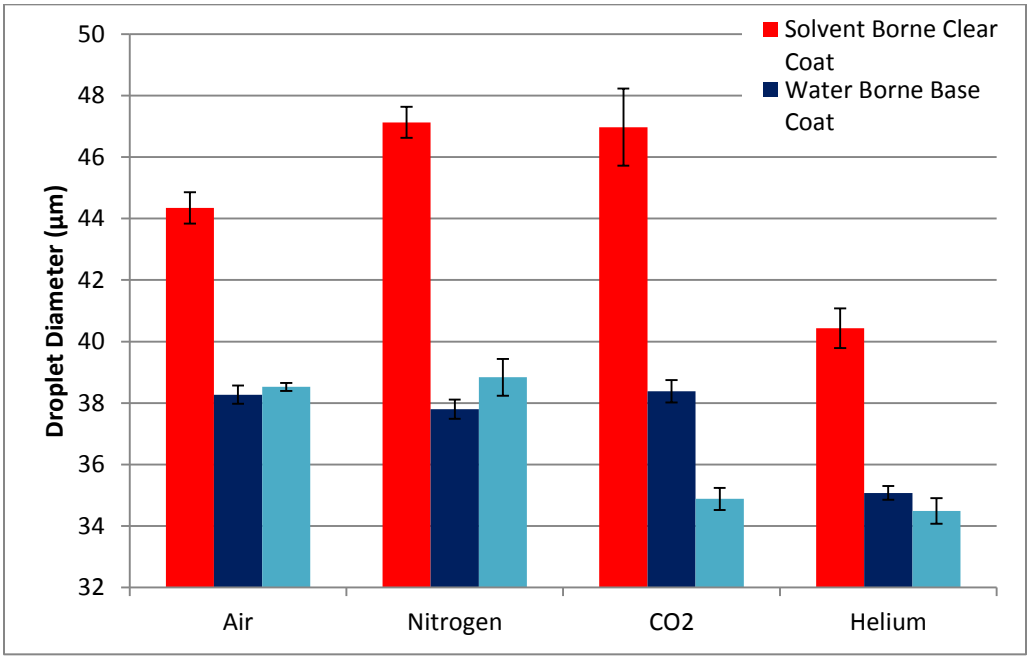

Figure 4.29: Atomizing gas vs. droplet diameter for spray for solvent-borne clear coat, water-borne metallic base coat, and water with a liquid flow rate of 300 cc/min and an atomizing gas pressure of 0.2 MPa at 20 cm from the nozzle.

The data shown in Figure 4.29 shows several trends in droplet sizes. The conditions of the experiments were a liquid flow rate of 300 cc/min, an atomizing gas of

air at a pressure of 0.2 MPa at 20 cm from the nozzle. Each of the experiments was conducted 10 times and a 95% confidence interval was constructed. The most obvious trend in the experiments is that the clear coat produced sprays with the highest droplet size regardless of the atomizing gas used; this trend indicates that the type of liquid sprayed was a major factor controlling the formation of droplets. To verify, the same experiment was tested at 30 cm, and the same trend was present. This trend follows from a realization that the surface tensions of different liquids were dissimilar, with water and water-borne base coat having very close surface tensions and, consequently very similar trends in droplet sizes. Any differences between the behaviors of these two liquids could be a result of the water-borne base coat having additives in solution other than only water.

Another trend in Figure 4.29 that is worthy of further investigation is the difference in droplet sizes for a single liquid when using different gases. The clear coat had similar droplet sizes with nitrogen and CO_2 atomizing gases, whereas the other liquids had dissimilar droplets sizes with these two gases. Interestingly, water produced distinct results for air atomization in comparison to the other gases. For all liquids, the use of He as an atomizing gas decreased droplet sizes the most.

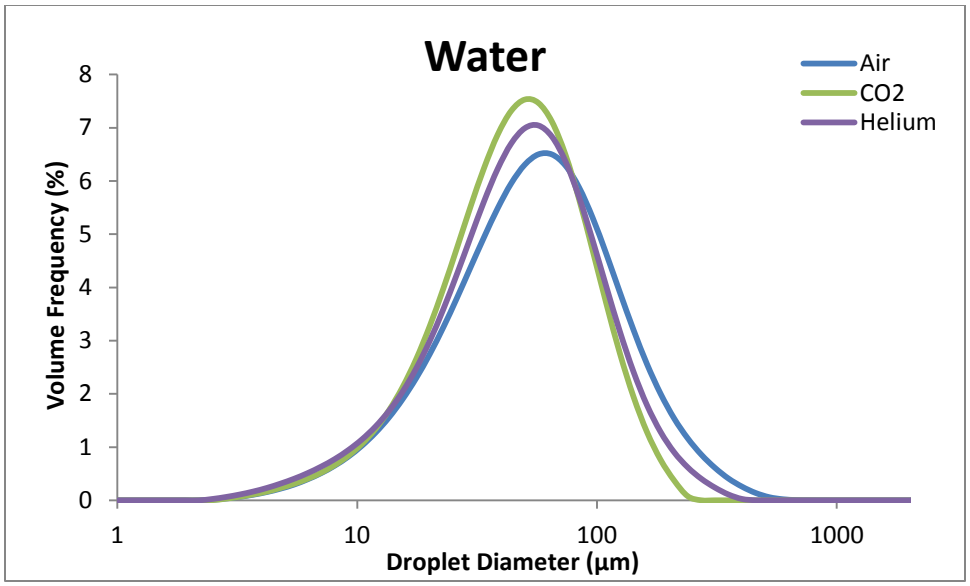

Figure 4.30: Histogram of the volume frequency of different droplet sizes for sprays with an atomizing liquid of water and atomizing gases of air, nitrogen, CO2, and helium.

Figure 4.30 shows that the CO_2 produced volume fractions with the smallest droplet size and the narrowest distribution for water; in contrast, air produced sprays with the widest distribution and the largest droplet sizes. Furthermore, the differences observed in Figure 4.30 are primarily on the high end of the droplet sizes; under 20 µm, the distributions were all almost identical.

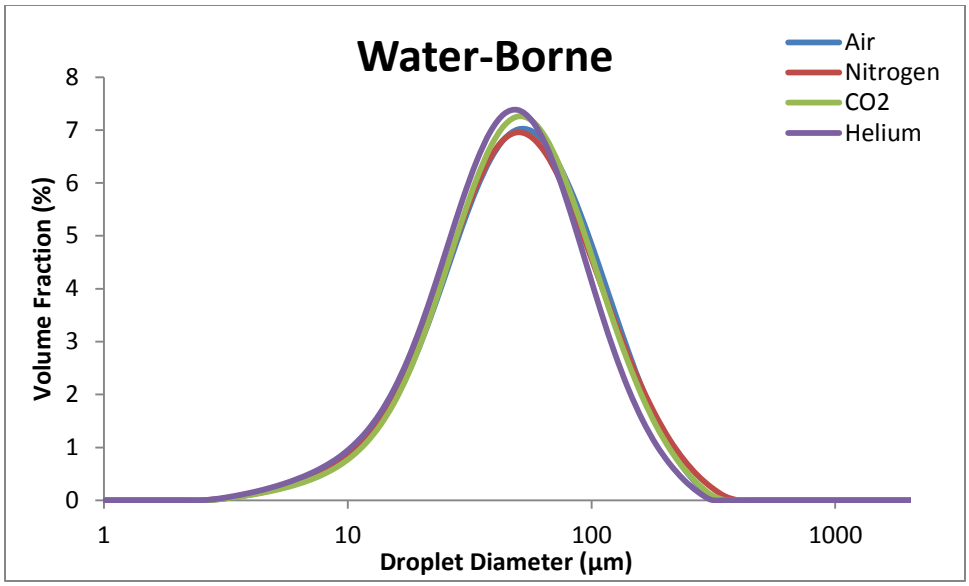

Figure 4.31: Histogram of the volume frequency of different droplet sizes for sprays with an atomizing liquid of water-borne metallic base coat and atomizing gases of air, nitrogen, CO2, and helium.

Figure 4.31 shows differences in the droplet size distributions for all of the atomizing gases for water-borne metallic base coat with the differences relatively minor. Even helium, which has a significantly different D_{32} from the other atomizing gases, had a behavior similar to the other gases. As before, the difference in the droplet size distributions originated primarily in the presence of larger droplet sizes, and very low percentages of very large droplets were present for He; this influence was enough to create a statistically significant difference in the droplet sizes. This graph also shows that the atomizing gas used with the water-borne metallic base coat had less of an effect on droplet sizes than it did for other liquids that were studied.

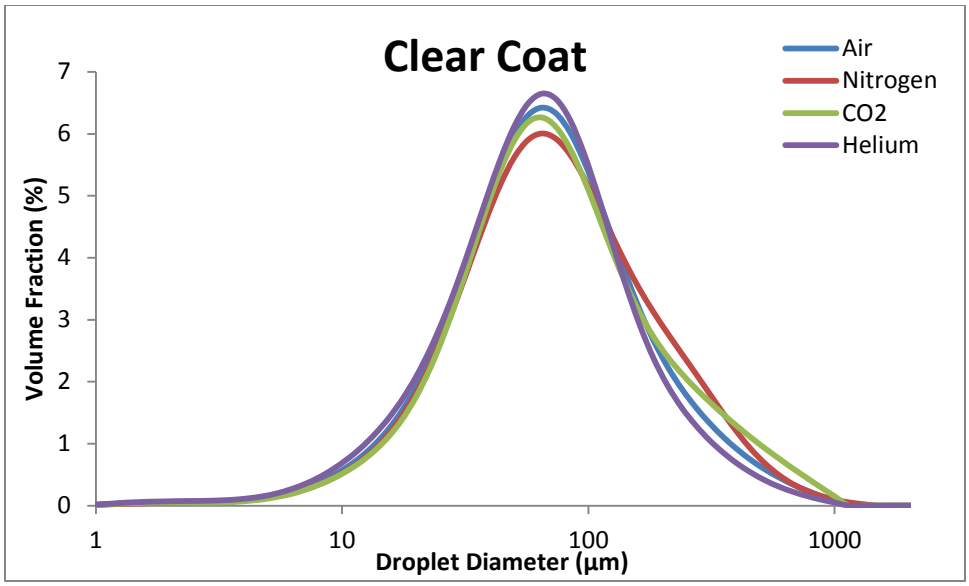

Figure 4.32: Histogram of the volume frequency of different droplet sizes for sprays with an atomizing liquid of solvent-borne clear coat and atomizing gases of air, nitrogen, CO2, and helium at 20 cm from the nozzle.

Figure 4.32 shows a much greater variation in the droplet distributions was measured for solvent-borne clear coat than for the other liquids. In particular, the distribution for CO2 had a much higher concentration of large droplets than any other atomizing gas. Similarly, the droplet distribution for nitrogen had a higher percentage of droplets at the larger droplet sizes even though all droplets were smaller than 1000 µm; CO_2 atomizing gas produced some droplets that were larger than 1000 µm. In Figure 4.32, air and the helium produced very similar curves to each other, but distinct from nitrogen and the CO_2.

A main conclusion gleaned from these graphs is that the atomizing gas and the liquid being sprayed are both important factors in overall droplet size distributions of sprays, i.e. droplet size distributions were different liquids sprayed with identical gases and were also different for the same liquid atomized with different gases. This

conclusion is most clearly evident for the clear coat, where the droplet sizes were much larger than the water-borne base coat and the water. Additionally, the differences for the atomizing gases for the clear coat were much more drastic than in the other liquids. These differences suggest that the solvent-borne paints were more sensitive to operating conditions of the atomizer than were the other liquids.

Additionally, the water-borne metallic clear coat produced a much more consistent droplet size across the different gases than water and the clear coat. However, differences in droplet sizes are not statistically significant (i.e. the confidence intervals overlap) for the air, nitrogen, and CO_2 but are significant for helium. These trends are most consistent and uniform for water, which suggests that the base coat contains additives that help to stabilize droplet sizes and have less of an influence on droplet size distributions even under different operating conditions of the atomizer. Overall, it was clear that changing the atomizing gas has the greatest effect on clear coat sprays.

4.5 EFFECT OF HEATING AND IONIZATION OF THE ATOMIZING GAS ON ATOMIZATION OF DROPLETS

This section presents the results of experiments which investigated heating and ionizing of various atomization gases using the three different liquids discussed in the previous section.

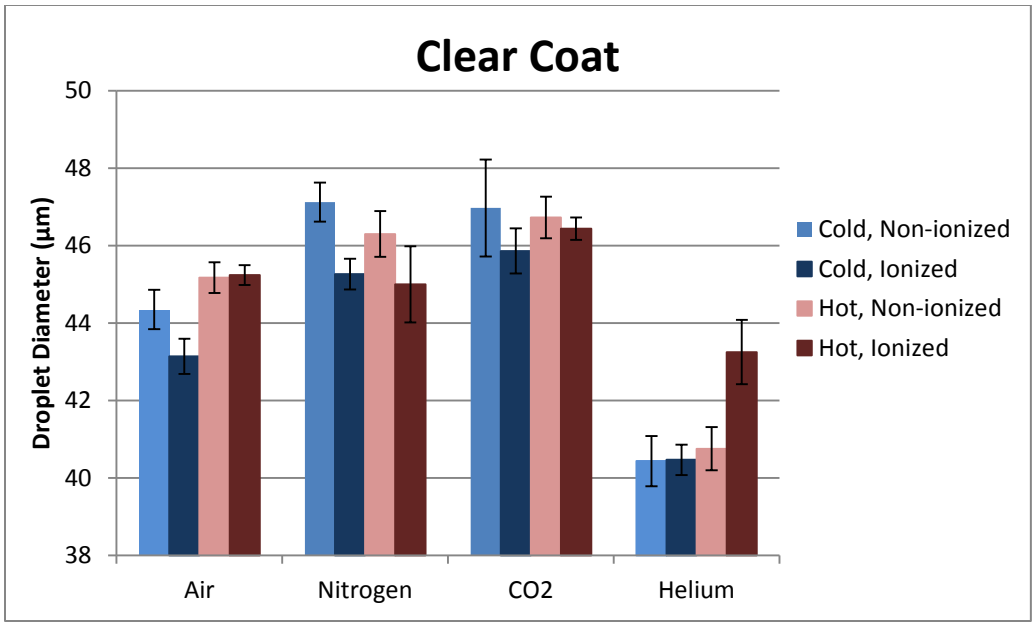

Figure 4.33: Droplet diameter vs. atomizing gas composition with heating and ionization. The liquid used was solvent-borne clear coat and the flow rate was 300 cc/min. The atomizing gas pressure was 0.2 MPa at 20 cm from the nozzle.

Figure 4.33 presents results for the clear coat, the liquid that provided the most distinctive results for the three liquids; for clarification, the clear coat is not water-borne. In general, the heating and ionizing of the atomizing gas often had a significant effect on droplet sizes although trends are not totally consistent. For air, heating of the atomizing gas had the most significant impact on droplet diameters; whereas for nitrogen and the CO_2 the impact of heating was insignificant. In general, differences in the droplet sizes between these heated and unheated atomizing gases were less than the standard error for the experiments.

The impact of ionizing He during atomization was the most apparent. Heated and ionized He gas produced a significantly higher increase in droplet diameters than did the use of heating and ionizing for the other three gases. These data signify that the

interaction of heating and ionization may play a significant role in the behavior of He as an atomizing gas. A possible influence for this result is that the electrical conductivity of helium is much higher that the conductivity of the other three gases (Fischer, Hackmann et al. 1969).

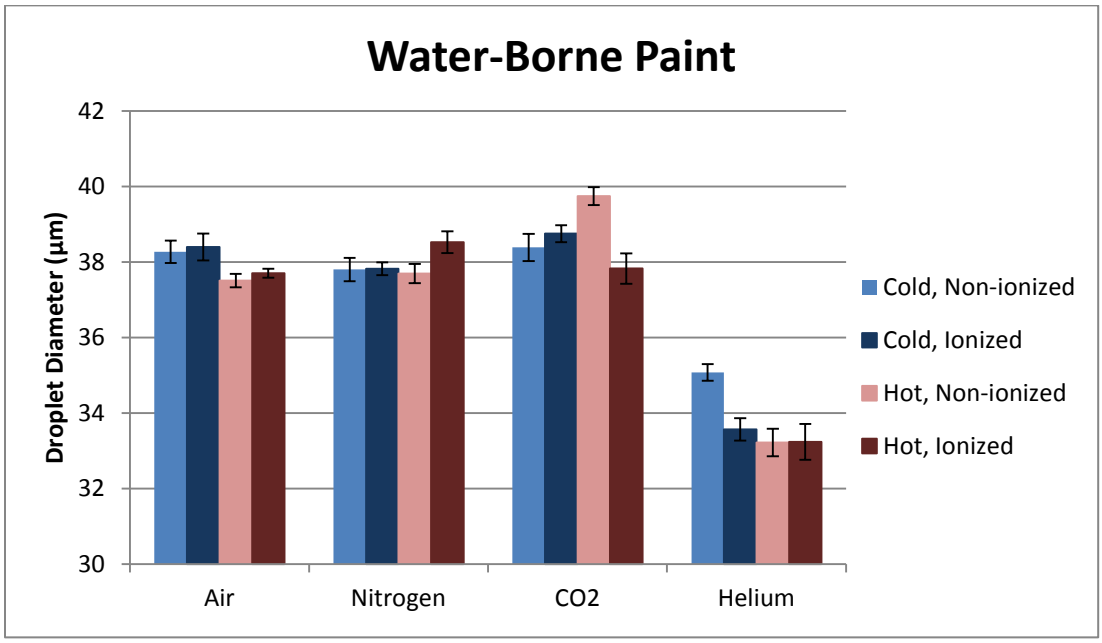

Figure 4.34: Droplet diameter vs. atomizing gas composition with heating and ionization. The liquid used was water-borne metallic base coat and the flow rate was 300 cc/min. The atomizing gas pressure was 0.2 MPa at 20 cm from the nozzle.

For the water-borne metallic base coat, the impacts of heating and ionizing the atomization gas on droplet diameters were minor. The air and the nitrogen data were identical within confidence intervals of each other. This implies that the impact of heating and ionizing these two similar gases was effectively zero, and may be influenced by the chemical composition of the water-borne base coat, which although based on water is a non–Newtonian fluid (Xu and Koelling 2005).

Tests with the He atomization gas again provided the most differences in droplet diameters for all the gases with the unheated, non-ionized result having a significantly higher diameter than the other three experimental conditions. This result implies that ionization and the heating impacts He to a much greater degree than for air, nitrogen and CO_2. These latter three gases are much denser than He, and this density difference combined with the physical properties of the liquid could be minimizing the effect of the heating and ionization.

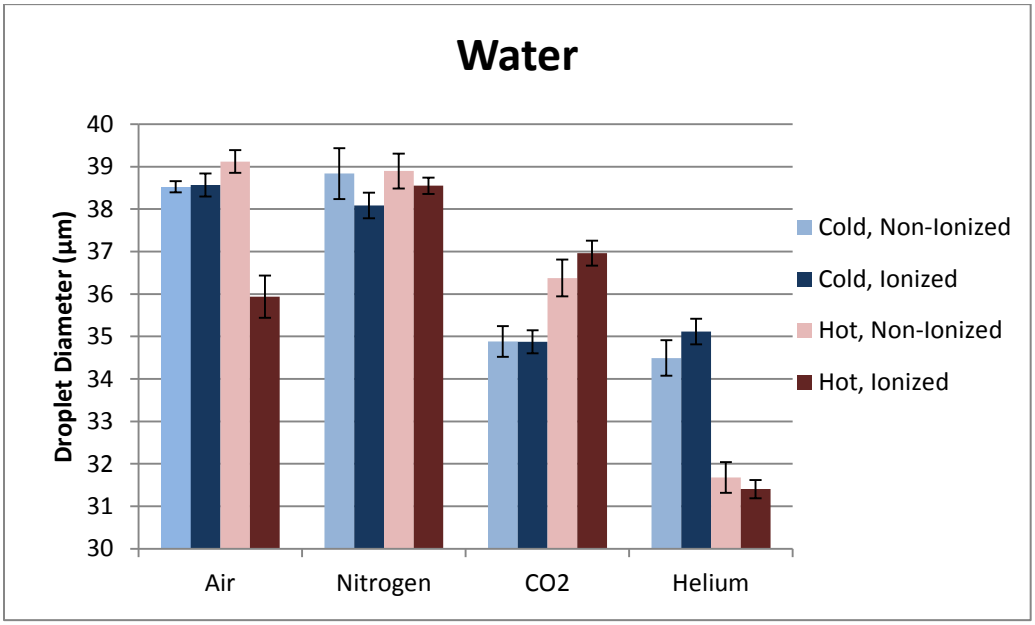

Figure 4.35: Droplet diameter vs. atomizing gas composition with heating and ionization. The liquid used was solvent-borne clear coat and the flow rate was 300 cc/min. The atomizing gas pressure was 0.2 MPa at 20 cm from the nozzle.

Figure 4.35 presents the results for the droplet sizes when the water flow rate was 300 cc/min and the atomizing gas pressure was 0.2 MPa. The results differ greatly from those of the water-borne metallic base coat, one reason for which could that water is a Newtonian fluid with no additives or metal flakes. Interestingly, the water droplet sizes

did not follow the same trend as those for the water-borne base coat; air and nitrogen atomizing gases behaved similarly except after heating and ionization were introduced and the average droplet size decreased by almost 3 μm.

Additionally, the effect of heating on the droplet size was significant for CO_2 and helium with effects that were inverse of each other. Heating of CO_2 as the atomizing gas increased droplet sizes, while heating helium reduced droplet sizes; these complicated trends complicates an overall understanding of the important factors influencing droplet diameters. In fact, ionization of the atomizing gas was not a significant factor in any of the results produced using water, as is evidenced by the fact that ionized and non-ionized experimental diameters always have shown overlapping confidence intervals.

A statistical analysis was performed for the data that was gathered in the last set of experiments. The droplet size data was entered into analysis of variance (ANOVA) software and the effects as well as their first order interactions were tested. The results are shown in Figure 36.

Effect Tests

Source	Nparm	DF	Sum of Squares	F Ratio	Prob > F
Paint Type	2	2	650.53536	273.4221	<.0001*
Atomizing Gas	3	3	175.30509	49.1209	<.0001*
Heating	1	1	0.06720	0.0565	0.8142
Ionization	1	1	1.45673	1.2245	0.2799
Paint Type*Atomizing Gas	6	6	25.02063	3.5054	0.0131*
Paint Type*Heating	2	2	3.33027	1.3997	0.2669
Paint Type*Ionization	2	2	0.07760	0.0326	0.9680
Atomizing Gas*Heating	3	3	4.15740	1.1649	0.3446
Atomizing Gas*Ionization	3	3	1.45556	0.4079	0.7488
Heating*Ionization	1	1	0.09381	0.0789	0.7814

Figure 36: Results of an ANOVA analysis of the factors as well as their first order interactions

The overall effects of the heating and the ionization were not statistically significant to the final results. The factors that were significant were the liquid composition (listed as the paint type), the atomizing gas, and the interaction of the atomizing gas and the liquid composition. More research is needed to determine if higher levels of heating or ionization would significantly affect the droplet size, and if the energy used to heat and ionize the atomizing gas is worth the additional energy costs.

CHAPTER FIVE

5.0 CONCLUSIONS

The following conclusions can be drawn from the results presented in this thesis:

1. The nozzles have the following characteristics (spray pattern, gas velocity, and droplet size) which when optimized would significantly improve the spray characteristics and transfer efficiency.
2. The Weber number formula is useful in determining the secondary atomization behavior of the spray which shows the ideal distance between the nozzle and the target, which this study confirms to be between 15 and 20 cm.
3. The use of different atomizing gases significantly affects the average droplet size of a spray.
4. The ionization and heating of the atomizing gas did not consistently affect the droplet size of the spray.

5.1 CONTRIBUTION OF THIS THESIS

In summary, this thesis provided the following contributions to the research community:

1. A novel method for calculating the Weber number in the spray was developed.
2. The method for measuring the Weber number in the spray was used to determine the best application distance from the nozzle.

3. The use of different atomizing gases shows the effect of different gases on the average droplet size.

5.2 FUTURE WORK

This thesis has answered questions about the efficacy of heating and ionization on the average droplet size, but there are many questions that arose during the research which have opened new avenues of investigation. Some of these are:

1. Validation of the Weber number method for prediction of the breakup of droplets in the spray. The method developed in this thesis is based on known scaling laws, but its accuracy in actual prediction should be validated with direct observation of the droplets with a high speed camera and magnification.
2. Measurements of the droplet size distribution of overspray have never been studied. Measurements of the overspray would give a more complete picture of the spray process and which droplet sizes are most likely to attach to the target.

REFERENCES

Akafuah, N. K., et al. (2009). "Estimation of Liquid Volume Fraction and Droplet Number Density in Automotive Paint Spray Using Infrared Thermography-Based Visualization Technique." Atomization and Sprays **19**(9): 847-861.

Akafuah, N. K., et al. (2010). "Infrared thermography-based visualization of droplet transport in liquid sprays." Infrared Physics & Technology **53**(3): 218-226.

Allen, T. (1990). Particle size measurement. London ; New York, Chapman and Hall.

Astarita, T. and G. Cardone (2008). "Convective heat transfer on a rotating disk with a centred impinging round jet." International Journal of Heat and Mass Transfer **51**(7-8): 1562-1572.

Avdelidis, N. P. and A. Moropoulou (2004). "Applications of infrared thermography for the investigation of historic structures." Journal of Cultural Heritage **5**(1): 119-127.

Aydin, T. O., et al. (2008). "Dynamic range independent image quality assessment." Acm Transactions on Graphics **27**(3).

Ayres, D., et al. (2001). "Prediction of the droplet size and velocity joint distribution for sprays." Fuel **80**(3): 383-394.

Braun, J. H. and D. P. Fields (1994). "Gloss of Paint Films .2. Effects of Pigment Size." Journal of Coatings Technology **66**(828): 93-98.

Canon USA (2015). "About EOS 5D Mark II." Retrieved January 18, 2015.

Canon USA (2015). "EF 28-135mm f/3.5-5.6 IS USM Specifications." Retrieved January 18, 2015.

Cao, J. M. (2002). "On the theoretical prediction of fuel droplet size distribution in nonreactive diesel sprays." Journal of Fluids Engineering-Transactions of the Asme **124**(1): 182-185.

Çengel, Y. A. and M. A. Boles (2011). Thermodynamics : an engineering approach. New York, NY, McGraw-Hill.

Chemco Manufacturing (2000). "Fiberglass Paint Arrestors." Retrieved January 17, 2015.

Chimonas, G. (1986). "The Combined Rayleigh, Kelvin-Helmholtz Problem." Physics of Fluids **29**(7): 2061-2066.

Cini, R., et al. (1971). "Dependence of Water Surface Tension on Temperature." Chimica & L Industria **53**(8): 793-&.

Cini, R., et al. (1972). "Temperature Dependence of Surface-Tension of Water by Equilibrium Ring Method." Journal of Colloid and Interface Science **41**(2): 287-&.

Clark, M. R., et al. (2003). "Application of infrared thermography to the non-destructive testing of concrete and masonry bridges." Ndt & E International **36**(4): 265-275.

Daly, B. J. (1967). "Numerical Study of 2 Fluid Rayleigh-Taylor Instability." Physics of Fluids **10**(2): 297-&.

Daly, B. J. (1969). "Numerical Study of Effect of Surface Tension on Interface Instability." Physics of Fluids **12**(7): 1340-&.

Drazin, P. G. (1970). "Kelvin-Helmholtz Instability of Finite Amplitude." Journal of Fluid Mechanics **42**: 321-&.

Dumouchel, C. and S. Boyaval (1999). "Use of the maximum entropy formalism to determine drop size distribution characteristics." Particle & Particle Systems Characterization **16**(4): 177-184.

Durst, F. a. Z., M. (1975). Laser Doppler measurements in two-phase flows. LDA-Symposium, Copenhagen, Denmark.

Elshanawany, M. S. and A. H. Lefebvre (1980). "Airblast Atomization - Effect of Linear Scale on Mean Drop Size." Journal of Energy **4**(4): 184-189.

Eurosider (2008). Spray Painting Device with Ionization of the Carrier Fluid. W. I. P. Organization. Italy.

Fischer, E., et al. (1969). "Calculation of Electrical Conductivity of Helium from Integral Arc Measurements." Zeitschrift Fur Naturforschung Part a-Astrophysik Physik Und Physikalische Chemie **A 24**(9): 1427-&.

FLIR Systems (2015). "ThermoVision SC4000 Science Grade Infrered Camera." Retrieved January 23, 2015.

Gartenberg, P. K., et al. (1989). "Evaluation of the Mineral Status of Cattle in Northeast Mexico .1. Macroelements and Crude Protein." Nutrition Reports International **40**(2): 367-375.

Gieseke, J. A. P., G.W. (1980). Inertial Classification of Aerosols for Size Measurement. CSNI SpecialistsbMeeting on Nuclear Aerosols in Reactor Safety.

Gittens, G. J. (1969). "Variation of Surface Tension of Water with Temperature." Journal of Colloid and Interface Science **30**(3): 406-&.

Hickey, A. J. (2004). Pharmaceutical inhalation aerosol technology. New York, M. Dekker.

Hirleman, E. D. (1988). "Modeling of Multiple-Scattering Effects in Fraunhofer-Diffraction Particle-Size Analysis." Particle & Particle Systems Characterization **5**(2): 57-65.

Hund, J. P. (1985). "Air-Assisted Airless Finishing Combines 2 Systems." Wood & Wood Products **90**(5): 103-&.

Infrared Systems. "IR-160/301 Extended Area Blackbody Specifications." Retrieved January 23, 2015.

Infrared Systems (2014). "Infrared radiation blackbody, radiation sources & infrared detector preamplifiers." Retrieved January 22, 2015.

Ion Industries (1991). "Portable Camera Link DVR's." Retrieved January 15, 2015.

Johansso.K and J. C. Eriksson (1972). "Determination of Dgamma Dt for Water by Means of a Differential Technique." Journal of Colloid and Interface Science **40**(3): 398-&.

Joseph, D. D., et al. (1999). "Breakup of a liquid drop suddenly exposed to a high-speed airstream." International Journal of Multiphase Flow **25**(6-7): 1263-1303.

Juslin, L., et al. (1995). "Droplet Size Measurement .1. Effect of 3 Independent Variables on Droplet Size Distribution and Spray Angle from a Pneumatic Nozzle." International Journal of Pharmaceutics **123**(2): 247-256.

Juslin, L., et al. (1995). "Droplet Size Measurement .2. Effect of 3 Independent Variables on Parameters Describing the Droplet Size Distribution from a Pneumatic Nozzle Studied by Multilinear Stepwise Regression-Analysis." International Journal of Pharmaceutics **123**(2): 257-264.

Kautz, C. H., et al. (2005). "Student understanding of the ideal gas law, Part I: A macroscopic perspective." American Journal of Physics **73**(11): 1055-1063.

Kautz, C. H., et al. (2005). "Student understanding of the ideal gas law, Part II: A microscopic perspective." American Journal of Physics **73**(11): 1064-1071.

Kayser, W. V. (1976). "Temperature-Dependence of Surface-Tension of Water in Contact with Its Saturated Vapor." Journal of Colloid and Interface Science **56**(3): 622-627.

Kelvin, L. (1871). "Hydrokinetic solutions and observations." Philosophical Magazine **42**: 362-377.

Keng, E. Y. H. and C. Orr (1966). "Thermal Precipitation and Particle Conductivity." Journal of Colloid and Interface Science **22**(2): 107-&.

Khan, M. A. H., et al. (2003). "A case study of methods of series summation: Kelvin-Helmholtz instability of finite amplitude." Journal of Computational Physics **187**(1): 212-229.

Krautzberger GmbH (2013). "HS 25 HV3 Description." Retrieved January 23, 2015.

Krautzberger GmbH (2014). "Material pressure feeding containers." Retrieved December 9, 2014.

Kull, H. J. (1991). "Theory of the Rayleigh-Taylor Instability." Physics Reports-Review Section of Physics Letters **206**(5): 197-325.

Kuneš, J. and J. Kuneš (2012). Dimensionless physical quantities in science and engineering. London ; Waltham, MA, Elsevier.

Lahiri, B. B., et al. (2012). "Medical applications of infrared thermography: A review." Infrared Physics & Technology **55**(4): 221-235.

Lasheras, J. C., et al. (1998). "Break-up and atomization of a round water jet by a high-speed annular air jet." Journal of Fluid Mechanics **357**: 351-379.

Lefebvre, A. H. (1980). "Airblast Atomization." Progress in Energy and Combustion Science **6**(3): 233-261.

Lefebvre, A. H. (1989). Atomization and sprays. New York, Hemisphere Pub. Corp.

Li, X. G. and R. S. Tankin (1987). "Droplet Size Distribution - a Derivation of a Nukiyama-Tanasawa Type Distribution Function." Combustion Science and Technology **56**(1-3): 65-76.

Liu, H. (2000). Science and Engineering of Droplets: Fundamentals and Applications. New York, Noyes Pulications.

Lou, H. H. and Y. L. Huang (2003). "Hierarchical decision making for proactive quality control: system development for defect reduction in automotive coating operations." Engineering Applications of Artificial Intelligence **16**(3): 237-250.

Lowe, H. J. a. L., D.H. (1953). "The physics of electrostatic precipitation." British Journal of Applied Physics **4**(2): 40-47.

Lowes (2015). "Utilitech 500-Watt Halogen Portable Work Light Specifications." Retrieved February 12, 2015.

Malvern Instruments. "Spraytec Overview." Retrieved December 9, 2014.

Marmottant, P. H. and E. Villermaux (2004). "On spray formation." Journal of Fluid Mechanics **498**: 73-111.

McKnight, M. E. a. M., J.W. (1997). Advanced Methods and Models for Describing Coating Appearance. Proc. of Organic Coatings - Waterborne; High Solids; Powder Coatings, Athens, Greece.

Meiron, D. I., et al. (1982). "Analytic Structure of Vortex Sheet Dynamics .1. Kelvin-Helmholtz Instability." Journal of Fluid Mechanics **114**(Jan): 283-298.

Meola, C., et al. (2004). "The use of infrared thermography for nondestructive evaluation of joints." Infrared Physics & Technology **46**(1-2): 93-99.

Muhlenweg, H. and E. D. Hirleman (1998). "Laser diffraction spectroscopy: Influence of particle shape and a shape adaptation technique." Particle & Particle Systems Characterization **15**(4): 163-169.

Myszkowsi, K. (2008). High Dynamic Range Video.

Orr, C., et al. (1956). "Thermal Precipitation for Sampling Air-Borne Microorganisms." Applied Microbiology **4**(3): 116-118.

Paasche Airbrush (2012). "FABSF-3-T3 Details." Retrieved January 22, 2014.

Parker, K. R. (1997). Applied electrostatic precipitation. London ; New York, Blackie Academic & Professional.

Pilch, M. and C. A. Erdman (1987). "Use of Breakup Time Data and Velocity History Data to Predict the Maximum Size of Stable Fragments for Acceleration-Induced Breakup of a Liquid-Drop." International Journal of Multiphase Flow **13**(6): 741-757.

Planck, M. (1901). "Law of energy distribution in normal spectra." Annalen Der Physik **4**(3): 553-563.

Polidori, G. H., J.F.; Fohanno, S. (2003). On the Simultaneous Use of Particle Streak Velocimetry and Infrared Thermography for the Study of Transient Separated Natural Convection Flow in Water. PSFVIP-4, Chamonix, France.

Poropat, G. V. (1993). "Effect of System Point-Spread Function, Apparent Size, and Detector Instantaneous Field-of-View on the Infrared Image-Contrast of Small Objects." Optical Engineering **32**(10): 2598-2607.

Qiu, H. H. and M. Sommerfeld (1992). "A Reliable Method for Determining the Measurement Volume Size and Particle Mass Fluxes Using Phase-Doppler Anemometry." Experiments in Fluids **13**(6): 393-404.

Schick, R. J. (2008). An Engineer's Practical Guide to Drop Size. Wheaton, Illinois, Spraying Systems Co.

Schulz, A. (2000). "Infrared thermography as applied to film cooling of gas turbine components." Measurement Science & Technology **11**(7): 948-956.

Semiao, V., et al. (1996). "Spray characterization: Numerical prediction of Sauter mean diameter and droplet size distribution." Fuel **75**(15): 1707-1714.

Sharp, D. H. (1984). "An Overview of Rayleigh-Taylor Instability." Physica D **12**(1-3): 3-18.

Sher, I. and E. Sher (2011). "Analytical Criterion for Droplet Breakup." Atomization and Sprays **21**(12): 1059-1063.

Simco-Ion (2012). "Air Ionizing Cartridge Model 6110." Retrieved January 18, 2015.

Sirignano, W. A. (1999). Fluid dynamics and transport of droplets and sprays. Cambridge, U.K., Cambridge University Press.

Sommerfeld, M. and H. H. Qiu (1995). "Particle Concentration Measurements by Phase-Doppler Anemometry in Complex Dispersed 2-Phase Flows." Experiments in Fluids **18**(3): 187-198.

Strutt, J. W., Lord Rayleigh (1883). "Investigation of the character of the equilibrium of an incompressible
heavy fluid of variable density." Proceedings of the London mathematical society **14**: 170- 177.

Taylor, G. I. (1950). "The Boundary Layer in the Converging Nozzle of a Swirl Atomizer." Quarterly Journal of Mechanics and Applied Mathematics **3**(2): 129-139.

Taylor Wharton (2014). "Instructions for XL-45, XL-50 and XL-55." http://www.taylorwharton.com/assets/base/doc/products/cylinders/TW-287_XL-45_50_55_(with_dual_regulators).pdf. Retrieved December 16, 2014.

Tidrow, M. Z. (2000). "Device physics and state-of-the-art of quantum well infrared photodetectors and arrays." Materials Science and Engineering B-Solid State Materials for Advanced Technology **74**(1-3): 45-51.

Varga, C. M., et al. (2003). "Initial breakup of a small-diameter liquid jet by a high-speed gas stream." Journal of Fluid Mechanics **497**: 405-434.

Vargaftik, N. B., et al. (1983). "International Tables of the Surface-Tension of Water." Journal of Physical and Chemical Reference Data **12**(3): 817-820.

Weber, D. C. and E. D. Hirleman (1988). "Light-Scattering Signatures of Individual Spheres on Optically Smooth Conducting Surfaces." Applied Optics **27**(19): 4019-4026.

Xu, J. H. and K. W. Koelling (2005). "Temperature dependence of rheological behavior of a metallic automotive waterborne basecoat." Progress in Organic Coatings **53**(3): 169-176.

VITA

ANTHONY VICTOR ADORNATO

Place of Birth: Louisville, Kentucky

EDUCATION

Bachelor of Science in Mechanical Engineering, 2008-2013, University of Kentucky, Lexington, Kentucky

AWARDS AND HONORS

Boeing Fellowship, University of Kentucky, 2013-2015
President's Scholarship, University of Kentucky, 2008-2012
General Electric STAR Scholarship, 2008

PROFESSIONAL MEMBERSHIP

Member, American Society of Mechanical Engineers
Member, Society of Automotive Engineers